# Modeling and Characteristics of a Novel Multi-fuel Hybrid Engine for Future Aircraft

Yin, Feijia

**DOI**
10.4233/uuid:344b7d9c-f54c-4836-87ca-28582231a3d3

**Publication date**
2016

**Document Version**
Final published version

**Citation (APA)**
Yin, F. (2016). *Modeling and Characteristics of a Novel Multi-fuel Hybrid Engine for Future Aircraft*. [Dissertation (TU Delft), Delft University of Technology]. https://doi.org/10.4233/uuid:344b7d9c-f54c-4836-87ca-28582231a3d3

# Modeling and Characteristics of a Novel Multi-fuel Hybrid Engine for Future Aircraft

# Modeling and Characteristics of a Novel Multi-Fuel Hybrid Engine for Future Aircraft

Proefschrift

ter verkrijging van de graad van doctor
aan de Technische Universiteit Delft,
op gezag van de Rector Magnificus prof. ir. K. Ch. A. M. Luyben
voorzitter van het College voor Promoties,
in het openbaar te verdedigen op
dinsdag 13 september 2016 om 10:00 uur

door

**Feijia YIN**

Master of Science in Control Theory and Engineering,
Northwestern Polytechnical University, China
Geboren te Liquan, Shaanxi province, China.

Dit proefschrift is goedgekeurd door de promotoren:

| | |
|---|---|
| promotor | Prof. ir. J. P. van Buijtenen |
| copromotor | Dr. A. Gangoli Rao |

| | |
|---|---|
| Rector Magnificus | voorzitter |
| Prof. ir. J. P. van Buijtenen | Technische Universiteit Delft |
| Dr. A. Gangoli Rao | Technische Universiteit Delft |

Onafhankelijke leden:

| | |
|---|---|
| Prof. dr. ir. S. Klein | Technische Universiteit Delft |
| Prof. dr. ir. L. Veldhuis | Technische Universiteit Delft |
| Prof. dr. ir. H. W. M. Hoeijmakers | University of Twente |
| Prof. dr. P. Pilidis | Cranfield University |
| Dr. ir. W. P. J. Visser | TU Delft / B&B Agema |
| Prof. dr. ir. P. Colonna | Technische Universiteit Delft, |
| reserve member | |

The research leading to these results has received funding from the China Scholarship Council (CSC) and the European Union Seventh Framework Programme (FP7/2007-2013) under grant agreement No. 284636.

Key words: hybrid engine, alternative fuels, low emissions, engine model development, performance optimization, operating strategy of dual combustors

ISBN 978-94-6186-711-7

Published and distributed by Feijia Yin
Email: feijia.yin@outlook.com



Printed in the Netherlands

# Summary

Civil air transportation has undergone significant expansion over the past decades and is continuing to grow. Nevertheless, the tendency of energy depletion and the severe environmental problems yield challenges in its further development. To mitigate the climate impact of civil aviation, the Advisory Council for Aeronautics Research in Europe (ACARE) has set ambitious objectives for the year 2050 to reduce the $CO_2$ emission by 75% per passenger kilometre, the NOx emissions by 90% and the perceived noise emission by 65% relative to the capacities of aircraft operating in the year 2000.

The conventional approach of increasing Bypass Ratio (BPR), Overall Pressure Ratio (OPR), and Turbine Inlet Temperature (TIT) to improve the cycle efficiency, and thereby reducing the fossil fuel consumption and the associated emissions is unlikely to meet the ACARE goals. Moreover, the high OPR and TIT aggravate the NOx emissions for a given combustion technique. A novel multi-fuel hybrid engine for a Multi-Fuel Blended Wing Body (MFBWB) aircraft conceived in the "*Advanced Hybrid Engine for Aircraft Development (AHEAD)*" project brings to light promising solutions in this regard.

The multi-fuel hybrid engine is a turbofan engine with the following added components: a Contra-Rotating Fans (CRF) system, two sequential combustors burning different fuels simultaneously, and a Cryogenic Bleed Air Cooling System (CBACS). The CRF can sustain the non-uniform flow ingested from the boundary layer of the airframe. The first combustor is the main combustor, where the Liquid Hydrogen (LH2) or the Liquid Natural Gas (LNG) is burnt to reduce $CO_2$. The second combustor, Interstage Turbine Burner (ITB), is located between the high pressure and the low pressure turbine burning kerosene or biofuel in a Flameless Combustion (FC) mode. With the thermal energy provided by different fuel sources, the volume required to store cryogenic fuels is less; meanwhile, the FC technique is beneficial to reduce NOx. By introducing the CBACS, LH2 or LNG is used as a coolant to cool down the bleed air.

According to fuel combinations, the hybrid engine is classified as LNG-kerosene version and LH2-kerosene version, where kerosene might be replaced by biofuel. By defining an "ITB energy fraction" as the ratio of the energy input of the ITB to the overall energy consumed, the fuel flow rates of two combustors are controlled. Using the developed model framework, the characteristics of the hybrid engine are studied and summarized in the following three aspects:

**Potentials of the ITB engine cycle**

The sequential combustor configuration of the hybrid engine forms a reheat cycle. By distributing the energy into two combustors, the heat addition to each combustor decreases; therefore, the TIT is lower. Consequently, the turbine cooling air and the associated loss in the turbine efficiency reduces. Moreover, the NOx produced from the upstream combustor dissociates again in the ITB, which helps to lower the overall NOx emissions. These remarkable features are appreciable when the OPR and BPR are forced to continuously increase, which causes a substantial increase in the TIT of a classical engine. A turbine with very high inlet temperature has to be cooled substantially. Eventually, the gain in cycle efficiency might be canceled by the loss in the turbine efficiency. Moreover, when the TIT is increased beyond 1800 K, the NOx exhibits an exponential increase. Hence following the evolution of the engine technology, the reheat cycle would be an option for the next step.

**Characteristics of the multi-fuel hybrid engine**

The features of the hybrid engine have been explored from various aspects. The isobaric heat capacity of the combustion products from LNG and LH2 is higher than that from kerosene, which is beneficial to the thermal efficiency. Using LNG and LH2 as a coolant, the bleed air temperature reduces substantially (maximum by more than 500 K), thereby, the turbine cooling air mass flow rate decreases by half. Moreover, the increase in fuel temperature is favourable to enhance the thermal efficiency. The hybrid engine has been optimized at cruise considering various ITB energy fractions. The optimized engine cycle is verified at critical operating points. The assessment of the standalone engine performance with baseline engines shows that the LH2-kerosene hybrid engine is superior to the LNG-kerosene hybrid engine in terms of the cycle efficiency and the $CO_2$ reduction. However, the mission analysis shows conflicting results. Due to the stronger installation effect, the MFBWB together with the LH2-kerosene hybrid engine scores lower, implying that the LNG-kerosene BWB would have the least climate impact.

**Operating strategy of the multi-fuel hybrid engine**

The operating strategy of the hybrid combustion system has been developed to enhance the steady state performance of the hybrid engine. The analysis exhibits that using an ITB is beneficial for the high pressure spool speed, the HPC exit temperature, and the HPT inlet temperature. However, the LPC surge margin and LPT inlet temperature conflict their limits as the ITB energy fraction increases. For the various thrust requirements at Sea Level Static (SLS) standard condition, a fuel control schedule together with a

variable bleed valve schedule is proposed. Moreover, another fuel control strategy is suggested for the flat rating at SLS.

# Samenvatting

De burgerluchtvaart is de afgelopen decennia aanzienlijk in omvang toegenomen en is nog steeds voortdurend aan het groeien. Desalniettemin blijven de neiging om de energievoorraden uit te putten en steeds ernstigere milieuproblemen uitdagingen vormen voor haar verdere ontwikkeling. Om het klimaateffect van de luchtvaart te beperken, heeft de Advisory Council for Aeronautics Research in Europe (ACARE) de ambitieuze doelstellingen gesteld om in het jaar 2050 de $CO_2$-uitstoot met 75%, de NOx-uitstoot met 90% en de geluidsoverlast met 65% te verminderen ten opzichte van een vliegtuigmotor uit het jaar 2000.

Het is onwaarschijnlijk dat de gebruikelijke aanpak om de omloopverhouding (BPR), algemene drukverhouding (OPR) en turbine-inlaattemperatuur (TIT) te verhogen ter vergroting van de efficiëntie van de verbrandingscyclus en daarmee het verbruik van fossiele brandstoffen en de bijbehorende uitstoot te verminderen, zal leiden tot het bereiken van de ACARE doelen. Bovendien hebben voor een gegeven verbrandingstechniek de hoge OPR en TIT een negatieve invloed op de NOx-uitstoot. Met betrekking hiertoe biedt een nieuwe multi-brandstof, hybride motor voor een multi-brandstof Blended Wing Body (BWB) vliegtuig, bedacht binnen het "Advanced Hybrid Engine for Aircraft Development (AHEAD)" project, veelbelovende perspectieven.

De multi-brandstof hybride motor is een turbofan motor met de volgende extra componenten: een systeem van contra-roterende fans (CRF), twee opeenvolgende verbrandingskamers die verschillende brandstoffen tegelijk verbranden en een Cryogeen Bleed-Air koel systeem (CBACS). De CRF kan de non-uniforme instroming ten gevolge van de grenslaag van de romp weerstaan. De eerste verbrandingskamer, waar vloeibare waterstof (LH2) of vloeibaar aardgas (LNG) wordt verbrand om de $CO_2$-uitstoot te verminderen, is de belangrijkste verbrandingskamer. De tweede verbrandingskamer, de Interstage Turbine Burner (ITB), bevindt zich tussen de hogedruk- en lagedrukturbine en verbrandt kerosine of biobrandstof in een vlamloze verbrandingsmodus (FC). Met de thermische energie die aan de verschillende brandstoffen wordt onttrokken is het benodigde volume om cryogene brandstoffen op te slaan kleiner. Daarnaast is de FC techniek gunstig voor het verminderen van de NOx-uitstoot. Door de invoering van CBACS wordt LH2 of LNG gebruikt als koelmiddel om de bleed-air af te koelen.

Volgens de classificatie van brandstofcombinaties wordt de hybride motor geclassificeerd als LNG-kerosine en LH2-kerosine versie, waarbij kerosine zou kunnen worden vervangen door biobrandstoffen. Door het

definiëren van een "ITB energie fractie" als de verhouding van de energietoevoer van de ITB tot het totale vereiste energie, worden de brandstof-stroomsnelheden van twee verbrandingskamers gecontroleerd. Door middel van een grondig analyse-instrument, zijn de eigenschappen van de hybride motor bestudeerd en samengevat in de volgende drie aspecten:

**Potentieel van de ITB motorcyclus**

De sequentiële verbrandingsconfiguratie van de hybride motor vormt een her-verwarmingscyclus. Door het verspreiden van de energie in twee verbrandingskamers neemt de warmtetoevoeging van elke verbrandingskamers af, waardoor de TIT lager is. Zodoende nemen de benodigde hoeveelheid koellucht en het daarmee gepaard gaande verlies in turbine efficiëntie af. Bovendien zal de stroomopwaarts geproduceerde NOx opnieuw dissociëren in de ITB, waardoor de totale NOx-uitstoot afneemt. Deze opmerkelijke eigenschappen zijn opmerkelijk wanneer de OPR en BPR continu toenemen, wat een aanzienlijke verhoging van de TIT in een klassieke motor veroorzaakt. Een turbine met een zeer hoge inlaattemperatuur moet aanzienlijk afgekoeld worden. Uiteindelijk zou de winst in efficiëntie van de cyclus tenietgedaan worden door het verlies in turbine-efficiëntie. Bovendien vertoont de uitstoot van NOx een exponentiële groei wanneer de TIT hoger is dan 1800 K. Dientengevolge zou de her-verwarminscyclus een optie kunnen zijn voor de volgende stap in de evolutie van motortechnologie.

**Kenmerken van de multi-brandstof hybride motor**

De eigenschappen van hybride motoren zijn onderzocht vanuit verschillende perspectieven. De isobare warmtecapaciteit van de verbrandingsproducten van LNG en LH2 zijn hoger, wat gunstig is voor de thermische efficiëntie. Het gebruik van LNG en LH2 als koelmiddel verlaagt de bleed-air temperatuur aanzienlijk (ten hoogste met meer dan 500 K), waardoor het massadebiet van de koellucht van de turbine met de helft afneemt. Daarnaast is de stijging van de verbrandingstemperatuur gunstig voor de thermische efficiëntie. De hybride motor is geoptimaliseerd voor kruiscondities met inachtneming van verschillende ITB energiefracties. De geoptimaliseerde motorcyclus is geverifieerd op kritieke werkpunten. De beoordeling van de prestaties van de losstaande motor ten opzichte van referentiemotoren toont aan dat de LH2-kerosine hybride motor superieur is ten opzicht van de LNG-kerosine hybride motor met betrekking tot de cyclusefficiëntie en de $CO_2$-reductie. Echter, de missieanalyse blijkt tegenstrijdige resultaten te geven. Als gevolg van de sterkere invloed van het installeren van dit type motor scoort de multi-brandstof BWB samen

met het LH2-kerosine hybride motor lager, hetgeen impliceert dat de LNG-kerosine BWB de minste impact op het klimaat zou hebben.

**Operationele strategie van de multi-brandstof hybride motor**

De operationele strategie van het hybride verbrandingssysteem is ontwikkeld om de prestaties van de hybride motor in stabiele toestand te verbeteren. De analyse toont dat het gebruik van een ITB een gunstige uitwerking heeft op de snelheid van de hogedrukspoel, de HPC uitlaattemperatuur en de HPT inlaattemperatuur. Echter, de LPC surge marge en LOT inlaattemperatuur hebben conflicterende limieten als de ITB energiefractie toeneemt. Voor de verschillende stuwkrachteisen onder Sea Level Static (SLS) ISA-condities is een brandstofcontroleschema, samen met een schema voor de variabele ontluchter, voorgesteld. Daarnaast is een andere brandstofregelstrategie voorgesteld voor de flat rating bij SLS.

# Contents

# Nomenclature

### *Abbreviation*

| | | | |
|---|---|---|---|
| ACARE | = | Advisory Council for Aeronautics Reasearch in Europe | |
| AHEAD | = | Advanced Hybrid Engine for Aircraft Development | |
| ATAG | = | Air Transport Action Group | |
| BLI | = | Boundray Layer Ingestion | |
| BPR | = | Bypass Ratio | |
| BWB | = | Blended Wing Body | |
| CBACS | = | Cryogenic Bleed Air Cooling System | |
| CHEX | = | Cryogenic Heat Exchanger | |
| CRF | = | Coutra Rotating Fans | |
| CryoCombustor | = | Cryogenic fuel Combustion Chamber | |
| CTL | = | Coal to Liquid | |
| EINOx | = | NOx Emissions Index | $[g/kN]/[g/kg]$ |
| FPR | = | Fan Pressure Ratio | |
| GITB | = | Geared Interstage Turbine Burner | |
| GSP | = | Gas turbine Simulation Program | |
| GTF | = | Geared TurboFan | |
| GTL | = | Gas to Liquid | |
| HEX | = | Heat EXchanger | |
| HPC | = | High Pressure Compressor | |
| HPT | = | High Pressure Turbine | |
| ICAO | = | International Civil Aviation Organization | |
| IRA | = | Intercooled Recuperated Aero-engine | |
| ISA | = | International Standard Atmosphere | |
| ITB | = | Interstage Turbine Burner | |

| | | | |
|---|---|---|---|
| LDI | = | Lean Direct Ingestion | |
| LH2 | = | Liquid Hydrogen | |
| LHV | = | Lower Heating Value | $[J/kg]$ |
| LNG | = | Liquid Natural Gas | |
| LPC | = | Low Pressure Compressor | |
| LPT | = | Low Pressure Turbine | |
| LTO | = | Landing Take-Off | |
| MFBWB | = | Multi-Fuel Blended Wing Body | |
| OL | = | Operating Line | |
| OPR | = | Overall Pressure Ratio | |
| RR | = | Ram Recovery | |
| SL | = | Surge Line | |
| SLS | = | Sea Level Static | |
| SM | = | Surge Margin | |
| ST | = | Specific Thrust | $[N \cdot s/kg]$ |
| TO | = | Take-Off | |
| TIT | = | Turbine Inlet Temperature | [K] |
| TSFC | = | Thrust Specific Fuel Consumption | $[g/kN \cdot s]$ |
| UHBR | = | Ultra High Bypass Ratio | |
| UHC | = | Unburnt Hydro Carbon | |
| VBV | = | Variable Bleed Valve | |
| VHBR | = | Very High Bypass Ratio | |
| VSV | = | Variable Stator Vane | |

***Greek symbol***

| | | |
|---|---|---|
| $\eta$ | = | efficiency |
| $\pi$ | = | pressure ratio |
| $\xi$ | = | turbine cooling air fraction |
| $\kappa$ | = | gas constant |
| $\varepsilon$ | | heat exchanger effectiveness |

| | | | |
|---|---|---|---|
| $\Delta$ | | variation | |

## *Symbol*

| | | | |
|---|---|---|---|
| $c_p$ | = | constant pressure specific heat | $[J/kg \cdot K]$ |
| cryo | = | cryogenic | |
| D | = | diameter | $[m]$ |
| FN | = | net thrust | $[kN]$ |
| $\dot{m}$ | = | mass flow rate | $[kg/s]$ |
| N1 | = | low pressure spool speed | $[rpm]$ |
| N2 | = | high pressure spool speed | $[rpm]$ |
| $p$ | = | pressure | $[Bar]$ |
| $Q$ | = | heat | $[J]$ |
| $S$ | = | entropy | $[J/kg \cdot K]$ |
| $T$ | = | Temperature | $[K]$ |
| $V$ | = | Velocity | $[m/s]$ |
| $W_c$ | = | compressor power | $[W]$ |
| $W_t$ | = | turbine power | $[W]$ |

## *Subscript*

| | | |
|---|---|---|
| 0 | = | free stream |
| 18 | = | bypass nozzle exit |
| 2 | = | low pressure compressor inlet |
| 25 | = | high pressure compressor inlet |
| 3 | = | high pressure compressor exit |
| 31 | = | combustion chamber inlet |
| 4 | = | high pressure turbine inlet |
| 45 | = | high pressure turbine exit |
| 46 | = | low pressure turbine exit |
| 8 | = | core nozzle exit |

| | | |
|---|---|---|
| $f_1$ | = | fuel of the first combustion chamber |
| $f_2$ | = | fuel of the second combustion chamber |
| $itb$ | = | inter-stage Turbine Burner |
| $mainCC$ | = | main combustion chamber |
| $j$ | = | jet |
| $t$ | = | stagnation condition |
| $th$ | = | thermal |
| $tot$ | = | total |
| $prop$ | = | propulsive |

# List of Figures

# List of Tables

# Chapter 1 Introduction

As the world population continuously expands and the urbanization becomes more rapid in many developing countries, a rapid growth in civil aviation is to be expected. The growth in aviation on one hand implies more fuel to be required, on the other hand, aggravates the climate impact of the air transportation. Therefore, the imperatives for the future commercial aviation would be to develop more fuel efficient and more sustainable civil aviation.

## 1.1 Air-traffic growth and challenges in aviation

Over the last decades, the aviation industry has undergone significant expansion along with the strong growth of the world economy. According to the report from the Air Transport Action Group (ATAG) [1], the number of passengers has more than doubled since the mid-1980s, whereas, the freight traffic has increased by almost three times on a tonne-kilometre performed basis. The jet-powered aircraft has proven itself as an essential way of traveling. The efficiency of moving people and goods has enabled it to be integrated successfully into the modern society. As the world population increases, and the urbanization becomes more rapid in many developing countries, air traffic is likely to grow further. The aircraft manufacturers have predicted that the world civil aircraft fleet would more than double by 2031[2]. This scenario draws attentions on climate effects of aviation.

In 1999, the Intergovernmental Panel on Climate Change (IPCC) published a report under the title of "*Aviation and the global atmosphere*". It was the first time the IPCC reported an assessment of climate effects for a specific industrial subsector [3]. Lee et al. have also discussed the aviation and global climate change in the literature [4, 5]. Aircraft emit gasses such as carbon dioxide ($CO_2$), nitrogen oxide (NOx), water vapor ($H_2O$), and particles (soot). Scientific understanding tells that these emissions can directly or indirectly alter the concentrations of greenhouse gasses in the atmosphere, including carbon dioxide ($CO_2$), ozone ($O_3$), and methane ($CH_4$). Furthermore, water vapor can form condensation trails (contrails), and might also produce extra cirrus clouds. The synthetic consequence of these variances ultimately influences the radiation balance of the earth, aggravating global warming. Although aviation only shares a little portion of all the pollutants formed due to anthropogenic activities, as the air traffic grows further the emissions from aviation can no longer be ignored.

To reduce the climate impact of aviation, the Advisory Council for Aeronautics Research in Europe (ACARE) has set ambitious objectives for the year 2050 with an aim to reduce $CO_2$ emission by 75%, NOx by 90% and noise by 65% in reference to an engine operating in year 2000 [6]. Moreover, emission standards set by International Civil Aviation Organization (ICAO) for engine certifications are also becoming stricter. As a result, a sustainable air transport system is highly required.

## 1.2 Development of sustainable aviation

According to the previous discussions, one of the imperatives for the future commercial aviation would be reducing its climate impact, namely, reducing the aircraft emissions. Different emission species are subject to distinguished factors. For instance, carbon dioxide ($CO_2$) is a product of combusting hydrocarbon fuels. Therefore, an efficient aircraft-engine integration system having lower fuel consumption is beneficial to reduce $CO_2$ emission. Moreover, the application of fuels containing less or no carbon also contributes to lower $CO_2$ emission. The NOx emissions are formed under rather complicated circumstances and are dependent on miscellaneous factors, e.g. the engine cycle parameters, the chemical reaction mechanism, the combustion technique, etc. Since each of the factors is coupled, the evaluation in NOx emission is never a straightforward task.

Development of civil aviation tends to follow the path of continuously making the aircraft more fuel-efficient and less noisy. Over the past 40 years, aircraft have been 20 decibels quieter [7] mainly due to the reduction in jet noise[8]. The fuel efficiency has been improved by 70%, among which the majority (40%) has been due to the engine technology advancement and the remaining (30%) has been realized by the advancement in aircraft aerodynamics, aviation structures, lightweight material, passenger density, etc. This can be observed from Figure 1.1. Therefore, an efficient engine would be highly appreciated.

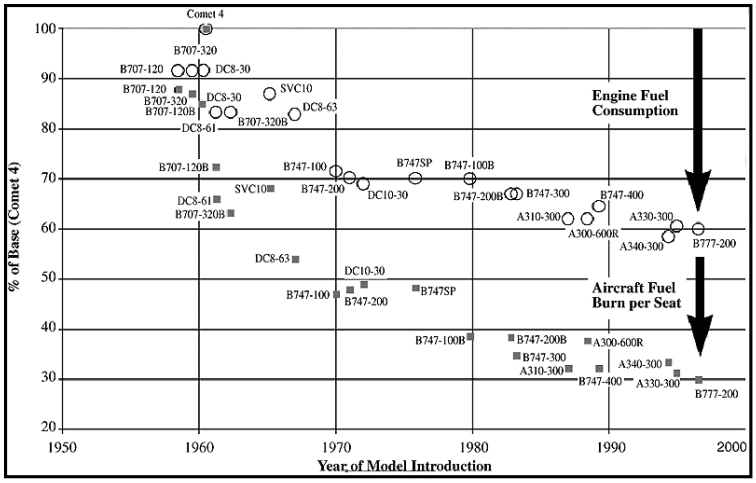


*Figure 1.1: Fuel efficiency of the air transportation (Figure source: http://www.grida.no/publications/other/ipcc_sr/?src=/climate/ipcc/aviation/avf9-3.htm )*

Historically, efficient propulsion has been realized by improving the engine efficiency. This is achieved by the continuous increase in the component efficiencies,

the engine pressure ratio, the maximum operating temperature, and the bypass ratio as far as a turbofan engine is concerned. However, while increase the operating pressure and maximum temperature for achieving thermal efficiency benefits, it has been observed that the NOx emissions would increase due to high temperature. The trade-off between engine efficiency, hence low $CO_2$ emission, and low NOx emissions make the future engine and airframe design process increasingly complex. Moreover, higher bypass ratio to improve the propulsive efficiency results in bigger fan diameter and higher speed mismatch between the fan and other low pressure components. This leads to heavier engines, which can offset the fuel consumption gain of higher propulsive efficiency. The traditional approach in reducing the fuel consumption is challenged by its negative environmental impact. The incidental effects on $CO_2$ emission reduction are hence also restricted. Alternative solutions attract increasingly public attentions.

## 1.3 Research objective and scope

Considering all the factors discussed above, a project named Advanced Hybrid Engine for Aircraft Development (AHEAD) was co-funded by the European Commission with an aim to improve the sustainability of aviation [9]. The hybrid engine proposed in AHEAD is a novel propulsion system with a distinct architecture compared to a conventional turbofan engine. During the conceptual investigation phase, there are many questions to be answered before it becomes mature. The main objective of this thesis can be summarized as follows.

- Developing a model framework for the feasibility analysis of the hybrid engine.
- Identifying the design parameters of the hybrid engine to form a proper design space.
- Optimizing the hybrid engine cycle.
- Evaluating the performance of the hybrid engine.
- Analyzing the off-design performance of the hybrid engine cycle to develop fuel control strategies making use of the operating flexibility of the dual combustor system.

Following the above thoughts, the overall contents of this thesis are constructed as the following.

Chapter 2 discusses the improvements in aircraft engines. Development of the state-of-art regarding engine architectures and cycles is presented. Three innovative engine concepts are highlighted: the geared turbofan, the open rotor, and the intercooler and recuperated aero engine concept. Additionally, the reheat cycle which has a potential to mitigate the environmental impact of aviation is described.

Chapter 3 introduces initiatives of the multi-fuel hybrid engine concept. Firstly, a Multi-Fuel Blended Wing Body (MFBWB) is elaborated on. Afterward, the fundamental requirements of the MFBWB propulsion system are discussed. Accordingly, a multi-fuel hybrid engine concept is conceived. The multi-fuel hybrid engine is a classical turbofan engine with several additional components: 1) a contra-rotating fans system; 2) a multi-fuel sequential combustion system, of which the second combustor is an Interstage Turbine Burner (ITB). 3) A Cryogenic Bleed Air Cooling System (CBACS).

Chapter 4 describes the model framework comprehensively. The entire model consists of four modules: 1) an engine performance module; 2) a CBACS module; 3) an emission prediction module; 4) an optimizer module. The engine performance module is developed using Gas turbine Simulation Programme (GSP). To improve the quanlity of predicting the engine performance, an in-house turbine cooling module is implemented. The core element of the CBASC is a Cryogenic Heat Exchanger (CHEX), with which the effects of using cooled bleed air on the turbine cooling requirement can be assessed. The in-house emission prediction module has been developed for a conventional RQL combustion technique and the hybrid combustion system separately. For the conventional combustion, a multi-reactor network has been created using Cantera's reactor networks. Depending on the structure of the network, the fuel surrogates, and the input parameters, the exhaust gas compositions can be predicted. Whilst, the emission prediction tool for the hybrid combustion system has been specially developed by the research group in TUDelft within the AHEAD framework. Chemkin® has been selected for modeling. The optimizer is constructed using MATLAB® optimization tool. The modules developed in this chapter can be flexibly activated to execute different tasks.

The analysis in chapter 5 is focused on the potential of the reheat cycle as the next step in the evolution of civil aircraft engines. The engine performance module, the emission prediction module and the optimizer in chapter 4 are implemented. An ITB turbofan having very high BPR, OPR, and TIT is created. To realize the very high BPR, a geared driven fan system will have to be applied. Fuels injected into two combustors are kerosene. Parametric analysis is firstly performed within a full range of the cycle design parameters. Accordingly, a proper design space can be defined to optimize the ITB engine cycle at cruise condition. The energy added to the ITB is controlled and indicated by various ITB energy fractions. Finally, the performance and the NOx emissions of the reheat cycle are assessed on an imaginary baseline Geared Turbofan engine optimized at the same state-of-art technology level.

The characteristics of the multi-fuel hybrid engine are analyzed in chapter 6. Based on the engines studied in chapter 5, replacing the kerosene in the first combustor by LNG or LH2, two hybrid engine models, i.e. an LNG-kerosene hybrid engine and an LH2-kerosene hybrid engine, are formed. Firstly, parametric analysis has been performed to understand the effects of the alternative fuels and the CBACS on the engine performance. Furthermore, the hybrid engine is optimized at cruise

and verified at different critical operating points. Various ITB energy fractions are considered. The standalone engine performance and emissions (mainly $CO_2$ and $H_2O$) are evaluated on three baseline engines representing the evolution of engine technologies. Furthermore, a mission analysis is performed to assess the installed performance of the hybrid engine.

Chapter 7 is devoted to exploring the operating strategy for the hybrid engine. The first part of this chapter is to develop a fuel control schedule at the SLS ISA condition on various thrust requirements. To protect the LPC surge margin from violating its limit, a Variable Bleed Valve (VBV) schedule is also suggested at lower thrust setting. In the second part, the flat rating at SLS is performed for the hybrid engine. Accordingly, a different fuel control schedule is proposed.

Eventually, the conclusions are drawn, and recommendations are presented in Chapter 8.

# Chapter 2 Evolution of aero-engine technology

The history of gas turbines can date back to the beginning of 20th century when a British engineer, Sir Frank Whittle and a German scientist, Hans von Ohain, independently developed a gas turbine for aircraft propulsion. Also, in the same period, the first gas turbine for power generation was operational in 1939 in Neufchateau, Switzerland. Ever since the exploration of gas turbine designs in the different parts of the world has never stopped.

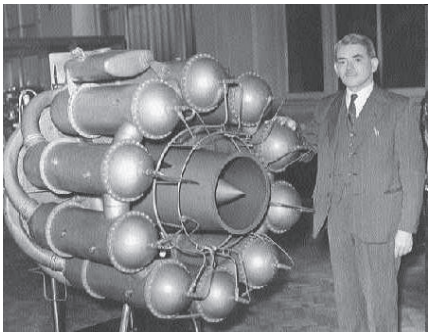

**This is where and how it all started!**

*Figure 2.1: Sir Frank Whittle and his engine (Source: http://www.solarnavigator.net/inventors/frank_whittle.htm, 24 March 2015)*

The aspiration to make engines stronger, lighter and more efficient has occupied scientists and engineers for decades [10]. Since the world's first jet engine was tested successfully, the aircraft propulsion has undergone the great evolution from the simple turbojet engine followed by the low bypass turbofan engine to the high bypass turbofan engine until the current very high bypass engine. The improvements in aircraft engine technologies have contributed significantly to the overall fuel burn reduction of the fleet [11]. Many of the design and manufacturing process innovations are responsible for this tremendous progress.

There are three categories of parameters often considered as criterions to evaluate the improvement of engine technologies. The first group includes engine design parameters: BPR, OPR, and TIT. Limits of these parameters define the design space of an engine. The second category is cycle dependent parameters, i.e. the thermal efficiency, the propulsive efficiency, and the overall efficiency. These parameters exhibit the quality of a given cycle. Furthermore, there are also constraints, which are boundaries of each engine operating condition. These constraints are due to thermal limits, mechanical limits, and emission limits. This chapter attempts to provide an overview of the technology improvement associated with various parameter categories.

## 2.1 Gas turbine engine cycle

The fundamental working principle of a gas turbine is to convert chemical power into mechanical power through a Joule-Brayton cycle. The working process can be described by a T-S diagram as can be seen in Figure 2.2. The air is firstly compressed by a compressor (C) to increase its pressure. Then the pressurized air enters into a combustion chamber (B) where the chemical power is added in the form of fuels. Ultimately, the hot gas is expanded by a turbine (T) to convert the chemical energy into the mechanical power. The solid line represents an ideal working process, whereas, the dashed line represents a real working process. Analysis of both processes can be found in texts on gas turbine theory [12].

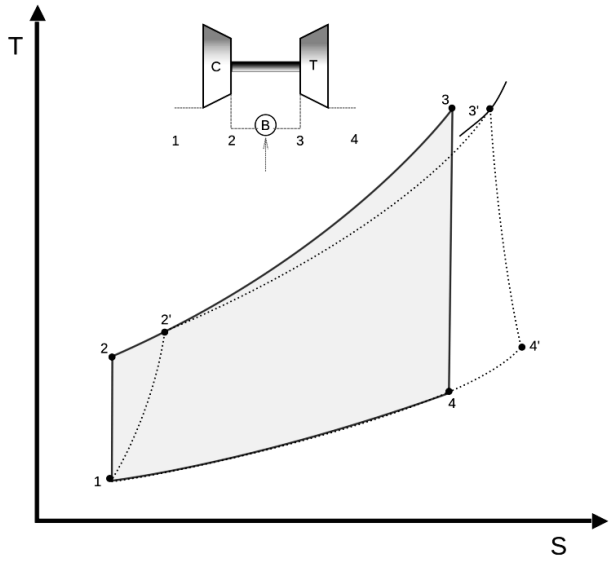


*Figure 2.2: T-S diagram of a Joule-Brayton cycle.*

The performance of the real working process differs from that of an ideal process for various reasons.

1) The compression and expansion processes are not adiabatic and reversible, hence leading to an increase in entropy.
2) The fluid friction and heat addition cause pressure losses in the combustion chamber, ducts, and heat exchanger if applicable.
3) Incomplete combustion results in a loss.
4) The exhaust gas at high temperature leads to heat loss
5) The exhaust gas having high velocity contains residual kinetic energy in the jet wake.

These various losses occurring in different processes are visualized using a Sankey Diagram in Figure 2.3. If deducting different forms of losses described above, only a minor portion of the total chemical power (approximately 40% in a modern civil aircraft engine) is converted into the mechanical power. To assess the performance of a real gas turbine cycle, different efficiencies are introduced.

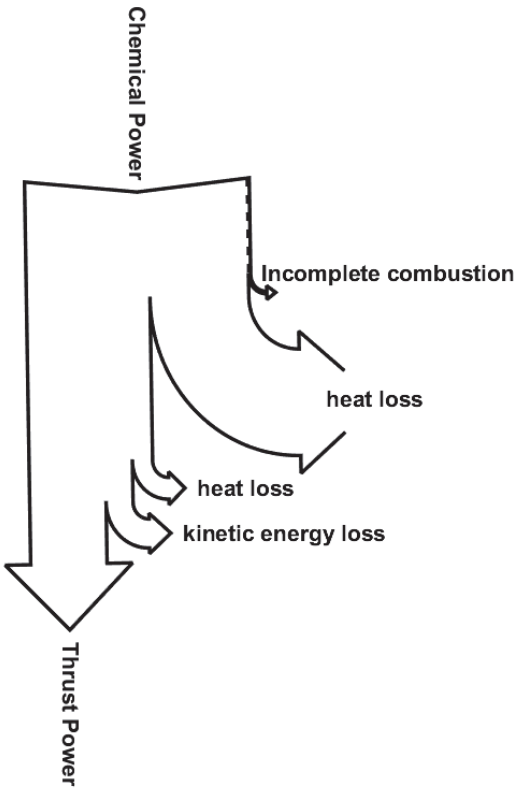


*Figure 2.3: Sankey diagram of jet engine power*

## 2.2 Performance evaluation criterion

The focus on developing commercial aircraft engines has changed from the question of whether it can safely fly an aircraft to whether it can economically and sustainably fly an aircraft. The objective of making an engine more fuel efficient and more environmental friendly becomes increasingly desirable. The engine fuel consumption is associated to three criterions, the thermal efficiency, the propulsive efficiency, and the total efficiency (a product of the thermal efficiency and the propulsive efficiency).

### 2.2.1 Thermal Efficiency

Thermal efficiency, symbolized by $\eta_{th}$, measures how efficiently the chemical energy can be converted to the mechanical power. In a gas turbine cycle, the chemical energy is supplied by the total quantity of fuel injected, whereas, the mechanical power output is the remaining power produced from the turbine by subtracting the amount of the power required by the compressor. It also refers to the amount of the kinetic energy available. This efficiency can be quantified by definition in Eqn. (1);

$$\eta_{th} = \frac{Kenetic\ energy}{Thermal\ energy\ input} = \frac{W_t - W_c}{\dot{m}_f \times LHV_f} = \frac{\Sigma\left\{{}^1/_2 \cdot \dot{m}_a \cdot \left(V_j^2 - V_0^2\right)\right\}}{\dot{m}_f \times LHV_f} \tag{1}$$

where $W_t$ and $W_c$ are the turbine work output and compressor work requirement respectively; $\dot{m}_f$ and $\dot{m}_a$ are the fuel flow rate and the air mass flow rate; $LHV$ is the Lower Heating Value of a given fuel; $V_j$ and $V_0$ are the jet velocity and the free stream velocity.

Research has been done to analyze the reasons responsible for the thermodynamic losses that are present in an aircraft gas turbine cycle [13, 14]. They are summarized from several sources: the component losses, the irreversible combustion process, and the exhaust heat loss. The latter two are the inherent features of the cycle itself; therefore, they cannot be eliminated. However, they can be minimized by varying relevant design variables, for example, the engine pressure ratio, the turbine inlet temperature, etc.

### 2.2.2 Propulsive Efficiency

The thermal efficiency alone cannot represent the performance of an aero engine. Ultimately, the kinetic energy has to be converted into the thrust power. The propulsive efficiency quantifies losses occurred during this process. The propulsive efficiency $\eta_{prop}$ is defined as the ratio of the thrust power to the total kinetic energy [12], represented by Eqn.(2),

$$\eta_{prop} = \frac{Thrust\ power}{Kinetic\ energy} = \frac{FN \cdot V_0}{\Sigma\left\{{}^1/_2 \cdot \dot{m} \cdot \left(V_j^2 - V_0^2\right)\right\}} = \frac{\Sigma\{\dot{m} \cdot (V_j - V_0)\} \cdot V_0}{\Sigma\left\{{}^1/_2 \cdot \dot{m} \cdot \left(V_j^2 - V_0^2\right)\right\}} \tag{2}$$

where the $FN$ is the net thrust of an engine; the notation of sum is valid when the objective is an unmixed turbofan.

To completely convert the kinetic energy into the thrust power, the jet velocity has to be equal to the free stream velocity, which gives the propulsive efficiency of 1. However under this circumstance, there would be no thrust at all. Hence, it is unavoidable to have the residual kinetic energy in the jet wake. Any effort of

improving the propulsive efficiency is to reduce the residual kinetic energy. The engine Fan Pressure Ratio (FPR) and BPR are parameters directly affecting the residual kinetic energy.

### 2.2.3 Overall efficiency

As one can see that neither the thermal efficiency nor the propulsive efficiency individually can fully represent the performance of a given cycle; therefore, an overall efficiency $\eta_{tot}$ as a product of the two efficiencies has been introduced. By multiplying the thermal efficiency and propulsive efficiency, the expression of the overall efficiency can be conveniently obtained. Since the numerator of the thermal efficiency is cancelled out by the denominator of the propulsive efficiency, eventually the overall efficiency becomes a ratio of the thrust power to the total thermal energy consumed, shown in the Eqn. (3),

$$\eta_{tot} = \frac{FN \times V_0}{\dot{m}_f \times LHV_f} = \eta_{th} \times \eta_{prop} \tag{3}$$

Apart from the efficiencies mentioned above, the Thrust Specific Fuel Consumption (TSFC) is also a factor to evaluate the performance of a given cycle. The definition is given in the Eqn. (4),

$$TSFC = \frac{\dot{m}_f}{FN} \tag{4}$$

If the Eqn. (4) is introduced, the Eqn. (3) can be reformulated to the Eqn. (5),

$$\eta_{tot} = \frac{V_0}{TSFC \times LHV_f} \tag{5}$$

With the given fuel and flight speed, the TSFC is inversely proportional to the total efficiency. Therefore, the overall efficiency can explicitly indicate the fuel efficiency of a given system. Improving the overall efficiency is beneficial in reducing the engine specific fuel consumption.

The engine thermal efficiency, propulsive efficiency, and overall efficiency are depending on various engine cycle parameters. Therefore, improving the engine efficiency essentially means varying the associated design variables to achieve minimum fuel consumption.

## 2.3 Cycle design parameters

Cycle design parameters formulate a design space, within which the engine cycle is optimized. Depending on the architecture of the engine, the selection of design

parameters differs accordingly. As far as a commercial turbofan engine is concerned, it is common practice to use the BPR, the TIT, and the OPR as design parameters.

### 2.3.1 Bypass Ratio

The BPR defines the ratio of the air mass flow rate through the engine bypass to that of the core. In the turbofan engine, the thrust is produced by propelling a large amount of the inlet air through the bypass at a lower velocity. The aim of such engine configurations is to improve the propulsive efficiency hence reducing the TSFC. Moreover, the jet noise decreases substantially because of the lower jet velocity. From Figure 2.4, one can observe that the BPR has increased substantially from 4 at the early 1970s until very recently close to 10. Moreover, with the very recent Geared Turbofan by Pratt & Whitney [15], the BPR can even reach 12.

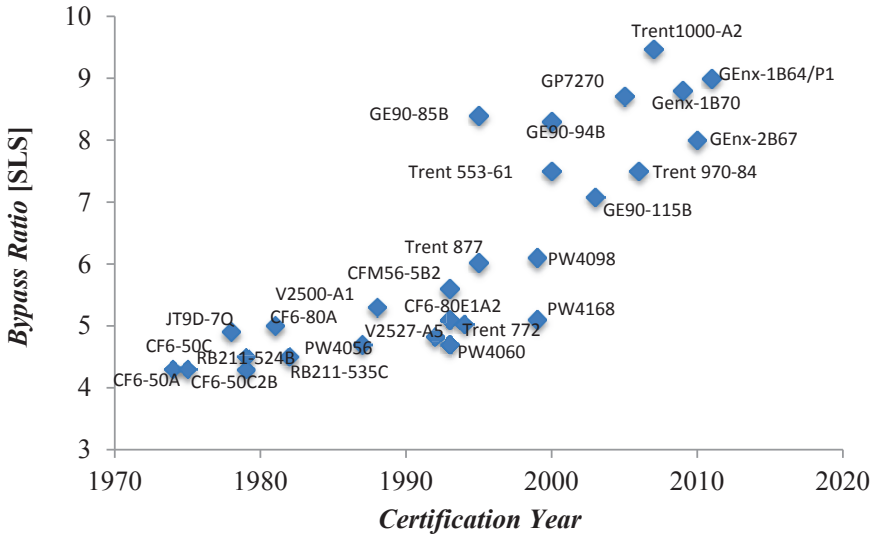


*Figure 2.4: Improvement of the engine bypass ratio.*

As the BPR constantly increases, the drawbacks become more prominent. Increasing the BPR not only increases the engine size and the associated drag but also slows down the rotational speed of the Low Pressure (LP) spool. Consequently, the Low Pressure Turbine (LPT) coupled on the LP shaft rotates slower as well, leading to an increase in the number of LPT stages for a given power output, thus increasing the engine weight.

### 2.3.2 Overall Pressure Ratio

The OPR is the ratio of the stagnation pressure at the exit of the High Pressure Compressor (HPC) to that at the inlet of the fan. The thermal efficiency of an engine cycle is proportional to the OPR. In Figure 2.5, it can be observed that the OPR of commercial turbofans has been more than doubled over decades. The OPR of recent engines has reached 45 even towards to 50 and above. According to the latest engine technology, it is very likely that the OPR will reach 60 shortly.

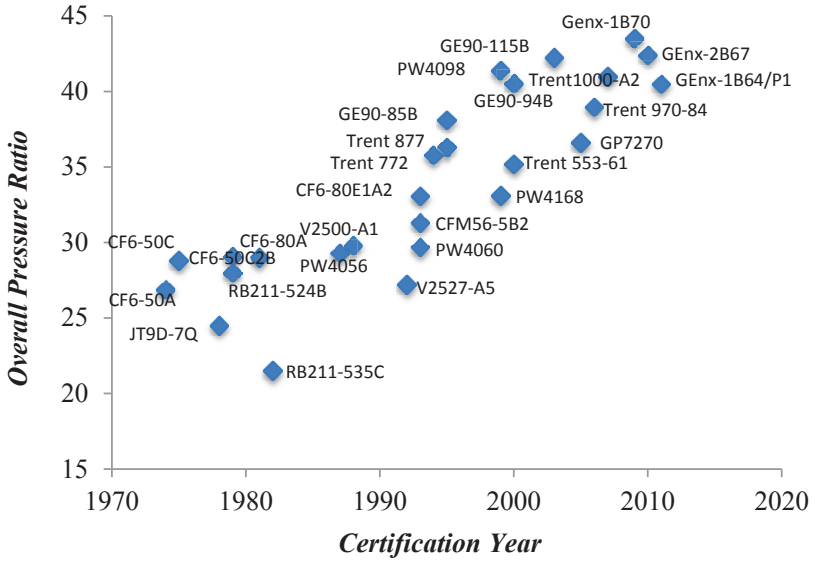


*Figure 2.5: Improvement in the overall pressure ratio*

Although a higher OPR is beneficial to increase the thermal efficiency, the compressor exit temperature and pressure are higher as well. On one hand, with the hotter air, the amount of air bled off for turbine cooling becomes higher, which penalizes the thermal efficiency. On the other hand, a large amount of research conducted by combustion engineers has proved that the NOx emission is proportional to the compressor exit pressure and temperature [16, 17]. Therefore, the high OPR tends to increase the NOx emission unless if an advanced combustion technique is used. A statistics of historical NOx emission measured data from ICAO is presented in Figure 2.6. In this figure, all the sample engines are classified according to their in-service periods. The tendency of increasing the NOx emission against the OPR is explicitly illustrated. A step change mainly due to the improvement in the combustion technology from one period to another is also observed. Moreover, at the bottom of the figure, a solid line is drawn to represent the expected NOx emission for the year 2050 proposed by ACARE. Following the current technology development trend, it would be very unlikely to meet this

requirement. Breakthroughs have to be made either in combustion techniques or engine designs. Also, increasing the OPR leads to smaller blades at the last stage of the compressor, hence decreasing the compressor efficiency.

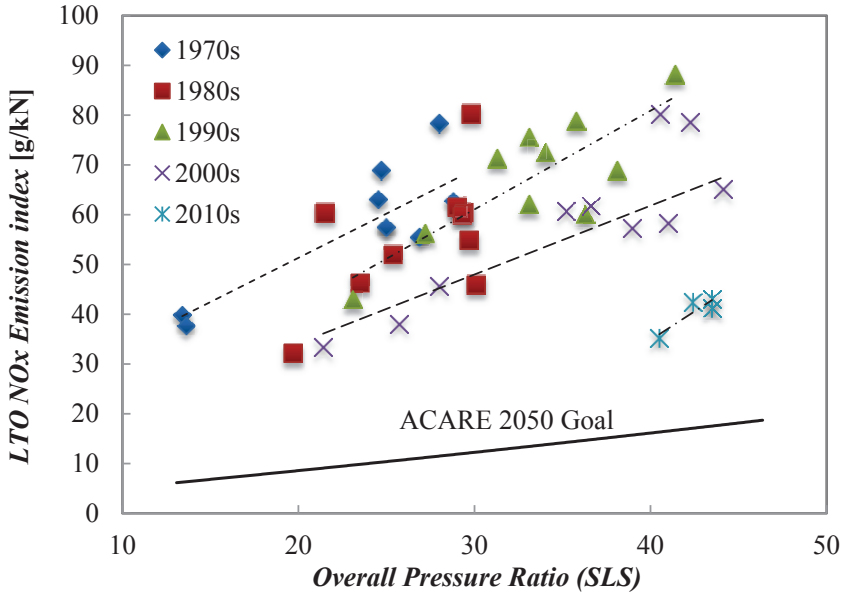


*Figure 2.6: LTO EINOx on the engine overall pressure ratio*

### 2.3.3 Turbine Inlet Temperature

The engine TIT increases correspondingly with the OPR but is confined by the material limits. Figure 2.7 shows the historical trend in the TIT and the development of turbine materials regarding the maximum allowable metal temperature. The average increase in the TIT has been approximately 18 °K/year, which is much more than that of the metal temperature (3 °K/year). Despite the practical restrictions proposed by the materials, the breakthroughs in manufacture processes enable the application of the sophisticated turbine cooling system. As a result, the TIT has increased significantly over periods. However, as the OPR and TIT continuously increase, a substantial amount of cooling air would be required. The improvement of the thermal efficiency realized in this perspective might be canceled out. Moreover, the NOx emission increases exponentially when the TIT is beyond 1800 K. As a result, the tendency of increasing the TIT tends to be flat.

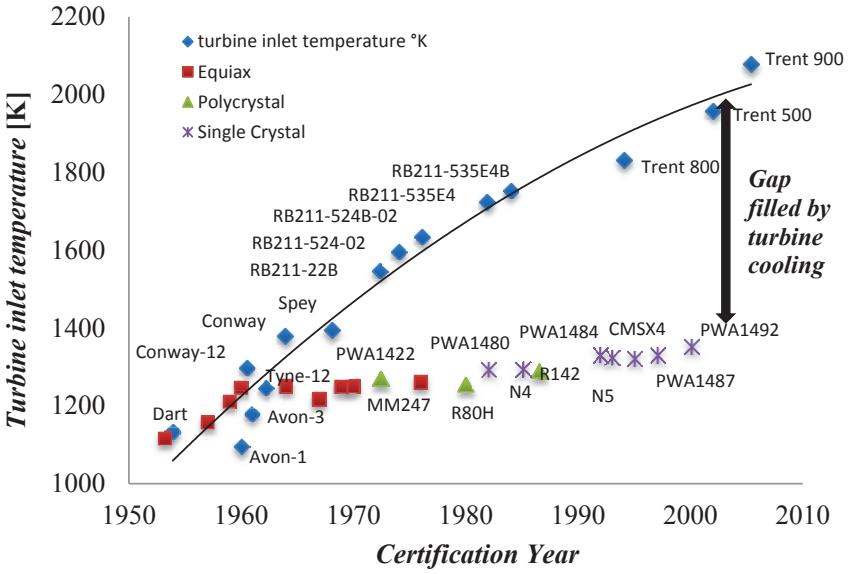


*Figure 2.7: Trend of turbine operating and metal temperature (Figure reproduced by data from Rolls-Royce: The jet engine).*

To summarize the preceding discussions, the thought of improving the engine efficiencies to reduce the TSFC has encountered its bottleneck. Figure 2.8 gives an overview of this perspective. Attention should be paid to the tendency of the parameter behavior rather than values indicated on the grids. One can see that the variations are restricted by several lines, which have been drawn beforehand. Taking the thermal efficiency as an example, the factors limiting the improvement in the thermal efficiency have become the NOx emission rather than the achievable OPR and TIT. Moreover, the propulsive efficiency can be improved through increasing the BPR, which makes the engine bigger and heavier, aggravating installation penalties. Hence, it is not practical to constantly enlarge the engine BPR. Accordingly, the engine propulsive efficiency is limited.

The classical approach to improving the economic efficiency of commercial aircraft is becoming less effective. The stringent reduction goals in aircraft emissions have introduced more challenges. Alternative solutions are advocated to satisfy the new requirements.

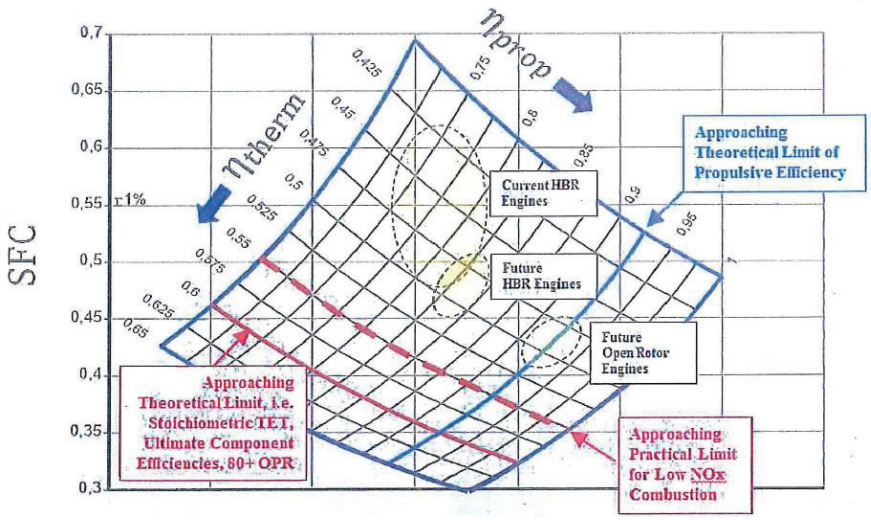


*Figure 2.8: Variation of the specific fuel consumption versus thermal and propulsive efficiency [18].*

## 2.4 Alternative solutions

The alternative solutions to further improve the cycle efficiency and to reduce the emissions can be considered from the following two aspects: innovations in engine architectures and alternative fuels.

### 2.4.1 Innovative engine configurations

Various innovative engine architectures have been conceived to overcome restrictions imposed by the conventional approach. Among all the candidates, four representative architectures are discussed here. They are the Geared Turbofan (GTF), the Open Rotor concept, the Intercooled and Recuperated Aero-engine (IRA), and the Interstage Turbine Burner (ITB) turbofan engine.

#### 2.4.1.1 The geared turbofan engine

To enable the further increase in the BPR, a geared driven fan concept has been conceived and investigated for about two decades. Conventionally, the fan is connected with other LP components via the identical shaft, hence rotating at the same speed. As the BPR increases, the fan diameter becomes bigger, and the corresponding fan tip speed is higher. Therefore, the fan tip noise increases. To meet the regulation rule in jet engine noise, the fan rotational speed has to decrease as the BPR increases, which restricts the LP spool speed.

The principle of using a geared driven fan system is to decouple the fan from the LP shaft such that each component rotates at its optimal speed. The following advantages can be realized:

- The BPR increases further, hence improving the propulsive efficiency.
- The fan can rotate even slower and is, therefore, less noisy.
- The LPC and LPT rotate faster, leading to the less number of the LPT stages and the associated maintenance cost, weight, etc.

Despite the above benefits, the propulsion system becomes more complex, which not only reduces the reliability of the system but also increases the maintenance cost. After a comprehensive analysis, the geared driven fan system has finally entered its certification stage. The schematic of the matured GTF engine is presented in Figure 2.9. It is stated that the geared turbofan can reduce the gate to gate fuel burn by around 16%, and slash the noise by up to 75% [19, 20]. The GTF concept is undoubtedly a step change to improve engine efficiencies, to reduce emissions and to minimize the fan noise.

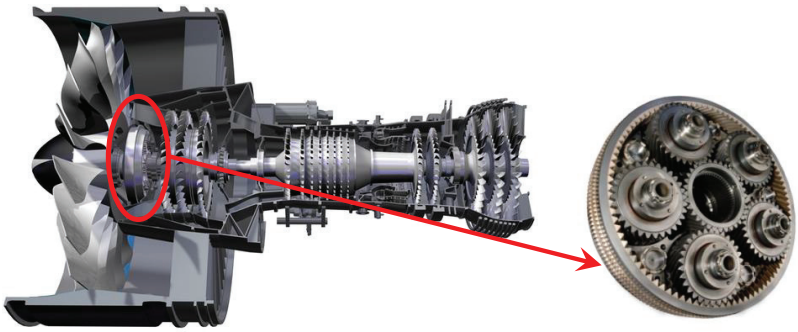

*Figure 2.9: Schematic of a geared turbofan concept (Source: http://theflyingengineer.com/flightdeck/pw1100g-gtf/, 22 Jan 2015).*

### 2.4.1.2 The open rotor engine

Interests in the open rotor concept date back to 1970s when the fuel price increased significantly [21]. The desire of having a more fuel efficient engine became increasingly strong. Therefore, the open rotor was considered. From Figure 2.10, one can see that at a relatively low flight speed, the turboprop engine is more efficient. However, its efficiency reduces sharply due to a more dominant shock loss at higher speed. Moreover, the propeller noise generated at high flight speed is also barely acceptable. This unfavorable feature together with the drop in the fuel price, later on, forced the early open rotor research to be shelved.

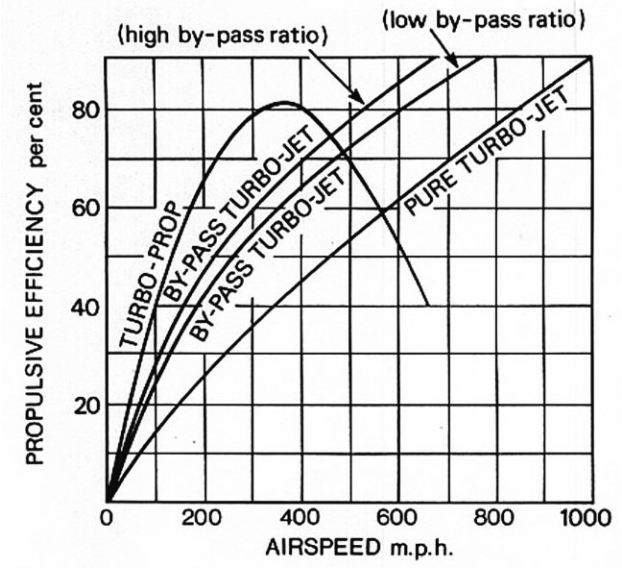


*Figure 2.10: Propulsive efficiency of various engines (Rolls-Royce, 1992).*

As the improvement in conventional turbofans tends to stagnate, and the environmental concern becomes increasingly critical, the open rotor draws attentions again [22]. With the development of aero-acoustic design technologies, the noise of open rotors is expected to be reduced to an accepted level. One of the open rotor layouts is depicted in Figure 2.11. The ongoing research on the open rotor has demonstrated positive achievements regarding the increase in flight speed and noise reduction [23, 24]. With the advanced technology, it wouldn't be too ambitious to hope that the open rotor to be the next step.

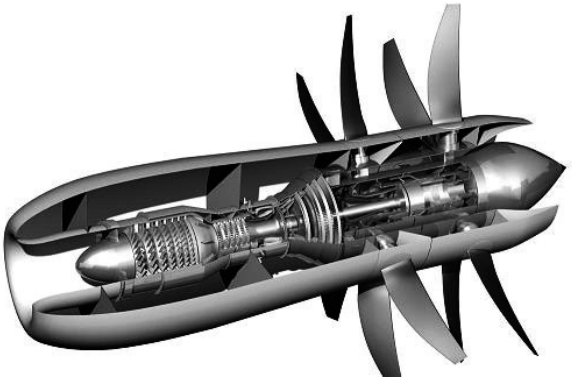

*Figure 2.11: Open rotor engine architecture (Source: http://www.theregister.co.uk/2009/06/12/nasa_open_rotor_trials/, 22nd Jan 2015).*

### 2.4.1.3 The Intercooler and Recuperated Aero-engine (IRA)

The GTF and open rotors mainly focus on the improvement in engine propulsive efficiency. The IRA engine concept aims to improve the thermal efficiency. Earlier research about this engine core concept has been performed by MTU Aero Engines [25], and later on in another large research project [26]. One of the proposed IRA concepts is depicted in Figure 2.12, where the schematic of the intercooler and the recuperator are pointed out respectively. The intercooler is a heat exchanger where the LPC exit flow is cooled by the bypass flow before entering the HPC. By doing this, the required HPC work to achieve a given pressure ratio reduces. However, since the air temperature exiting the HPC is lower, the fuel flow rate increases at a given TIT. Hence, the intercooler alone doesn't improve the thermal efficiency.

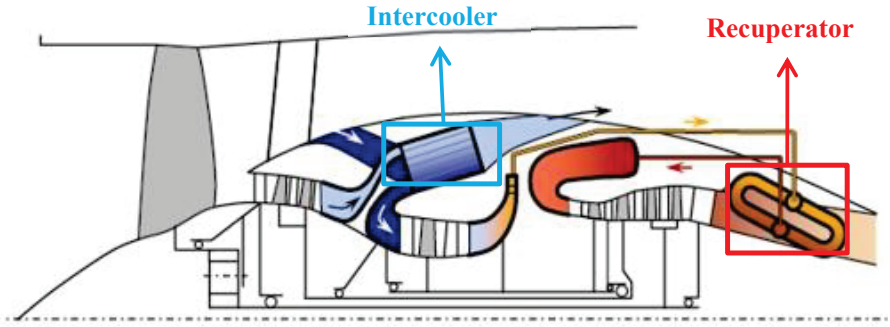


*Figure 2.12: Intercooled recuperated aero engine [27].*

Research in [28] has confirmed that one of the major losses in a gas turbine cycle is the exhaust heat loss. By using a recuperator, the exhaust heat from the turbine can be brought back to the combustion chamber. Therefore together with the intercooler, the IRA engine improves the thermal efficiency significantly. This entire principle can be understood from a typical IRA engine cycle shown in Figure 2.13. Due to the intercooler, the HPC inlet temperature reduces to the state 25 through the isobar. The actual HPC compression process happens from the state 25 to 3. One can clear see that for the identical pressure ratio; the latter process requires less work. On the other hand, because of the recuperator, the combustor inlet temperature increases from the state 3 to 31 on the isobars. Therefore, the fuel consumption decreases for a given TIT. Meanwhile, the turbine exit temperature reduces from the state 5 to state 7, which helps to reduce the exhaust heat loss. The innovative IRA engine core provides an opportunity to improve the engine fuel consumption and to reduce the emissions. The overall benefits realized by this engine core have been presented in [29]. The current development would be focused on the compact heat exchanger design.

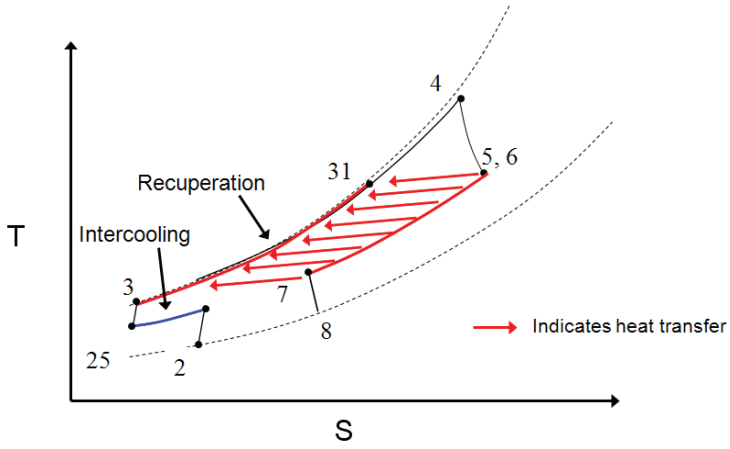


*Figure 2.13: A typical intercooler recuperated engine cycle in T-S diagram*

2.4.1.4 Interstage Turbine Burner engine

Interstage Turbine Burner (ITB) is located in the duct between the HPT and the LPT. It has been considered as a possible substitution for an afterburner engine. The afterburner works at the downstream of the LPT, where the flow pressure is low; therefore the thermal efficiency of the afterburner engine is poor. The ITB, on the other hand, operates under the relatively high pressure condition; therefore, the thermal efficiency is better than that of an afterburner engine. Furthermore, the Specific Thrust (ST) of the ITB engine is higher than that of a single combustor engine. In [30-32], the advantages of turbofans and turbojets with the ITB have been discussed. Moreover, the ITB has been applied in industrial gas turbines due to its operating flexibility and potentials to reduce emissions [33].

Despite the advantages described above, the ITB engine is by nature less efficient than a conventional turbofan. Therefore, it is not common to see such an engine configuration in a commercial aircraft, where the economic efficiency plays an important role. However, considering the additional challenges of low emissions faced by the civil aviation in future, the ITB engine would be one the most promising candidates in the next step of the engine evolutions.

The dual combustor system offers the operating flexibility to realize various objectives. If one starts from a conventional single combustor engine cycle as depicted in Figure 2.14 A), there are three possibilities to achieve an ITB engine cycle. The first one is to maintain both combustor exit temperatures identical to the baseline engine; accordingly, a reheat cycle as presented in Figure 2.14 B) is formulated. Such a configuration delivers the maximum specific power but at the worst thermal efficiency. If one attempts to maintain the thermal efficiency of the reheat cycle identical to the baseline engine, the first combustor exit temperature of

the ITB engine has to be higher than that of the baseline engine, meanwhile, the ITB exit temperature needs to be below a certain temperature (named as the critical temperature) as illustrated in Figure 2.14 D). Furthermore, the operating strategy presented in Figure 2.14 C) produces the same amount of the specific power as the baseline engine in the case A). However, the turbine inlet temperatures in this configuration are much lower than the baseline engine, which is beneficial to reduce the HPT cooling air and the associated NOx emissions. Most importantly, with the ITB engine configuration, different types of fuels can be combusted simultaneously, which offers a unique opportunity for alternative fuels as discussed later.

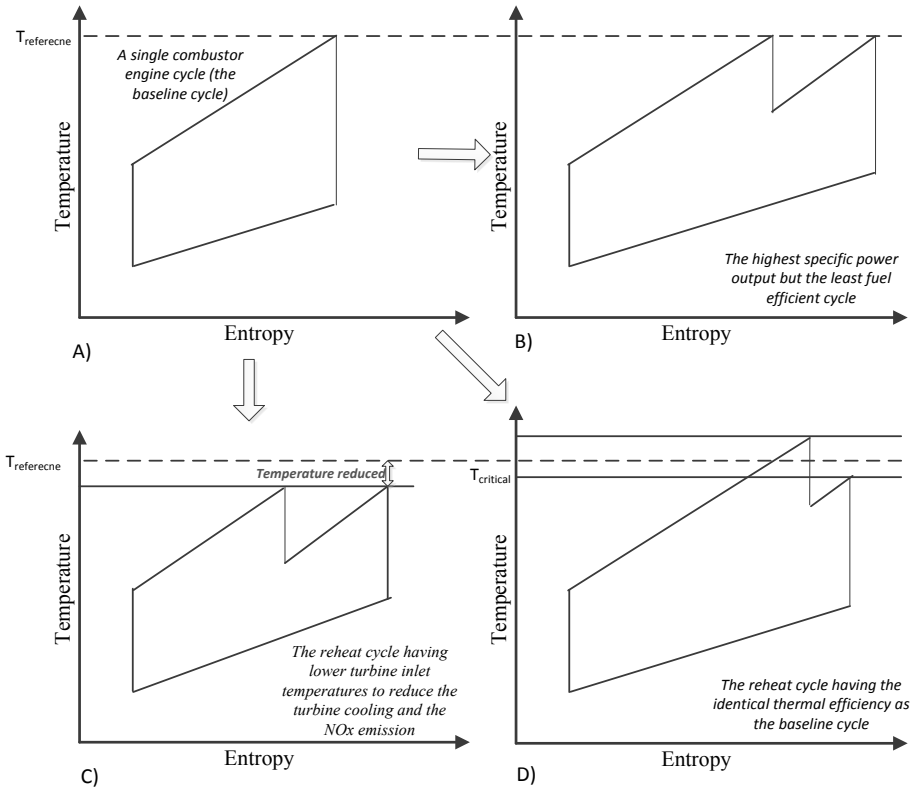


*Figure 2.14: T-S diagram of reheat cycle for different purposes.*

### 2.4.2 Alternative fuels

Despite the improvement in cycle efficiency discussed in the preceding sections, it is still challenging to reduce the environmental impact as expected. Taking the $CO_2$ emission as an example, the $CO_2$ emission is directly related to the system efficiency and the fuel burnt. As discussed earlier, the reductions in $CO_2$ emission by improving the cycle efficiencies would still be difficult to satisfy the ACARE

emissions reduction goal. The ICAO Committee on Aviation Environmental Protection (CAEP) has performed an assessment to predict the developing trend in the $CO_2$ emission by civil aviation as depicted in Figure 2.15. A gap starting from the year 2020 exists between what the aircraft technology and operational changes can deliver and the ICAO goal. This gap needs to be filled in with alternative fuels and other measures.

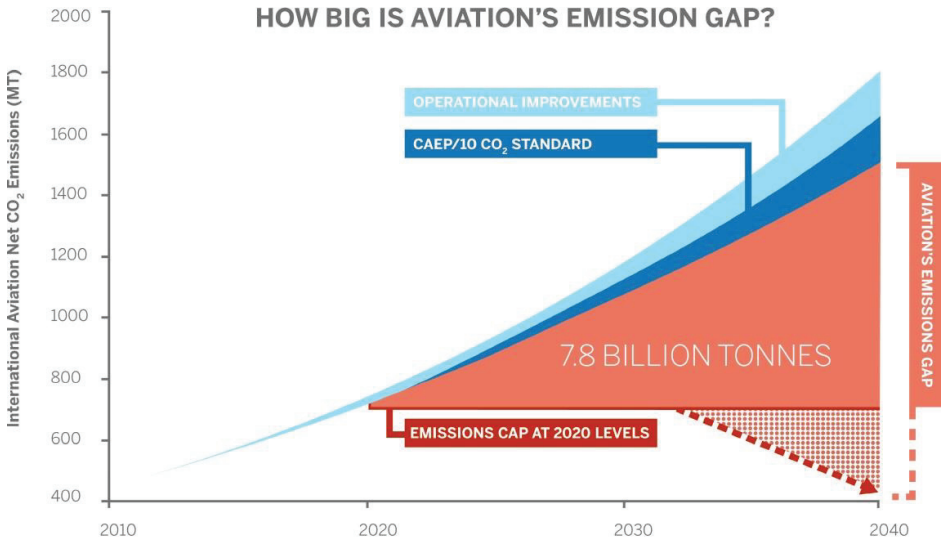


*Figure 2.15: Schematic of $CO_2$ emission reduction roadmap (Graph source: "overview of ICAO's environment work"(ICAO 2015)).*

Apart from the environmental perspective, other motivations also play essential roles. The crude oil is a limited natural resource which is subjected to exhaustion. It has been reported in the literature that the world's crude oil production is close to its maximum and after reaching this peak it will start to decrease [34-36]. Although predictions of the exact time are not always reliable, it confirms that the depletion of crude oil is a certain event. Given the growth rate in air traffic and the caused increase in fuels, if action is not taken immediately to determine the satisfactory replacement of current aviation fuel, the global aviation industry will face a big difficulty. Furthermore, the market competitiveness of the civil air transportation depends largely on its energy cost. Over periods, the fuel price has risen significantly, which is not favored by airliners. With the intention of maintaining the economic benefits, the airlines develop their interests in alternative fuels.

A question that arises immediately is what would be an ideal candidate to replace the current kerosene fuel. The commercial engine and aircraft research communities have investigated various possibilities. A prediction of the future fuel scenario for long range aircraft has been made in Figure 2.16. In the near term, biofuels\synthetic

aviation fuels are suggested. Such fuels are also called “drop-in” fuels because these fuels can be implemented directly to the existing airplanes. These fuels are less restricted by crude oil resources. Moreover, the production process of these fuels is sustainable. From a long-term perspective, in 50 years, aircraft and engines would be designed to use the low-carbon or non-carbon fuels, e.g. Liquid Natural Gas (LNG) and Liquid Hydrogen (LH2), to reduce emissions.

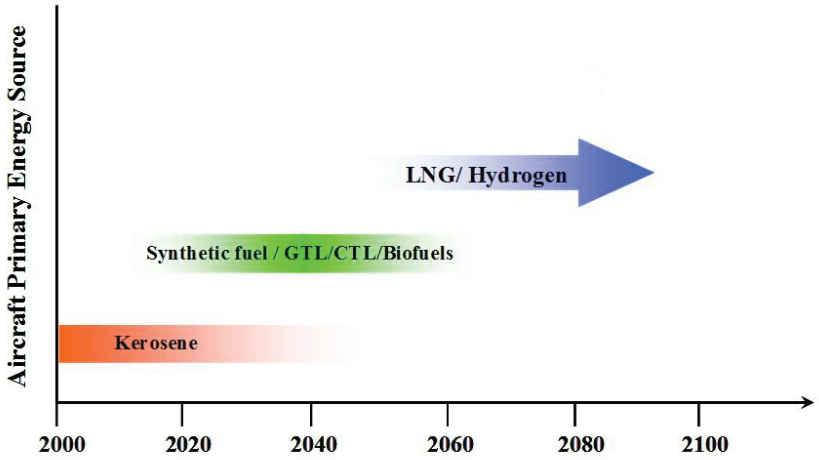


*Figure 2.16: Future fuel scenario for long-range commercial aero engines*

## 2.5 Summary

The development of aircraft engine technologies has been discussed in this chapter. Over the past decades, the engine pressure ratio, the bypass ratio, and the burner exit temperature have increased significantly to improve the cycle efficiency. However, due to various limitations, the conventional approach of improving the cycle efficiency becomes less effective. Alternatively, various innovative engine configurations have been proposed, among which four concepts have been elaborated in this chapter. They are the geared turbofan engine, the open rotor engine; the intercooler recuperated aero engine and the Interstage Turbine Burner engine. All these engines have a large potential to reduce the fuel consumption. However, it is still challenging to meet the emission reduction goal proposed by the ACARE. Alternative fuels would be an attractive solution, in particular, to reduce the $CO_2$.

# Chapter 3 A novel multi-fuel hybrid engine concept

The increased concern for the climate change has added a new imperative for the future aviation to reduce the emitted greenhouse gases. As a result, developing a sustainable aeronautical propulsion system has taken precedence over the general more affordable and economic engines requirement. The reduction in greenhouse gases can be achieved from various aspects. The innovative engine architectures discussed in the preceding chapter can be beneficial in reducing the fuel consumption and the associated emissions. Moreover, the advancement in combustion techniques is helpful to reduce emissions. Furthermore, burning sustainable fuels can reduce $CO_2$. Following this thought, a multi-fuel hybrid engine concept has been conceived within a European project "*Advanced Hybrid Engine for Aircraft Development (AHEAD)*" for a Multi-Fuel Blended Wing Body (MFBWB) aircraft. In this chapter, the features of the MFBWB aircraft are firstly introduced. Accordingly, the specifications of its propulsion system are presented. These requirements are regarded as criterions to formulate the multi-fuel hybrid engine. Finally, a selected multi-fuel hybrid engine configuration is described.

## 3.1 Background of the multi-fuel hybrid engine concept

To reduce the climate impact of aviation, natural gas and hydrogen have been highlighted due to their outstanding advantages in $CO_2$ reduction. However, the challenges of applying these fuels in conventional aircraft have kept engineers and scientists busy for quite some time. One practical difficulty is to store these fuels. These fuels are gases at room temperature and must be stored either in the cryogenic form or at very high pressure. Given the tank material available, the heavy weight of the high pressure tank makes the latter option impractical. Therefore, the cryogenic storage becomes an option. But this introduces other challenges, among which the large volume requirement is prominent.

From Figure 3.1, it can be observed that the mass-energy density of both LH2 and LNG are higher than kerosene, which is beneficial to reduce the fuel weight. Especially, the mass-energy density of LH2 is about three times than that of the kerosene; hence, the total mass would be decreased by more than 60%. However, the volumetric energy density of LH2 is only one-fourth of kerosene. Thereby, the required volume to store LH2 would be four times larger. Furthermore, cryogenic fuels have to be preserved in cylindrical tanks with the well-insulated system to prevent them from leaking and boiling off, which requires extra volume. This dimension increase would cause the additional aerodynamic drag, hence more energy consumption. Therefore, the LH2 alone is not attractive for the commercial aviation. Lessons have also been learned from various research [37-39]. One of the recent activities in this aspect was the Cryoplane project under the 5th Framework of the European Commission [38, 40-42]. It was reported that replacing the kerosene by LH2 for a given mission, the system energy consumption increases by

approximately 10% due to the increased aircraft wetted surface area caused by pressure vessels used for the LH2 storage [43].

On the other hand, although LNG is less efficient in $CO_2$ reduction, it is more practical to be applied. The mass-energy density of LNG is higher than kerosene, and the volumetric energy density of LNG is moderate. Moreover, LNG is currently one of the cheapest fuels. In addition, Russians already successfully tested the LNG airplane in the past. Although the project was discarded due to the dissolution of the Soviet Union, the successful attempts can still provide us precious experiences for the further development of LNG planes.

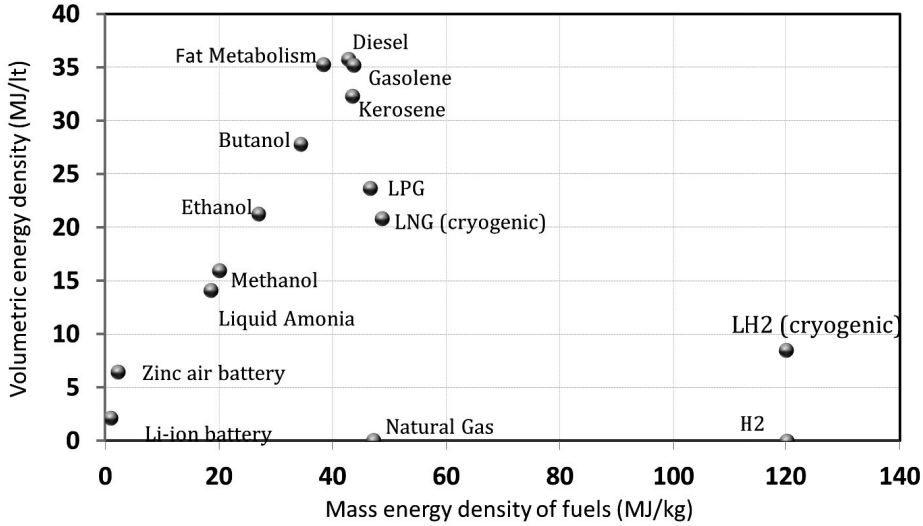


*Figure 3.1: Energy density of various fuels*

To summarize, the difficulties of using cryogenic fuels in a conventional aircraft is to accommodate the cylindrical tanks together with the thick insulation layer. If the availability of free space were not a restriction, LH2 and LNG would be perfect candidates to realize the sustainable aviation.

### 3.1.1 Multi-Fuel Blended Wing Body aircraft

The analysis above shows the co-existence of opportunities and challenges to utilize cryogenic fuels in future aviation. The solution provided in the AHEAD project is a Multi-Fuel Blended Wing Body (MFBWB) configuration. By using such a configuration, the total energy is provided by different fuels simultaneously. The fraction of each energy source can be controlled such that the overall mission performance is optimized.

The Blended Wing Body (BWB) aircraft itself has been investigated widely by various research groups [44-47]. Its lift-to-drag ratio is significantly higher than a conventional aircraft; hence, the BWB itself is more efficient. Furthermore, the inherent feature of the BWB aircraft offers large free space, which makes it more competitive in transporting payload. However, the idea of designing a passenger aircraft with multiple fuels based on the BWB configuration has never been explored. A schematic of the AHEAD MFBWB is depicted in Figure 3.2. The central fuselage is reserved as the passenger compartment. Space at both sides can perfectly accommodate the cryogenic fuel tanks. The internal wing space is still used to store normal liquid fuels. The ratio between two fuels can be adjusted such that the penalty of using cryogenic fuels is minimized. The preliminary design of the MFBWB has been performed by Delft University of Technology (TU Delft).

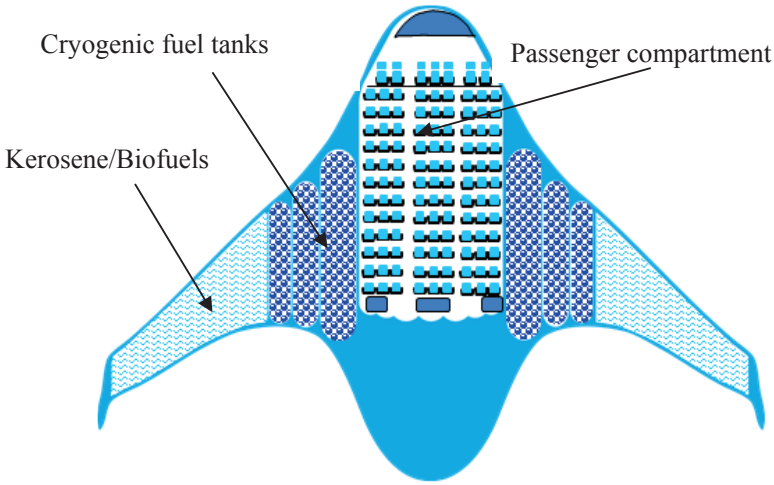


*Figure 3.2: A schematic of the Multi-Fuel Blended Wing Body [48]*

To demonstrate the effects of the multi-fuel configuration (LH2-kerosene combination and LNG-kerosene combination as examples) on the overall fuel mass and volume, the following study is performed. The additional weight and volume of fuel tanks and the insulation layer are not considered. The analysis has been conducted for a given flight mission. It is assumed that the mission energy consumption remains constant in all cases. Since the energy densities of fuels differ from one to another, the fuel mass and volume vary accordingly for a given energy content. The baseline is a pure kerosene aircraft.

The results are presented in Figure 3.3 a) and b), where the figure a) shows the fuel combination of LH2-kerosene and the figure b) shows the LNG-kerosene situation. The solid line represents the variation in the total fuel mass, whereas, the dashed line indicates the variation in the overall fuel volume. The $y$ axial on the left hand is the relative mass defined by the Eqn. (6), and the $y$ axial on the right hand is

the relative volume defined by the Eqn. (7). The $x$ axis is the energy fraction of LH2 or LNG defined by the Eqn. (8). The LH2 energy fraction of 0 indicates a pure kerosene case, and the value of 1 implies a pure LH2 case. Any point in between is a multi-fuel configuration. The same philosophy holds for the LNG-kerosene combination.

$$relative\ mass = \frac{m_{LH2/LNG} + m_{kerosene}}{m_{kerosene}} \tag{6}$$

$$relative\ volume = \frac{v_{LH2/LNG} + v_{kerosene}}{v_{kerosene}} \tag{7}$$

$$LH2/LNG\ energy\ fraction = \frac{m_{LH2/LNG} \times LHV_{LH2/LNG}}{m_{kerosene} \times LHV_{kerosene} + m_{LH2/LNG} \times LHV_{LH2/LNG}} \tag{8}$$

Using only LH2 enlarges the volume by 4 times but reduces the fuel weight by 60%. Furthermore, using the only LNG increases the volume by 1.6 times with the weight reduction of about 15%. As the LNG or the LH2 energy fraction increases, the $CO_2$ reduces accordingly. If the additional weight and volume of fuel tanks and the insulation layer are included, the magnitudes of variations will differ. Moreover, increasing the LH2 or LNG energy fraction reduces the $CO_2$ emission. Optimization can be performed to find out the most beneficial energy fraction of the LH2 or LNG.

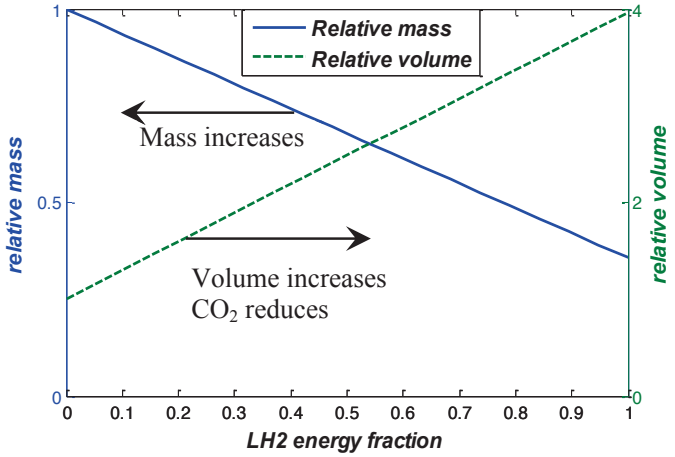


*(a) LH2 & kerosene*

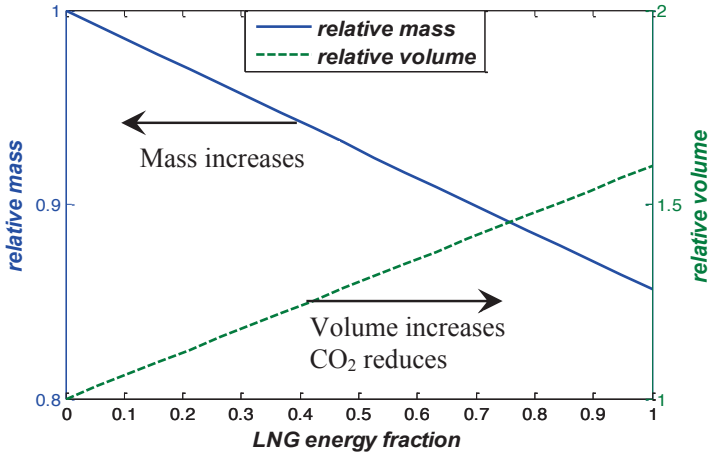


*(b) LNG & kerosene*

*Figure 3.3: Total fuel mass and volume variation for a given mission*

### 3.1.2 Propulsion system requirements of MFBWB

As a complete system, the aircraft and its propulsion system are inextricable. Whenever a novel aircraft concept is conceived, the question raised immediately is what kind of engine is required. The futuristic propulsion system for MFBWB aircraft is expected to suffice the following requirements:

- *Multi-fuel Capability*: The engine of the MFBWB aircraft should be able to burn multiple fuels simultaneously.
- *High efficiency*: Efficient propulsion system enables the MFBWB more competitive compared to the current state-of-art.
- *Low Emissions*: The emission reduction goal proposed by ACARE plays an important role to motivate the MFBWB system. Moreover, the soot emission affects the local air quality and the formation of contrail cirrus; therefore, it should also be reduced.
- *Aircraft & Engine Integration*: Research on the BWB aircraft has shown confidences in reducing fuel consumptions by a highly integrated aircraft & engine system, where the engine ingests the boundary layer developed over the airframe [49, 50]. By doing this, the propulsive efficiency of the system increases. To enable the ingestion of the boundary layer flow, the engine has to be embedded. Such a configuration helps to shield the fan noise and to reduce the wetted surface. However, the embedded propulsion system also causes negative effects and challenges [51]. The non-uniformity of the boundary layer causes flow distortion. Therefore, an improved fan system would be appreciated

if one intends to utilize the Boundary Layer Ingestion (BLI) technique for the MFBWB in the future.

## 3.2 Multi-fuel hybrid engine concept

To satisfy various requirements of the MFBWB propulsion system, different engine configurations have been proposed. Ultimately, the engine configuration depicted in Figure 3.4 is scored the best and will be thoroughly studied in the current thesis. Several novel features are present in this multi-fuel hybrid engine:

- Hybrid sequential combustion chambers
- Multi-fuel capacity
- Counter rotating shrouded fans
- Cryogenic Bleed Air Cooling System (CBACS)

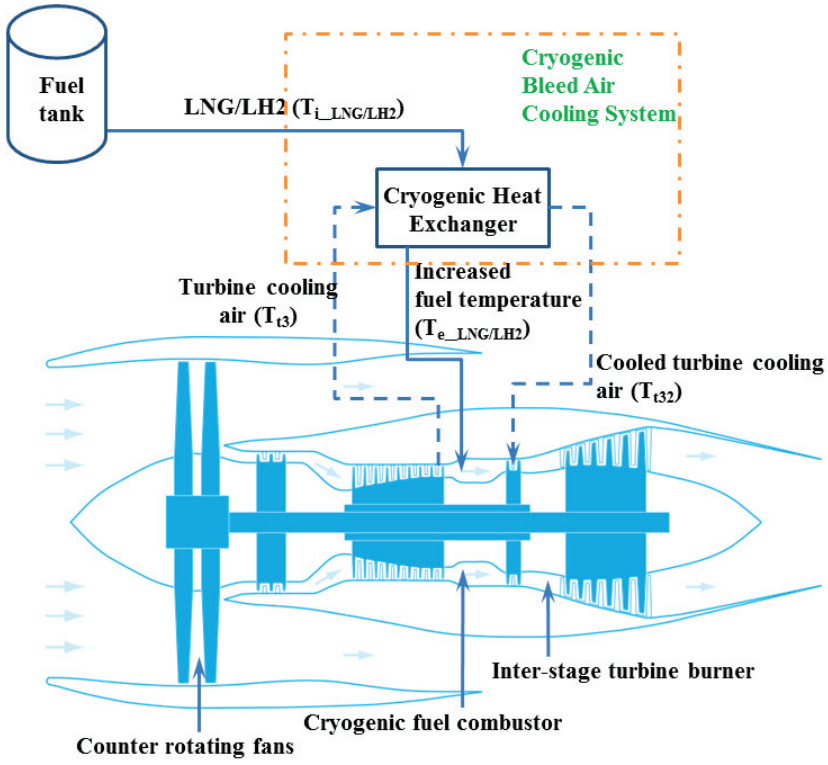


*Figure 3.4: Layout of the multi-fuel hybrid engine*

*Hybrid Sequential Combustor System*: The hybrid sequential combustion chamber system enables different fuels burnt simultaneously. In the hybrid engine, the cryogenic fuel (LH2 or LNG) is burnt in the first combustor (named as CryoCombustor). The CryoCombustor is the main burner. The kerosene or biofuels are combusted in the ITB in the Flameless Combustion (FC) mode [52, 53]. This burner operates flexibly on or off depending on the operating conditions.

The advantage of the hybrid sequential combustion system is low emissions. The CryoCombustor can reduce $CO_2$ emission significantly. The LNG or LH2 contains very low or even no carbon, therefore, burning such fuels produces very less $CO_2$ or eliminates $CO_2$ as the LH2 is concerned. Moreover, the NOx emissions are expected to be lower for multiple reasons. As discussed in the section 2.4.1, the sequential combustor configuration itself has a potential to reduce the NOx emissions. Furthermore, the Flameless Combustion (FC) applied in the ITB is a low NOx technique and has been widely used in industry [54, 55]. The FC takes place at low $O_2$ concentration and high temperatures (above the auto-ignition temperature of the fuel) as shown in Figure 3.5. To achieve a low $O_2$ concentration, a large recirculation volume is required, which is challenging in a conventional engine configuration. The ITB is at the downstream of the first combustion chamber. Using hydrogen or methane in the first combustion chamber increases the water vapor concentration and reduces the $O_2$ concentration of the gas, thereby creating a high temperature vitiated environment at the inlet conditions of the ITB. This is ideal to for the FC to take place [56].

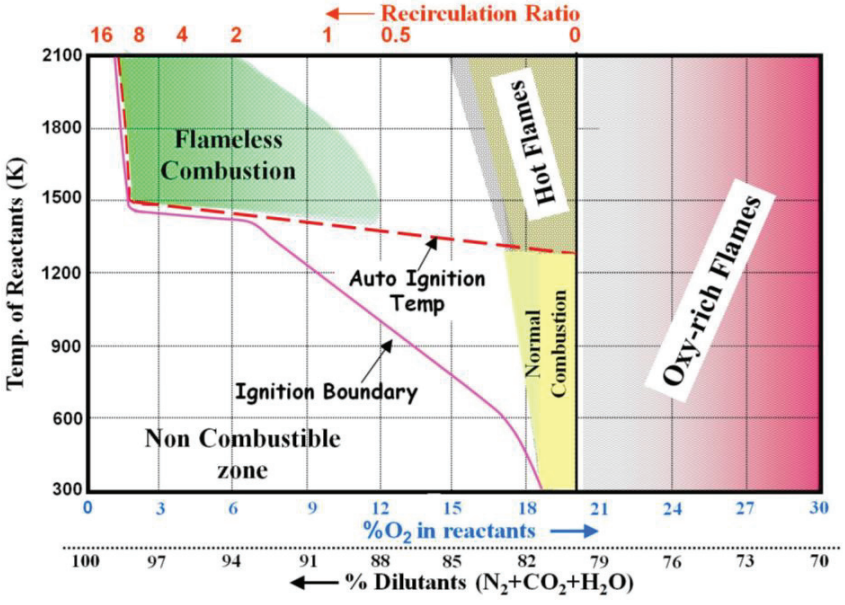


*Figure 3.5: Schematic of different combustion regimes [57]*

Although the hydrogen combustion generally produces more NOx emissions at given equivalence ratio due to its high flame temperature (about 100 K more than that of the kerosene)[37], the flammability limit is wider. Therefore, the combustion in the Cryocombustor can take place at very lean conditions [58-60] which is beneficial to reduce NOx emissions.

*Cryogenic Bleed Air Cooling System (CBACS)*: The LH2 or LNG used in the first combustion chamber is an excellent heat sink. Figure 3.6 presents the efficiency gain by using the LH2 to cool different components in a gas turbine engine. It shows that the most benefits are achieved by cooling the turbine cooling air. This gives confidences of using a cooled bleed air system in the hybrid engine.

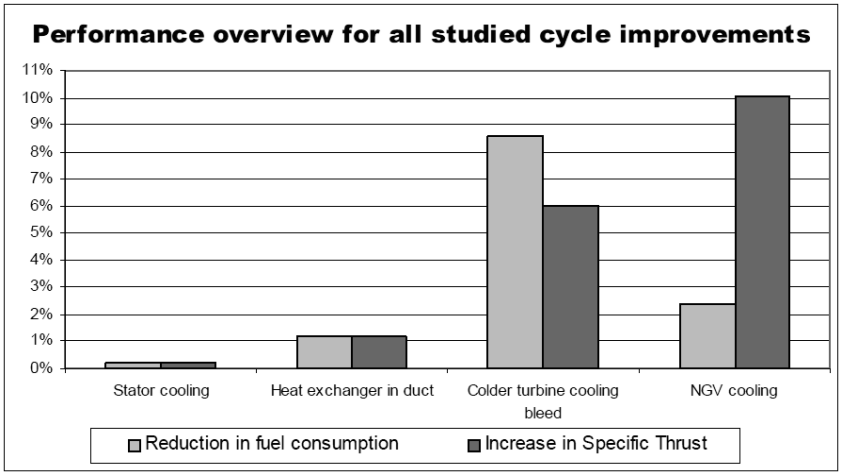


*Figure 3.6: Implementation of LH2 as heat sink for various gas turbine cooling [61]*

In the hybrid engine, a CBACS is used the enable the bleed air to be cooled by LH2 or LNG. The cooled bleed air is then used for the turbine cooling. This helps to reduce the turbine cooling air, hence improves the thermal efficiency. Moreover, after cooling the bleed air, the fuel temperature increases, which is helpful to improve the thermal efficiency.

*Contra Rotating Fans (CRF):* The future MFBWB aircraft tends to use the BLI technique to improve the propulsive efficiency of the system. The boundary layer flow field is non-uniform. The normal single stage fan with an ultra high bypass ratio is quite sensitive to the coming flow quality. Therefore, a CRF system is considered in the hybrid engine. An example layout of the CRF is depicted in Figure 3.7. Such fan system can sustain the non-uniform flow better than a single stage fan, for the reason that each stage of the CRF is less loaded than that of a single stage fan for a given fan pressure ratio. Research on the CRF has been conducted to analyze the performance from various perspectives. For example in Ref. [62] the acoustic

effects of this fan system are studied. In Ref. [63-65] the fan characteristics are provided by a fan map, where the fan efficiency and pressure ratio at various rotational speeds are given.

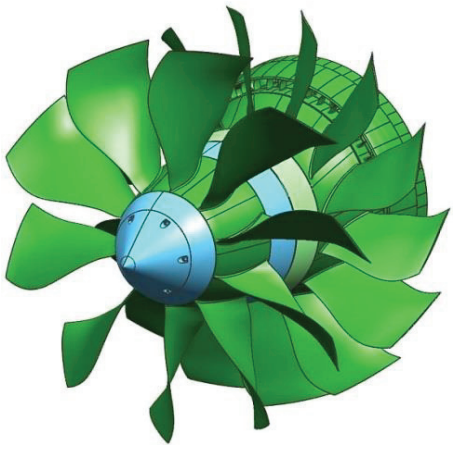

*Figure 3.7: Contra-rotating fans (Picture source: Snecma).*

## 3.3 Summary

In this chapter, the motivations of the multi-fuel configuration and the associated aircraft engine configurations are introduced. The LNG and LH2 can reduce $CO_2$ significantly. However, the volume to store these fuels are large, which is challenging in a conventional aircraft with a compact design. The large available free space in a BWB aircraft sheds light on this thought. Nevertheless, to balance the overall performance of the aircraft system and the low emissions goal, an MFBWB concept was proposed. Correspondingly, a novel Multi-Fuel Hybrid Engine concept is conceived. A further detailed analysis on this specific engine architecture will be performed in the following chapters.

# Chapter 4 Engine model framework

This chapter is devoted to the complete model framework. It consists of an engine performance module within which an in-house turbine cooling module is included to improve the accuracy in the cycle performance prediction, a Cryogenic Bleed Air Cooling System (CBACS) module, a generic emission prediction module, and an optimizer module. In the following paragraphs, the modeling philosophy will be elaborated.

## 4.1 The engine performance module

In general, engine performance model is classified into three categories: the design condition model, the steady state model, and the dynamic model. The modeling philosophy of each condition also differs from each other.

### 4.1.1 The various operating conditions

A typical flight mission is given in Figure 4.1. It undergoes through taxi, take-off, climb, cruise, descent, approach, and landing. A broad range of ambient conditions and flight speeds are covered, which brings forward challenging requirements for an engine. A well-designed aircraft engine should be able to perform successfully at each operating point over this mission.

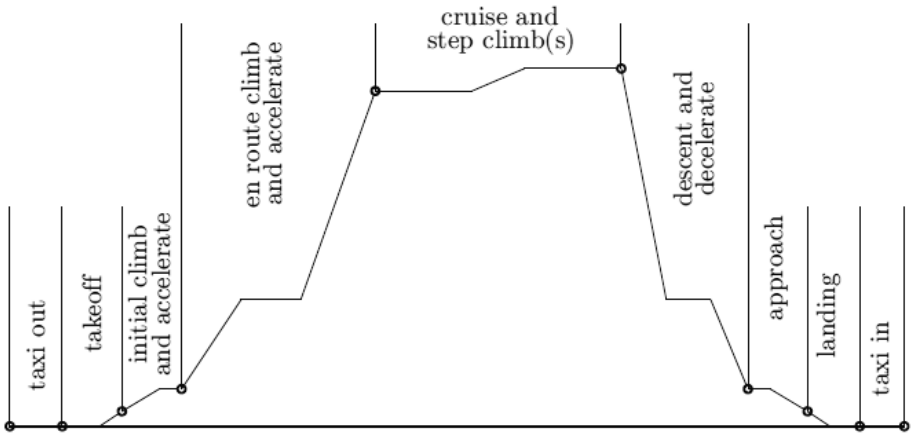


*Figure 4.1: A typical commercial flight mission profile*

Among various operating points over a flight mission, it is important first to identify the design condition of an engine. There are several possibilities as shown in Figure 4.2, among which the cruise performance is critical in particular as a long-

range mission aircraft is concerned. During a practical engine design process, all these points would be involved. A final engine design is selected depending on the criterion of the overall performance optimization [66].

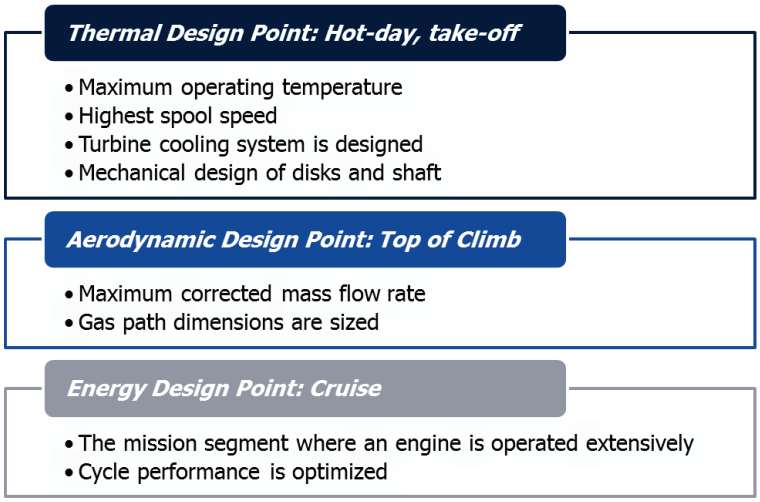


*Figure 4.2: Critical operating points*

Once an engine design condition is determined, the performance at the steady state conditions and through the transient process can be studied. Under most circumstances, an engine works at the equilibrium condition also named as steady state. Whenever the flight condition (inlet temperature, pressure, or flight speed) changes or the power setting varies, the initial equilibrium is destroyed, in other words, the engine will be operating at a dynamic state, which is also called transient. During this process, it is vital to have a sophisticated fuel control system in combined with other variable geometry controls, for example, the Variable Stator Vanes (VSV), the Variable Bleed Valves (VBV), and the adjustable nozzle area. Therefore, the transient engine model plays important roles to develop the control system for an engine. This thesis mainly focuses on the design and the steady state performance of the hybrid engine; therefore, the modeling procedures in this regard will be described in the following contents.

### 4.1.2 The various modeling environment

The non-linear characteristics of gas turbine engines require sophisticated modeling and simulation tools. Conventionally, different modeling tools focusing on various disciplines, for example, aero-thermodynamics, structure, cost analysis, etc. are provided to gas turbine designers. Hence, the earlier engine performance model mainly predicts the whole engine performance at the 0-D dimension, implying that only the average temperature, pressure, and gas properties at the inlet and the exit of

each component are calculated. However, in the modern engine design processes, the Multi-Disciplinary Optimization (MDO) method has drawn broad attentions. Therefore, the recent engine modeling tools tend to extend their scopes.

One example is Gasturb [67]. Gasturb is a user-friendly tool for gas turbine performance simulation. It can be used to analyze the thermodynamic performance of a predefined set of engine cycles at both design and off-design conditions. Moreover, Gasturb also enables the preliminary gas turbine sizing.

Another representative tool is NPSS (Numerical Propulsion System Simulation) [68, 69] developed by a consortium of US research institutes, government agencies, industry, and universities. It can conduct different levels of simulation fidelity from a simple thermodynamic model to a full 3D whole engine CFD (Computational Fluid Dynamics) simulations, as described in [70].

Apart from software discussed above, there are also other tools available. For instance, PROOSIS (Propulsion Object Oriented Simulation Software) developed under European project framework [71].

Gas turbine Simulation Program (GSP) [72] is an object-oriented 0-D gas turbine simulation tool [73]. It is powerful in engine performance analysis. The component-based modeling environment of GSP provides the flexibility to create models for various gas turbine configurations. GSP has also been extended progressively to perform diverse analysis, for example, gas path analysis [74]. Moreover, although GSP itself is a 0-D modeling environment, Application Programming Interface (API) developed recently by GSP team allows running the engine model externally, which provides the potential to couple different disciplines.

The hybrid engine configuration is novel and non-standard. The tools to model this engine should be flexible and extensible such that the users can arbitrarily modify the engine model to perform the necessary analysis. Given these considerations, the GSP is selected for the hybrid engine modeling. Two models sharing a common modeling procedure have been created. These models correspond to a conventional turbofan configuration and an ITB turbofan configuration respectively. The model layouts are given in Figure 4.3 and Figure 4.4.

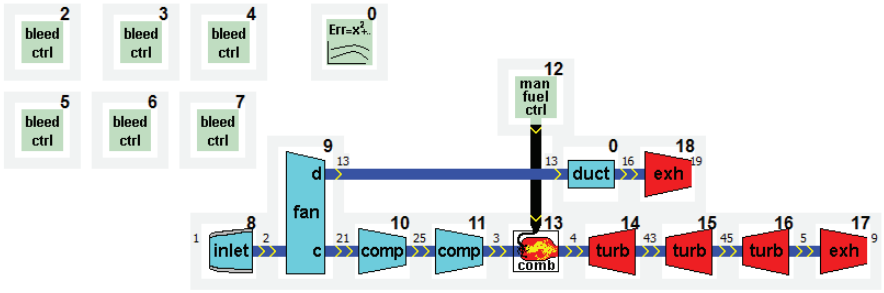


*Figure 4.3: Layout of a conventional turbofan engine model*

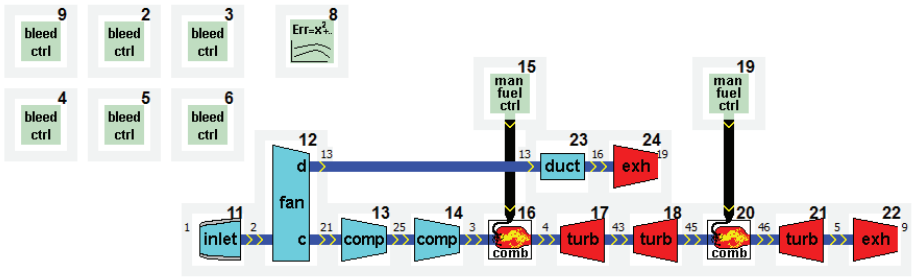


*Figure 4.4: Layout of an ITB turbofan engine model*

Each model consists of an inlet, fan, Low Pressure Compressor (LPC), High Pressure Compressor (HPC), the first combustion chamber, High Pressure Turbine (HPT), Low Pressure Turbine (LPT), convergent core nozzle, bypass duct, and convergent bypass nozzle. Moreover, the ITB engine model includes an additional combustion chamber between the HPT and LPT. Both engines are twin-spool configurations, where the HPC is driven by the HPT, and the fan and LPC are driven by the LPT.

### 4.1.3 The design condition modeling

*Inlet*: The inlet component defines the total inlet air mass flow. The total inlet conditions of the free stream are also calculated according to given ambient and flight conditions. The inlet pressure loss is represented by a Ram Recovery (RR) factor which is a function of the engine flight Mach number [75]. To determine the RR, the MIL-E-5008B standard is used [76]. According to this standard, the RR factor is equal to 1 at the flight Mach of 1. Above the Mach 1, the RR factor reduces according to the relation in Eqn. (9),

$$\pi_d = 1 - 0.075(M_0 - 1)^{1.35} \quad 1 < M_0 < 5 \tag{9}$$

*Fan:* In the fan component, the FPR and BPR are inputted. Thereby, the temperature ratio of an isentropic compression process can be obtained by the Eqn. (10),

$$\frac{T_{t2}}{T_{t1}} = \left(\frac{p_{t2}}{p_{t1}}\right)^{\frac{\kappa_a - 1}{\kappa_a}} \tag{10}$$

where $T_t$ and $p_t$ are the total temperature and pressure, and the subscripts 1 and 2 indicate the component inlet and exit respectively; $\kappa_a$ is the heat capacity ratio for air. Moreover, the notation definitions mentioned here are also valid in the later application if not mentioned otherwise.

However, due to various losses occurred during the compression, the actual work required to achieve the given pressure ratio is always higher than that of an isentropic process. Therefore, in a real cycle, by introducing an efficiency term, the Eqn. (11) can be obtained to calculate the temperature ratio for a given pressure ratio and component efficiency,

$$\frac{T_{t2}}{T_{t1}} = 1 + \frac{1}{\eta_f}\left[\left(\frac{p_{t2}}{p_{t1}}\right)^{\frac{\kappa_a - 1}{\kappa_a}} - 1\right] \tag{11}$$

where $\eta_f$ is the fan efficiency;

With the temperature ratio known, the Eqn. (12) determines the compression work requirement,

$$W_c = \dot{m}_a c_p (T_{t2} - T_{t1}) \tag{12}$$

where $W_c$ is the compression power; $c_p$ is the isobaric heat capacity; $\dot{m}_a$ is the air mass flow rate.

*Compressor:* A compressor follows the identical working principle as described in the fan module. Therefore, the Eqn. (11) would also be valid, with only the $\eta_f$ replaced by compressor efficiency ($\eta_c$). The compression work required by a compressor can be derived by the Eqn. (12).

*Cryogenic Combustion Chamber (CryoCombustor):* The CryoCombustor is located between the compressor and the turbine. It operates during the entire flight mission. The fuel flow rate (or the TIT), the combustion efficiency, and the combustion pressure loss can be specified for this component at the design condition. The combustion process is calculated based on the gas and fuel composition data and chemical equilibrium equations. The dissociation effects are taken into account [75].

*Turbine:* In the turbine component, the turbine design efficiency and the shaft speed are inputs. They are defined directly at the model reference point. The turbine drives the compressor coupled on the same shaft. Therefore, the work balance has to be maintained between the compressor and turbine, as shown in Eqn. (13),

$$W_t = \dot{m}_g c_p (T_{t1} - T_{t2}) = W_c / \eta_m \tag{13}$$

where $\eta_m$ is the mechanical efficiency of the shaft; $\dot{m}_g$ is the mass flow rate of the gas through the turbine; $W_t$ is the turbine power.

By following the energy balance between compressors and turbines, the turbine exit temperature is calculated. Accordingly, the expansion ratio of a turbine is given by the Eqn. (14),

$$\frac{T_{t2}}{T_{t1}} = 1 - \eta_t \left[ \left( 1 - \frac{p_{t2}}{p_{t1}} \right)^{\frac{\kappa_g - 1}{\kappa_g}} \right] \tag{14}$$

where $\eta_t$ is the efficiency (either polytropic or isentropic) of the turbine; $\kappa_g$ is the heat capacity ratio for gas. The turbine cooling air is considered and is calculated by an in-house turbine cooling module, which will be discussed in details in the later section.

*Interstage Turbine Burner:* The modeling procedure of the ITB follows the same philosophy as the main combustor. The fuel characteristics, the combustion efficiency, and the pressure loss are input parameters. However, the inlet gas composition of the ITB differs from that of the first combustor. The gas model provided in GSP can calculate this gas composition.

*Duct:* The relative pressure loss through the bypass duct is defined to indicate the percentage pressure loss with respect to the inlet pressure ($\Delta p_t / p_{t\_inlet}$). Therefore, increasing the FPR with the given pressure loss percentage results in the higher absolute pressure loss in the duct.

*Nozzle:* A fixed geometry convergent nozzle is used. The velocity coefficient or the thrust coefficient is used to represent the efficiency of the nozzle.

### 4.1.4 The steady state condition modeling

No matter it is at the design or the off-design conditions, the conservations of mass, energy, and momentum have to be always ensured. However, when a gas turbine works at its off-design condition, the component has been designed, and therefore, one cannot freely specify the values of parameters as straightforward as at the design condition. The off-design performance modeling determines the operating condition

of each component by a matching process. Therefore, the steady state modeling procedure is a thermodynamic matching process. It requires successive guesses of the operating point on component maps (will be explained in the later content). Iterations are often required to update the initial guess until other known conditions are satisfied. Then, the overall cycle performance can be calculated. In GSP, the Newton-Raphson solver is applied for iteration of the off-design calculation [77].

The off-design characteristics of a component are represented by a so-called performance map, which can be obtained through various tests and analysis. A typical compressor and turbine map can be found in Figure 4.5 and Figure 4.6. These maps are presented in a non-dimensional form. By performing the dimensional analysis [12], the performance of turbomachinery can be represented by a group of non-dimensioned parameters as following:

Pressure ratio: $\frac{p_{t2}}{p_{t1}}$

Temperature ratio: $\frac{T_{t2}}{T_{t1}}$

Non-dimensional mass flow rate: $\frac{\dot{m}\sqrt{RT_{t1}}}{D^2 p_{t1}}$

Non-dimensional rotational speed: $\frac{ND}{\sqrt{RT_{t1}}}$

where $D$ is the characteristic dimension (usually the diameter of the inlet of a compressor or turbine); $N$ is the rotational speed; $R$ is the gas constant. Since the diameter of a given component is constant, it is often dropped out of the formula. The same holds for the constant $R$.

By assembling these maps into the model, the off-design performance is then derived. In the current research modeling, since component maps are not available, generic maps for compressor and turbine are applied. All the maps are scaled according to the design performance of the hybrid engine.

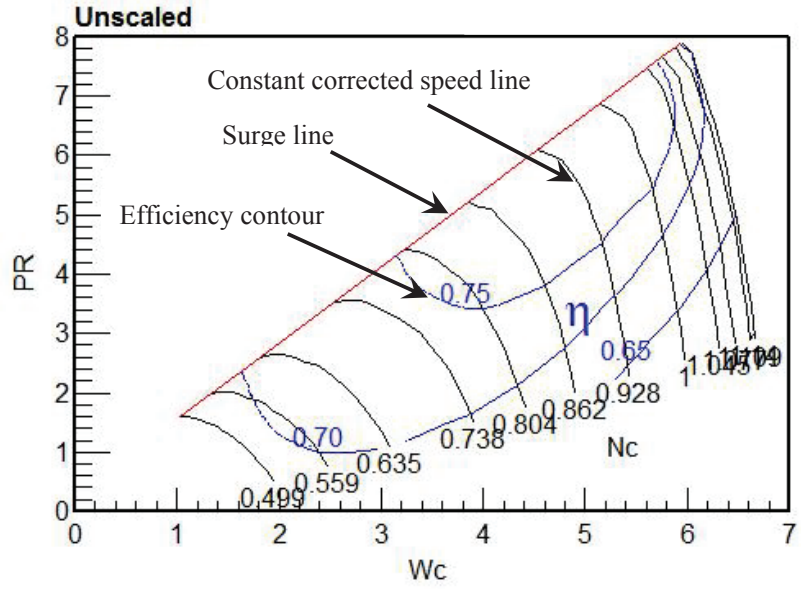


*Figure 4.5: Example of a compressor performance map*

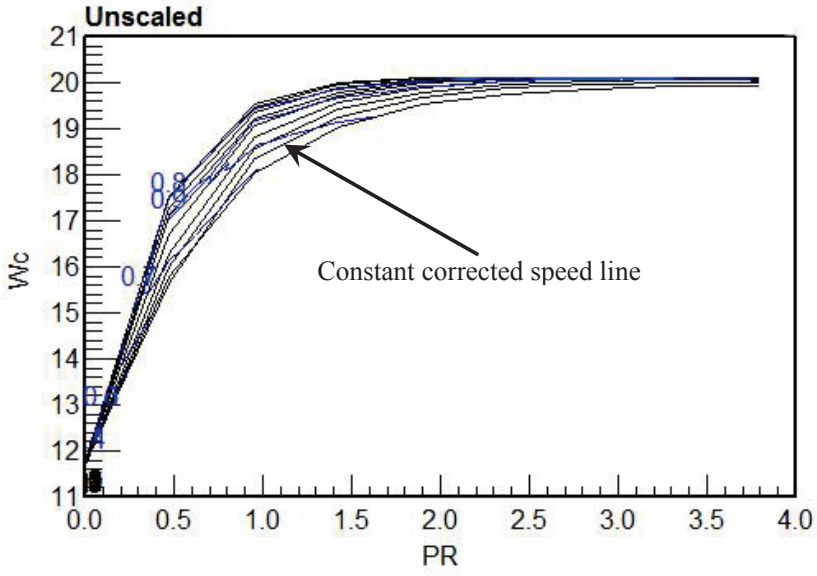


*Figure 4.6: Example of a turbine performance map*

Moreover, the hybrid engine uses contra-rotating fans. Research has been carried out by different organizations to study the performance of contra-rotating fans. Both experimental and simulation data can be found in the literature. By using the Smooth C [78] and data in the reference [65], a performance map of contra-rotating fans has been created and applied for the off-design performance analysis of the hybrid engine. The layout of the map can be seen from Figure 4.7. The design point of the fan is depicted on the map.

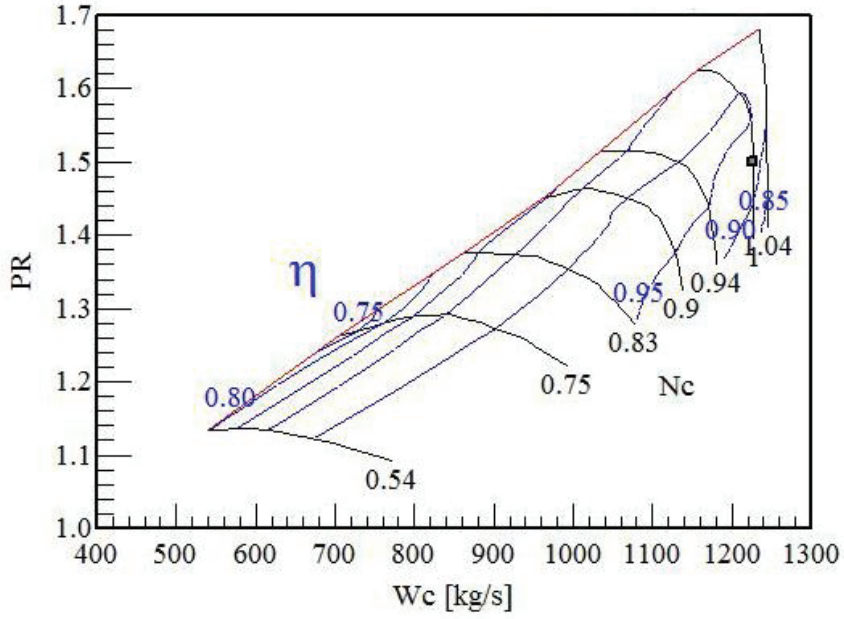


*Figure 4.7: Scaled contra-rotating fans map*

## 4.2 The turbine cooling module

In the preliminary gas turbine design phase, it is common practice to apply empirical correlations to predict turbine cooling mass flow rate. One example can be found in [79]. However, most of the correlations behave linearly. As the OPR and TIT increase substantially, the non-linear characteristics of cooling requirements are more dominant. If the linear correlations are still used, the discrepancies of the turbine cooling prediction will become larger, which might result in the significant performance deviation. Therefore, it is essential to have a turbine cooling prediction tool which can capture the nonlinear characteristics such that the impacts of the turbine cooling on the overall engine performance can be estimated accurately.

### 4.2.1 Overview of the cooling module

An overview of the turbine cooling flow path is depicted in Figure 4.8. The HPT and LPT cooling are considered individually. The cooling air is extracted from different stages of the HPC depending on the pressure at the mixing point, and the pressure loss occurred on the route. The bookkeeping has been considered in the way that the cooling flow of the turbine NGV mixes before the turbine expansion, implying that this flow always contributes to the turbine work output. However, the rotor cooling flow mixes with the mainstream after the turbine expansion. Therefore depending on the number of turbine stages, the rotor cooling has no contribution to the turbine work (single stage turbine condition) or partially expanded in the turbine (upstream of a multi-stage turbine).

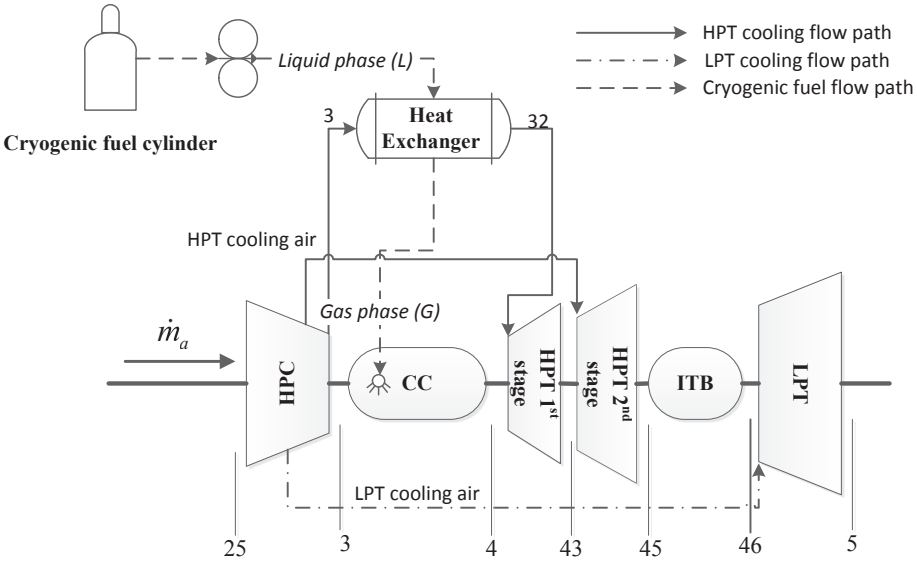


*Figure 4.8: Overview of the turbine cooling flow path*

Moreover, the first stage HPT cooling flow is cooled by a Cryogenic Bleed Air Cooling System (CBACS, indicated as a heat exchanger in the figure), and then the cooled bleed air flows further to the HPT stage. Detailed discussion on the CBACS is presented in the latter section. The reason for only cooling the HPT first stage cooling air can be understood as following. First of all, the majority of the bleed air is used for the first stage HPT. Therefore reducing this cooling quantity is most beneficial for the cycle efficiency. Moreover, the pressure of the cooling flow of each stage turbine differs. If one tends to cool the entire turbine cooling flows, different heat exchangers would be required; this leads to extra complexity and weight of the engine itself. Hence, it is decided only the first stage HPT cooling is cooled.

### 4.2.2 Turbine cooling mechanism

The in-house turbine cooling module has been developed in TU Delft [80]. The overall structure of the model is illustrated in Figure 4.9. In the turbine cooling module, both the internal and external cooling techniques are considered. The internal cooling consists of the rib turbulated cooling, the jet impingement cooling, and the pin fin cooling. The pin fins cooling and rib tabulated cooling are approaches to improve the heat transfer rate of given convection cooling application. Therefore, they follow identical heat transfer principle as the convection cooling. As for the external heat transfer module, the film cooling is considered. The mass flow rate of the turbine cooling is determined by performing the heat balance between the amount of heat absorbed by the cooling flow ($Q_{abs}$) and the amount of heat injected by the hot gas ($Q_{in}$).

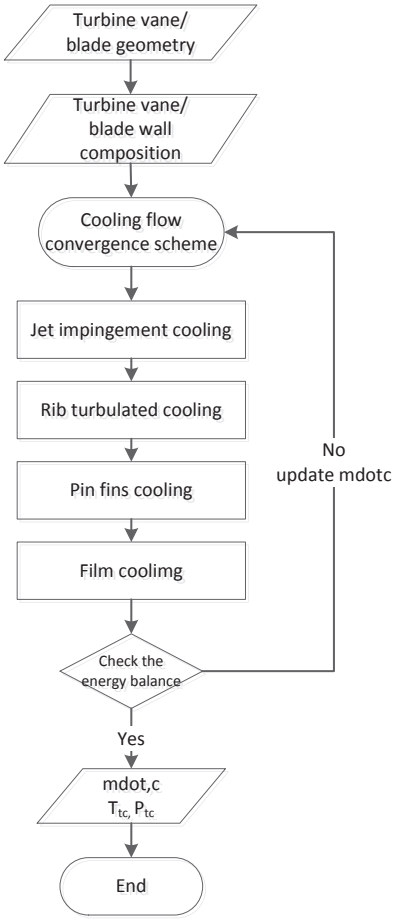


*Figure 4.9: Overview of the turbine cooling module.*

A turbine geometry data would be required to initiate the model. Since at the conceptual analysis phase, the geometry of the turbine blade has not been finalized. Therefore, the detailed information regarding the cooling arrangements is not available. A typical profile of a modern cooled turbine blade as presented in Figure 4.10 is considered. It can be seen that at the leading edge of the blade, the jet impingement cooling approach is applied, followed by the downstream convection cooling within channels. The ribs and pin fins are used at different locations in the channels to improve the heat transfer rate. Depending on the arrangements of ribs and fins, the performance varies. The cooling flow injected from the leading edge by the jet impingement forms a film layer outside the blade surface to protect the blade from the hot gas. Each of the cooling mechanisms is elaborated in the following paragraphs.

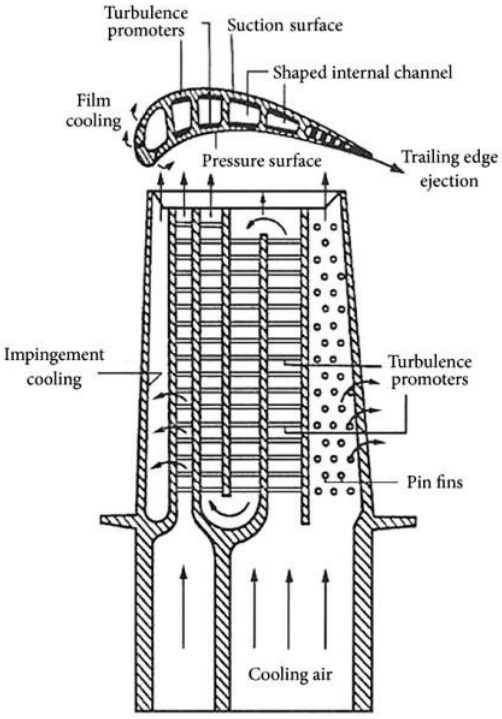


*Figure 4.10: Design concept of a modern cooled gas turbine blade [81].*

*Jet impingement cooling* is an efficient cooling technique and has been widely used for turbine cooling. The cool jet impinges on the hot surface at very high speed. Depending on the jet velocity, the orifice size, the distance of the orifice to the hot surface, and the arrangements of the orifice, very high heat transfer rate can be achieved. Although this cooling mechanism has the highest heat transfer rate, the higher pressure loss makes it unaffordable to be used widely over the entire turbine

blade or vane. The common practice is to apply it only to the leading edge, where the hottest gas temperature is encountered. In this turbine cooling model, empirical correlations provided by Florschuetz, et al. [82] is adopted to calculate heat transfer parameters. Method presented by Levy, et al. [83] is used to estimate pressure drops caused by this cooling technique.

*Rib turbulated cooling* is a form of enhanced forced convection cooling mechanism. The ribs are placed in the channels inside turbine vanes or blades such that the flow turbulence is promoted to achieve higher heat transfer efficiency. The angle and height of the ribs, the space between ribs, the continuity (continued/discrete) of ribs, the shape of ribs (V-shape / straight etc.), and channel aspect ratio are all needed to be considered carefully such that higher heat transfer performance can be achieved.

*Pin fin cooling* is another enhancement approach, by which the internal surface of a turbine blade increases hence improving the heat transfer coefficient. In a turbine blade, pin fins are applied internally at the trailing edge as can be seen in Figure 4.10. The configurations, such as the pin length, the pin diameter, the pin spacing, etc. are critical for its performance. In this turbine cooling model, the Nusselt number of pin fin cooling is calculated using correlations suggested by Metzger et al. [84]. A pressure loss induced by pin fin cooling is calculated by friction factor correlations in [85].

*Film cooling* is an external cooling method to increase the heat transfer resistance of a turbine vane or blade. Instead of directly cooling a turbine by bleed air, the cold air is ejected outside to form a film on the surface of a turbine vane or blade such that it can be protected from the hot gas. The performance of film cooling depends on many factors, for instance, the streamwise film cooling holes distance, the spanwise holes space, the holes size, the air injection angle, blowing ratio, etc. For calculation simplicity, the correlation for the laterally averaged film cooling effectiveness by Baldauf et al. [86] is applied. With the averaged film cooling effectiveness, the further calculation can be conducted to obtain the film temperature, hence the heat transfer coefficient.

The cooling model calculates the quantity of cooling air required for a single turbine vane or blade. By multiplying the number of blades or vanes, the total turbine cooling can be obtained. The calculation of cooling mass flow rate depends on several parameters, the maximum allowable metal temperature, the bleed air pressure, the bleed air temperature, the turbine operating temperature, and the turbine operating pressure. The location where the turbine cooling air is extracted depends on the pressure at the mixing point. Iterations are executed to balance the heat flux between the cooling air and the hot gas. This cooling model is validated by comparison to the NASA Energy Efficient Engine (E3) project as described in [87, 88]. Detailed information regarding this turbine cooling model and the turbine geometry definition can be found in [80].

### 4.2.3 Effects of cooling on turbine efficiency

When a turbine design is finalized, the turbine design efficiency is decided accordingly. However, in reality, it is common practice to extract some amount of air from the HPC to cool the turbine stage. The implementation of turbine cooling has both positive and negative effects. The advantage is the turbine can operate at much higher temperature than its material limit, which is beneficial to the cycle thermal efficiency and the specific power. The drawbacks caused by turbine cooling are multifold:

- Since not all the turbine cooling air is expanded through the turbine stage, a portion of the turbine power is wasted. This leads to deterioration in cycle efficiency;
- When the cooling air flows through the internal channel of a turbine blade, the pressure losses is not avoidable;
- The mixing process of the turbine cooling air with the mainstream causes losses;
- The cooling air coming out of the turbine blade destroys the aerodynamic performance of a turbine blade, leading to the reduction in turbine efficiency.

Therefore, the cooled turbine efficiency is always lower than the uncooled turbine. Horlock [89] has performed theoretical analysis on basic thermodynamics performance of turbine cooling. Moreover, Horlock, et.al [90] and Wilcock, et.al [91] have also simulated gas turbine cycle performance with cooled turbine modeling applied. Their analysis confirmed different orders of magnitudes in the reduction in cycle efficiency due to turbine cooling. The methodology for modeling an air cooled gas turbine has also been discussed by Young and Wilcock in [92].

Significant research has been conducted with an intention to redefine the turbine efficiency including the effects of cooling. Hartsel [93] has demonstrated two analytical models to estimate the cooled turbine efficiency (Harsel eff.). Kurzke [94] also redefined turbine efficiency (mainstream pressure mixed eff.) taking different bookkeeping for both single stage and multi-stage turbine. As for the mixing loss, the prediction is not straightforward. Young and Horlock [95] have attempted to provide distinguished definitions (fully reversible mixed eff.). Horlock and Leonardo[96] compared three definitions of cooled turbine efficiencies. In the current research, the cooled turbine efficiency is considered as a function of the turbine cooling air fraction. Based on the methodologies discussed in the literature, considering the technology improvement in future, the compromised effects by turbine cooling have been considered in this thesis (Thesis eff.). The comparison with different the methodologies is presented in Figure 4.11.

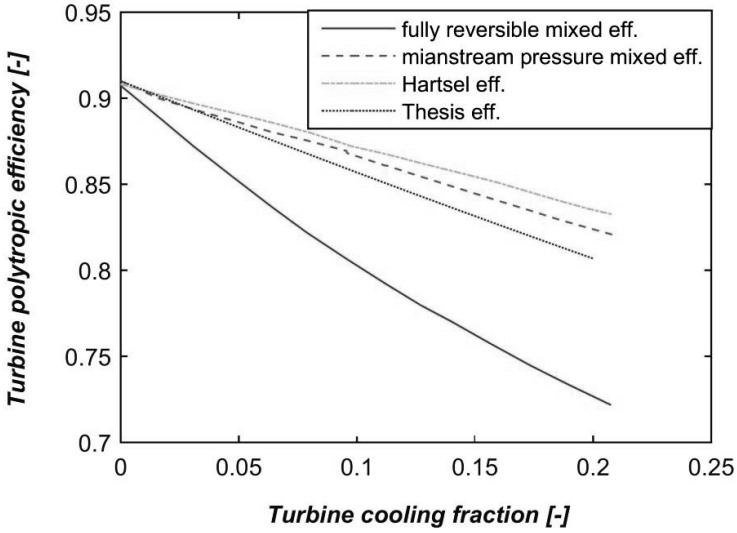


*Figure 4.11: Variation of turbine efficiency versus turbine cooling fraction (figure reproduced by data provided in [96]).*

In this thesis, assumptions are made to account for the turbine cooling air effects:

- The cooling air of the turbine NGV is assumed to mix completely with the mainstream before expansion in the rotor;
- The cooling air of the turbine rotor blade is assumed to mix with the mainstream after the expansion in the rotor;
- The half cooling air of the first stage turbine rotor is assumed to contribute to the turbine work output;
- Every 1% increase in the turbine cooling air reduces the turbine efficiency by 0.5% when compared to the uncooled state-of-art turbine efficiency.

## 4.3 The Cryogenic Bleed Air Cooling System module

This section introduces the modeling of the Cryogenic Bleed Air Cooling System (CBACS). Challenges of the Cryogenic Heat Exchanger (CHEX) are first presented. Afterward, the modeling philosophy of the CHEX is elaborated.

### 4.3.1 The cryogenic heat exchanger design

The core element of CBACS system is a CHEX. The bleed air extracted from the compressor is cooled by the cryogenic fuel; the fuel itself gets heated up, simultaneously. Quantities of the fuel flow and the bleed air participate in this

process are determined by the cycle performance calculation. The exit temperature of the bleed air is specified as an input.

Ultimately, the bleed air at the exit of the CHEX has to mix with the mainstream at the inlet of HPT. Therefore, the pressure drop of the bleed air through the entire CBACS should be minimized such that the total pressure loss of the bleed air through the entire CBACS is no more than that of the first combustion chamber. This becomes one of the critical criterions for the CHEX design. At the conceptual analysis phase, taking into account the pressure losses through pipes, the pressure loss of the bleed air in the heat exchanger is specified to be 1.5% of the inlet pressure. The pressure loss of the fuel is less critical since the fuel injected pressure is controllable by the fuel pump.

When the bleed air is cooled by the Cryofuel, the temperature of the Cryofuel increases simultaneously until the boiling point of the fluid is reached, beyond which the cryogenic fuel undergoes a phase change from liquid to gaseous. This leads to a significant change in the thermophysical properties of the fuel. Hence, the heat transfer rate and the pressure drop deviate from those of the single-phase condition. This feature also impacts the design of the heat exchanger. A detailed heat exchanger design for an LH2 heat exchanger has been conducted by the AHEAD partner Pratt & Whitney Rzeszów S.A. [97], whereas, the design of the LNG heat exchanger has been conducted by the research group in TU Delft [98]. To minimize the pressure loss, three units of the heat exchanger are considered such that the mass flow rate entering each unit is lower.

### 4.3.2 The heat exchanger effectiveness

Although the heat exchanger design follows a physical process of a typical two-phase flow heat exchanger design, in the engine performance calculation, it is convenient to consider the characteristics of a Heat Exchanger (HEX) from the effectiveness point of view such that it can be easily implemented both for design and off-design analysis.

The definition of the HEX effectiveness is given by the ε-NTU method presented in [99]. It is the ratio of the actual heat flux of two mediums to the maximum heat flux available. In the current heat exchanger case, the heat capacity of air is lower than that of the cryogenic fuel, and the minimum temperature the air flow can reach is the inlet temperature of the cryogenic fuel (LNG or LH2). However, the mass flow rate of the cryogenic fuel is much lower than that of the air. Eventually, the maximum heat flux is confined to the minimum enthalpy change of the two fluids as given in Eqn. (15),

$$q_{max} = min\left\{\dot{m}_a \cdot \left(h(T_{t3}) - h\left(T_{i\_cryo}\right)\right), \dot{m}_{cryo} \cdot \left(h(T_{t3}) - h\left(T_{i\_cryo}\right)\right)\right\} \tag{15}$$

Where $h$ represents the specific enthalpy; the subscript 3 indicates the inlet condition of the air, and $i\_cryo$ indicates the cryogenic fuel at the inlet;

After identifying the maximum heat flux, the thermal effectiveness of the heat exchanger can be defined by a ratio between the actual heat flux to the maximum heat flux as seen in Eqn.(16),

$$\varepsilon = \frac{q}{q_{max}} = \frac{\dot{m}_{cryo}\cdot\left(h(T_{e\_cryo})-h(T_{i\_cryo})\right)}{\dot{m}_a\cdot\left(h(T_{t3})-h(T_{i\_cryo})\right)} = \frac{\dot{m}_a\cdot(h(T_{t3})-h(T_{t32}))}{\dot{m}_a\cdot\left(h(T_{t3})-h(T_{i\_cryo})\right)} \quad (16)$$

where the subscript *32* indicate the exit condition of the bleed air; $e\_cryo$ indicates the cryogenic fuel at the exit.

### 4.3.3 The off-design characteristics of the heat exchanger

The off-design performance of the CHEX is simulated by a heat exchanger map as shown in Figure 4.12. In this map, the heat exchanger effectiveness is defined as a function of bleed air mass flow rate and the cryogenic fuel flow rate. As the engine operating condition changes, the quantity of the bleed air and the fuel flow differ from the design condition. The corresponding heat exchanger effectiveness can be obtained by looking up the given map. After knowing the heat exchanger effectiveness, the temperatures of the bleed air and the fuel at the exit of the heat exchanger can be calculated by reforming Eqn. (16).

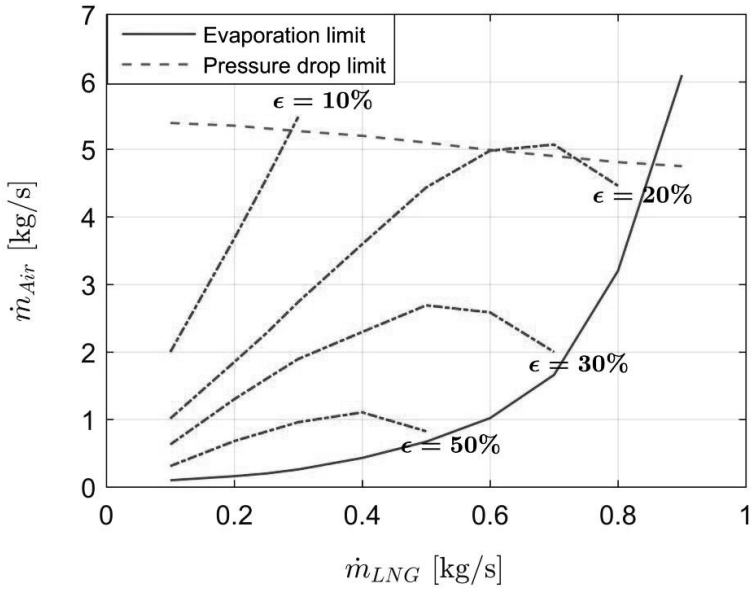


*Figure 4.12: Example of the LNG-air heat exchanger map*

## 4.4 The emission prediction module

This section elaborates the module for emission prediction purpose. As introduced earlier, the emissions from aviation have drawn significant public attentions. It has become one of the essential criterions to assess the performance of an aircraft system. Therefore, at the conceptual design phase, the importance of considering a low emissions system is emphasized.

### 4.4.1 Overview of the aero engine emissions

Fuel is injected into the combustor and mixed with the incoming air. After burning this mixture, ideally, emissions of $CO_2$, $H_2O$, $N_2$, $O_2$ and SOx (due to impurity of the fuel) are emitted. However, due to uncompleted combustion, the real combustion emissions would include more species on top of the ideal combustion emissions. These extra species are Unburnt Hydro Carbon (UHC), CO, NOx ($NO+NO_2$). This process is depicted in Figure 4.13.

These emissions contribute to the climate change in terms of affecting the Radiative Forcing (RF). The term RF is a measure of the importance of a potential climate change mechanism. It expresses the perturbation or change to the energy balance of the earth-atmosphere system in watts per square meter ($W/m^2$). Positive values of radiative forcing imply a net warming while negative values imply cooling [3]. To understand the effects of various emission species, at the first place, the quantity of each emission should be predicted.

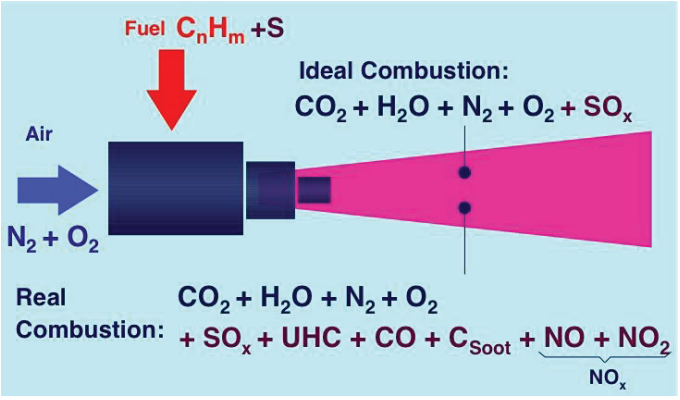


*Figure 4.13: Aircraft emissions (Figure source: http://adg.stanford.edu/aa241/emissions/emissions.html)*

Among various emissions species, the most effort is made to predict the NOx emission due to its complex formation mechanism. The thermal NOx dominates the NOx emission in aero-engines. It increases exponentially with the increase in the

peak combustion temperature above 1800 K. Several parameters, including the combustor local equivalence ratio, the residence time, the species concentration, and the temperature, are responsible for the NOx emission. Different empirical or semi-empirical equations can be found in the literature. For example, in Lefebvre's model in [100], a semi-empirical NOx emission prediction model has been given, where the NOx emission depends on combustion chamber volume, stoichiometric flame temperature, primary zone temperature, and combustor inlet pressure. Apart from those empirical correlations, Rizk and Mongia in [101] simulate different combustion zones by a number of reactors combined with a detailed chemical kinetic mechanism. This way a number of equations for the NOx prediction are formulated. In this approach, the effects of equivalence ratio and residence time are addressed. Some more NOx emission prediction models can be found in [102, 103],

Correlations are often derived under certain operating conditions, beyond which they might fail in predictions. For example, the gas composition at the inlet of the ITB differs from that of the first combustor, which leads to different formations of the NOx emissions. Moreover, the NOx formed in the first combustor might dissociate in the ITB, hence changing the NOx emitted eventually. Therefore, in the current research, an in-house emission prediction module developed by the research group in TU Delft has been used. Different tools for the conventional RQL combustion technique with pure kerosene and for the hybrid combustion system are considered. They structure of the module is introduced in the following paragraphs.

### 4.4.2 Emission prediction for conventional combustion

The aim of the current tool is to predict the combustion products of a gas turbine at various given operating conditions and given combustor geometry. A conventional RQL combustion technique is considered. The AeroComb developed by Shakariyants in [104] is used to calculate the geometry. This emission prediction tool uses multi-reactor networks. The reactors are created using Cantera's reactor networks [105]. Cantera is a free suite of an object-oriented software tool to deal with problems involving thermodynamics or chemical kinetics. A Cantera file contains information about the phase and composition of gasses, and reactions taking place in the reaction mechanism. It can be applied to model Perfectly Stirred Reactors (PSR), where all the gases are assumed to be homogeneously mixed. By creating an interactive network between different single reactors, a multi-reactor network is formed in a certain way to represent a gas turbine combustor reaction model. The setup of reactors is depicted in Figure 4.14

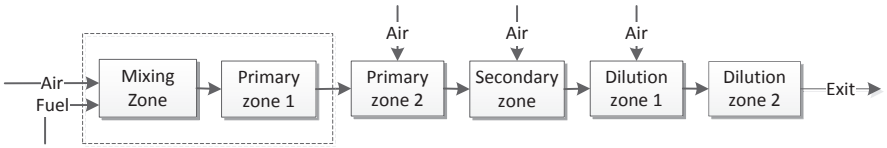


*Figure 4.14: Multi-reactor setup.*

The entire combustor contains three combustion zones, i.e. the primary zone (divided into two subsections), the secondary zone, and the dilution zone (divided into two sections). In addition, a mixing zone is placed before the primary zone. The combustor volume is calculated beforehand based on different operating conditions. By specifying equivalence ratios in different combustion zones, the air split ratio can be determined.

Kerosene is a complex fuel containing petroleum byproducts in which the dominant mass fractions are of higher hydrocarbon. Chromatograph of kerosene shows the presence of components ranging from butane to tricosane. The average chemical formula varies from $C_{10.9}H_{22}$ to $C_{12}H_{23}$. There is a variance of composition in kerosene from one source to another, and this has led to several surrogate compounds being proposed for kerosene by different researchers. Surrogates can be a mix representing the overall physical property of kerosene or chemical surrogate representing the chemical property. The mixture describing both these properties is called as comprehensive surrogates. Alkane part of surrogate fuels is well represented by n-Decane and few other compounds; however, the major problem lies with oxidation of aromatic cyclic hydrocarbons. The kerosene reaction is a complex one involving hundreds of species and reactions [106]. The complicated set of reactions occurring between free hydrogen atoms and aromatic hydrocarbons lead to the formation of soot, which is a very important emission to be predicted. In general, the prediction of emissions like NOx and CO is strongly dependent on the temperature and flow field, which are strongly dependent on the kinetics of reacting species. For the current study the Aachen Surrogate containing 77.7% n-Decane and 22.3% n-Propyl Benzene is used. This mechanism has been developed and tested at TU Aachen by Honnet et al [107] and consists of 119 species and 527 reactions. To predict the emissions, a detailed chemical reaction mechanism is required. Depending on the initiative conditions, different chemical reactions are activated. The combustion reactor has been validated with respect to an existing CF6 engine.

### 4.4.3 Emission prediction for the hybrid combustion system

The combustion system in the hybrid engine is a unique state-of-art. Design and analysis of this combustion system are of great importance. For the AHEAD project this development was carried out for the LH2 combustor at TU Berlin [60] and flameless combustor at Technion, Israel. Figure 4.15 shows the layout of this

combustion system, where the first combustion chamber is the hydrogen combustor and the second combustion chamber is the flameless combustor with a semi-bubble shape for the flow recirculation reason.

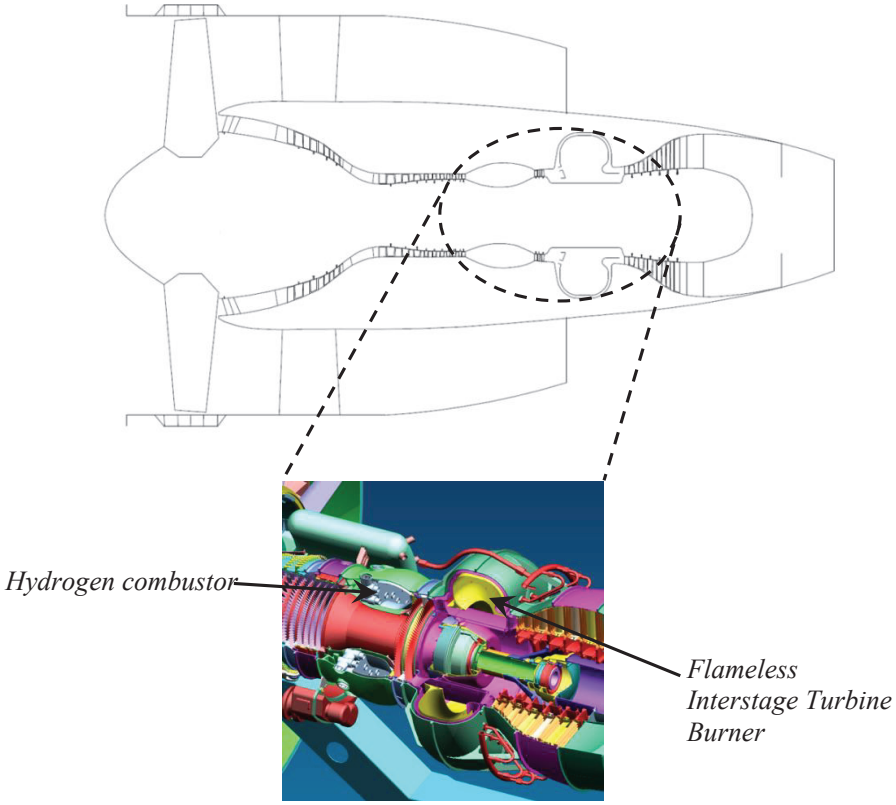


*Figure 4.15: Overview of the hybrid sequential combustion chamber (Courtesy: Pratt & Whitney Rzeszów).*

To assess the emissions produced by these two combustors, a reactor network has been constructed under the AHEAD framework in Chemkin®. A schematic of this network is shown in Figure 4.16. The inlet flow is split in the ratio of 80:20 for combustion and liner cooling respectively. The first reactor network has a single recirculation zone, which represents the flame attached recirculation at the center of the combustion chamber. The second combustion chamber is represented by two recirculation zones, one of which is the central recirculation zone while the other one corresponds to the smaller recirculation zone formed on the right side corner of the fuel exit. The reaction mechanism given by Honnet et al. [107] has been used for the simulation. It consists of 527 reactions and 163 species. The reaction mechanism is validated for the residence time and the variation in species with different experimental studies. The reactor network has been validated using the available

experimental data and the CFD results [108]. This rector network is then utilized to predict emissions of the hybrid engine. The more information on the hybrid combustion system has been presented by Rao, et.al in [108].

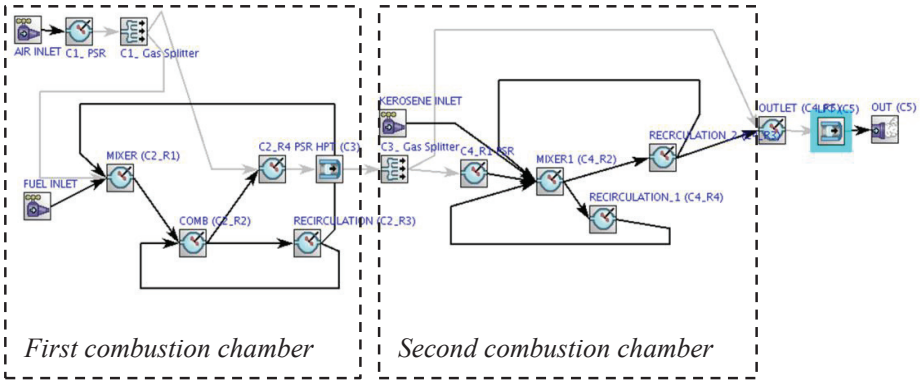


*Figure 4.16: Reactor network of the hybrid combustion system [108].*

## 4.5 Optimizer module

The purpose of this module is to perform optimizations with respect to different objectives and constraints. There are different numerical optimization algorithms. It is common practice to use the gradient-based method to optimize linear problems, whereas, the non-gradient based methods are often used to solve problems with non-linear characteristics. In this thesis, the MATLAB® optimization toolbox using genetic algorithm is applied [109]. Proper population size, the number of generations, the rate of crossover or mutation, and selection criteria are selected according to sensitivity analysis results. The genetic algorithm can deal with a variety of problems whether the objective function is linear or nonlinear, stationary or non-stationary, continuous or discontinuous [110, 111].

### 4.5.1 Single objective optimization definition

In this thesis, a single objective optimization framework is considered. A typical single objective optimization function can be constructed following the procedure from the Eqn. (17) - (20),

$$F(X) \tag{17}$$

Subject to

$$X \subset [L, U] \tag{18}$$

$$g_i(x) \leq 0, i = 1,2,\cdots,m \tag{19}$$

$$c_j(x) = 0, j = 1,2,\cdots,p \tag{20}$$

where $F(X)$ is the objective function (cruise TSFC in this thesis); $g(x)$ are inequality constraints; $c(x)$ are equality constraints; $X$ is the argument vector (consists of engine cycle design parameters, for instance, the engine OPR, TIT, BPR, FPR, etc.), which is bounded by the upper and lower constraints vectors $L$ and $U$. This upper and lower bounds form a design space for a specific engine design problem. Depending on the constraints, different engine cycle can be optimized within the design space.

### 4.5.2 Optimization constraints

The constraints considered for the optimization is presented in Table 4.1. They are defined with respect to the cycle efficiency, the thermal limits, the mechanical limits, and emissions. Increasing the BPR not only improves the engine propulsive efficiency but also enlarges the fan diameter. The consequent effects are multifold: firstly, a bigger fan increases the nacelle drag, hence, more thrust is required, which increases the engine fuel consumption; secondly, a bigger fan tends to create more fan noise. To reduce the fan tip noise, the LP shaft speed has to decrease, increasing the number of the LPT stages. As a result, the engine becomes heavier, increasing the fuel consumption. Therefore, an upper limit for the BPR is defined following the BPR development trend in Figure 2.4.

The OPR is limited due to three reasons. 1) It prevents the exit temperature of the compressor from exceeding the material limits; 2) The higher the OPR is, the smaller the blade size of the HPC last stage will be. As the blade height is smaller, the tip clearance loss becomes dominant, which penalizes the HPC efficiency. Detailed analysis of tip clearance effects has been performed in Ref. [112]. Ref. [113] gives an empirical equation to correct the HPC stage efficiency based on the actual last stage blade height. 3) According to the NOx emission prediction correlations discussed in the literature, the combustor inlet temperature and pressure play important roles in the NOx emission formation.

The HPT inlet temperature is another constraint. Conventionally, this parameter is limited by the maximum metal temperature of the turbine. As the sophisticated turbine cooling is applied, this temperature becomes progressively increasing as already discussed in Figure 2.7. However, the turbine efficiency deteriorates severely as the turbine cooling increases, which might cancel out the cycle efficiency gain by the high TIT. Moreover, the NOx emission is another factor in constraining the maximum TIT.

*Table 4.1: Technology requirements and constraints*

| *Parameters* | *Description* | *Comments* |
|---|---|---|
| BPR | Maximum | To minimize the installation penalty<br>To restrict the fan noise |
| OPR | Maximum | Confined by compressor material limits<br>To reduce the NOx emission<br>Confined by the HPC last stage efficiency |
| Tt4 | Maximum | To reduce the NOx emission<br>Confined by the turbine material limits<br>To minimize the HPT cooling |
| ITB energy fraction | Maximum | To minimize the negative effects on the cycle efficiency by the application of an ITB |
| Tt46 | Maximum | To minimize the LPT cooling |

The ITB energy fraction in this thesis represents the energy input of the ITB with respect to the total energy consumption of the dual combustors, as defined in Eqn. (21),

$$ITB\ energy\ fraction = \frac{energy_{itb}}{energy_{mainCC}+energy_{itb}} = \frac{\dot{m}_{f2}\times LHV_{f2}}{\dot{m}_{f1}\times LHV_{f1}+\dot{m}_{f2}\times LHV_{f2}} \quad (21)$$

where the subscripts $f_1$ and $f_2$ represent the first combustor fuel and the second combustor fuel respectively; in case of the hybrid engine, $f_1$ is cryogenic fuel, and $f_2$ is kerosene; $mainCC$ is the short name of the "main combustion chamber". The ITB energy fraction of 0 indicates that the ITB is switched off. Increasing the ITB energy fraction results in more energy injected in the ITB, hence less fuel consumption from the first combustor. This is beneficial to mitigate the volume requirement in case cryogenic fuels are used in the first combustor. However, a higher ITB energy fraction penalizes the thermal efficiency of the engine cycle.

The LPT inlet temperature is defined as a function of the HPT inlet temperature and the ITB energy fraction. In a conventional engine setup, this temperature is determined by the upstream work done by the engine high pressure system. There is no way to control this parameter alone. However, due to the implementation of the ITB in the hybrid engine, this parameter becomes adjustable. According to the research advancement in material, it is very likely that in the next 2-3 decades the turbine maximum metal temperature will reach 1300 deg. C [114]. Hence, a maximum temperature of 1500 K is given to minimize the LPT cooling.

## 4.6 Overall structure of various modules

Each module described above is inter-related following the way as presented in Figure 4.17. The single objective optimization framework has been conceived to minimize the engine cruise Thrust Specific Fuel Consumption (TSFC). The cooling fraction is estimated at the Hot-day take-off condition via the turbine cooling module. The final engine cycle is obtained when the turbine cooling scheme converged. Later, the engine performance module executes the performance calculations at various operating points, the output of which can be further applied for the emission calculation if necessary.

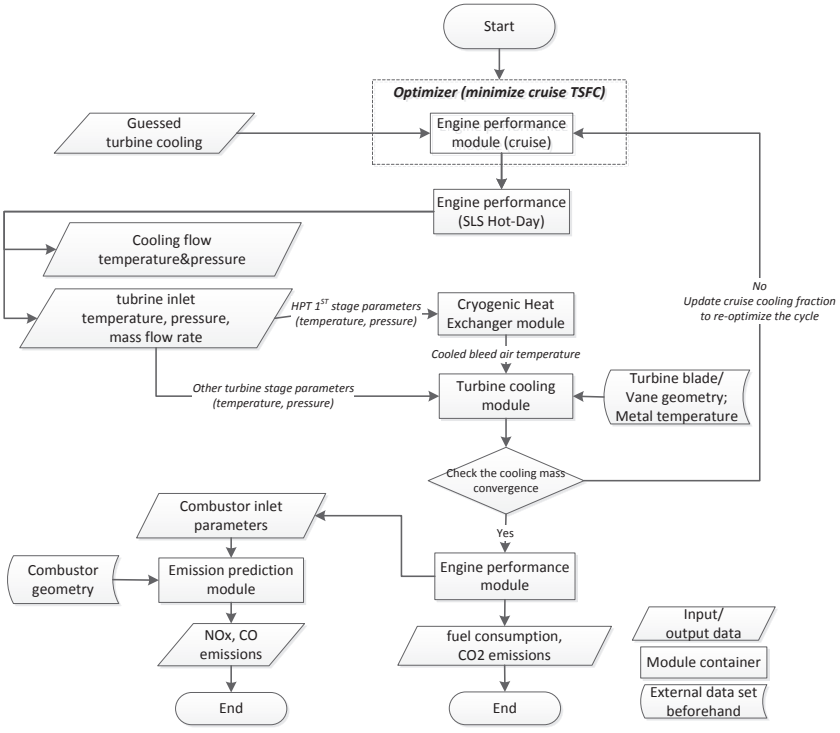


*Figure 4.17: Overview of the model structure*

## 4.7 State-of-art technology definition

This section identifies the state-of-art technology reflected at the component level. The non-isentropic compression or expansion happens due to the irreversibility of a process. The losses caused by this process can be defined by component efficiencies (either isentropic or polytropic efficiency). Any change of these parameters can influence the overall cycle performance. Neglecting these effects, one can easily overestimate the engine performance. In Table 4.2 different component performance

variables considered in the hybrid engine cycle are presented. The corresponding notations and datum values are also displayed.

*Table 4.2: Component performance parameters*

| *Component* | *Performance parameter* | *Notation* | *Datum value* | *Unit* |
|---|---|---|---|---|
| Fan | Polytropic efficiency | $\eta_{fan}$ | 93 | % |
| Geared Box | Gear ratio | GR | 4/2.5 | [-] |
| LPC | Polytropic efficiency | $\eta_{LPC}$ | 93 | % |
| HPC | Polytropic efficiency | $\eta_{HPC}$ | 91 | % |
| Main combustor | Combustion efficiency | $\eta_{CC}$ | 99.7 | % |
| | pressure ratio | $\pi_{CC}$ | 0.95 | [-] |
| HPT (uncooled) | polytropic efficiency | $\eta_{HPT}$ | 93 | % |
| ITB | Combustion efficiency | $\eta_{ITB}$ | 99.7 | % |
| | pressure ratio | $\pi_{ITB}$ | 0.97 | [-] |
| LPT (uncooled) | Polytropic efficiency | $\eta_{LPT}$ | 92.5 | % |
| HP shaft | Mechanic efficiency | $\eta_{mHPT}$ | 99.5 | % |
| LP shaft | Mechanic efficiency | $\eta_{mLPT}$ | 99.3 | % |
| Bypass duct | Pressure loss | $\Delta p_t/p_{tin}$ | 2 | % |

The heat added in the ITB is maintained intentionally lower than that in the main combustor to minimize the penalties in the cycle thermal efficiency. Therefore, the pressure loss of the ITB is defined 2% lower than that of the main burner. The mechanic efficiency of the LP shaft is defined taking the loss by the geared fan system into account. The bypass duct pressure loss is 2% of the fan bypass exit total pressure. Therefore, a higher FPR would also increase the duct pressure loss. The HPT uncooled polytropic efficiency is 0.93. Depending on the amount of cooling required, the actual HPT polytropic efficiency is derived. The same methodology holds for the LPT efficiency calculation with an uncooled LPT polytropic efficiency of 0.925 as a baseline. Moreover, to realize the ultra high bypass ratio, a geared fan system is considered in the future turbofan engine. Although for engine performance, no major changes would occur, the gear ratio of 4 is still considered to make the entire system complete. On the other hand, the gear ratio of geared contra-rotating fans system is assumed as 2.5. If not mentioned specifically, values provided in this table are utilized as baselines for later cycle calculations.

Additionally, since the LHV of the LH2 and LNG are different from that of the kerosene. To enable a fair comparison, the TSFC of the hybrid engine is redefined as in Eqn. (22), where the mass flow rate of the cryogenic fuel is normalized into the equivalent mass flow rate of kerosene with respect to the energy content.

$$TSFC = \frac{(\dot{m}_{cryofuel} \times LHV_{cryofuel})/LHV_{kerosene} + \dot{m}_{kerosene}}{FN} \tag{22}$$

## 4.8 Summary

This chapter gives an overview of the model framework. An engine performance module, a turbine cooling prediction module, a Cryogenic Bleed Air Cooling System module, a generic emission prediction module, and an optimizer module are elaborated. In addition, the baseline component efficiencies are also specified for the later analysis. In the following chapters, depending on the objectives of analysis, relevant modules will be applied with necessary modifications.

# Chapter 5 Characteristics of an ITB turbofan engine

The multi-fuel hybrid engine is built upon the basis of an ITB engine configuration due to its multi-fuel capacity with two combustion chambers. Therefore, before going for the complete analysis of the hybrid engine, this chapter is dedicated to investigating the applicability of an ITB turbofan engine for a single fuel. A Very High Bypass Ratio (VHBPR) turbofan engine representing the future state-of-art engine technology is considered as a baseline. Accordingly, a contemporary engine with an ITB is derived.

In the first part of this chapter, a parametric analysis is performed. By varying one or two design variables at a time, the effect of the individual parameter on the engine performance are studied. Furthermore, the ITB engine performance is optimized with respect to the ITB energy fraction defined in section 4.5.2 to ensure the minimum fuel consumption at cruise condition. Finally, the effects of the ITB on the turbine cooling air and the NOx emissions are evaluated. The engine performance module, the turbine cooling module, and the emission prediction module for the conventional combustion technique are involved in this chapter.

## 5.1 Engine configuration

By extrapolating the development trend of various engine design parameters discussed in Chapter 2, an imaginary VHBPR turbofan engine with a geared system representing the state-of-art technology in the year 2025-2030 is created as a baseline (named as advanced GTF). Accordingly, a contemporary engine with an ITB (named as Geared Interstage Turbine Burner (GITB) turbofan) is originated. Both engine layouts are displayed in Figure 5.1. The upper part of the figure is the GITB engine, whereas, the bottom part is the advanced GTF. Due to the implementation of an ITB, it is expected that the ITB engine would be slightly longer than the single combustor engine. The rest of the engine remains unchanged. The station number is defined in Table 5.1. The LPT inlet or the ITB exit is defined as the station 46.

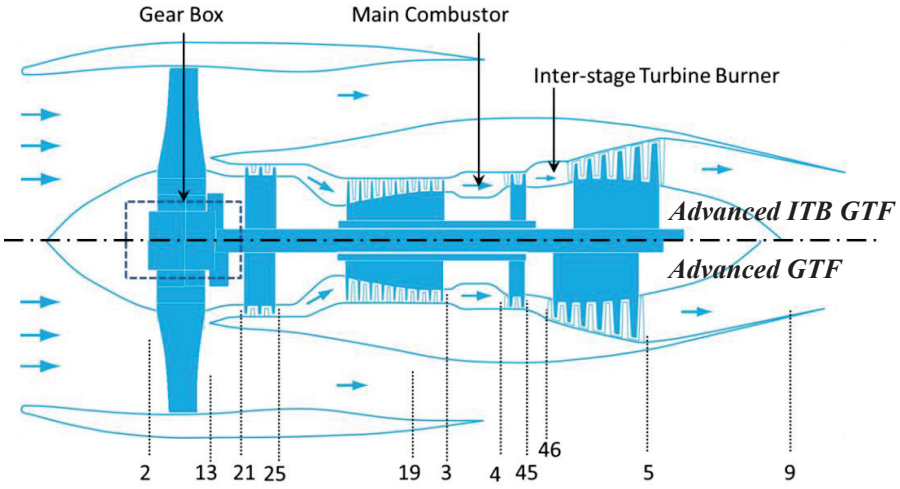


*Figure 5.1: Engine configuration comparison*

*Table 5.1: Engine station number definition*

| ***Station number*** | ***Description*** |
|---|---|
| 2 | Fan inlet |
| 21 | Fan core exit |
| 25 | LPC exit |
| 3 | HPC exit |
| 4 | Combustor exit |
| 45 | HPT exit |
| 46 | LPT inlet/ITB exit |
| 5 | LPT exit |
| 9 | Core nozzle exit |
| 13 | Fan bypass exit |
| 19 | Bypass nozzle exit |

## 5.2 Parametric analysis

Parametric analysis is performed to understand the effects of several key parameters on the engine performance. The component efficiencies in Table 4.2 are used. The datum values of design variables given in Table 5.2 are obtained from an optimized ITB engine cycle at cruise. The analysis is carried out over a specified range of each parameter with the rest remain at the datum value. The International Standard Ambient (ISA) condition at an altitude of 11 kilometers is considered, and the flight Mach number is 0.85, if not mentioned otherwise. For the sake of simplicity, the turbine cooling is not considered in this analysis, meaning that the uncooled turbine efficiency is applied in all cases.

*Table 5.2: Datum value of design variables at cruise*

| *Variables* | *Notation* | *Datum value* | *Unit* |
|---|---|---|---|
| Fan pressure ratio | FPR | 1.44 | [-] |
| Bypass Ratio | BPR | 15 | [-] |
| LPC pressure ratio | LPCPR | 5 | [-] |
| HPC pressure ratio | HPCPR | 9.69 | [-] |
| Overall pressure ratio | OPR | 70 | [-] |
| HPT inlet temperature | Tt4 | 1689 | K |
| ITB energy fraction | ITB energy fraction | 0.1 | [-] |

At this point, the efficiencies defined in Chapter 2 are reformatted to help the later analysis. In Chapter 2, the performance of an engine cycle has been defined by the total efficiency, which is a product of the thermal efficiency and the propulsive efficiency. As a turbofan engine is concerned, it is convenient to reformat the thermal efficiency defined in Eqn. (1) to Eqn.(23), which is again the product of the engine core efficiency ($\eta_{core}$) and the transfer efficiency ($\eta_{tr}$).

$$\eta_{th} = \eta_{core} \times \eta_{tr} \tag{23}$$

With the introduction of the transfer efficiency, a hypothetical station is made in the LPT when the power of the LPT has just driven the core section of the fan and the LPC, yet not powered the bypass section of the fan. This allows us to account for the losses when extracting the power from the LPT to raise the pressure of the bypass stream of the fan. In other words, the transfer efficiency describes the quality of the energy transferred from the core stream to the bypass. It is subject to the mechanical efficiency of the LP shaft, the efficiency of the LPT, the efficiency of the bypass section of the fan, the pressure loss through the bypass duct, etc. The core efficiency is the ratio that the energy available after the hypothetical station to the energy provided by the fuel.

The definition of the propulsive efficiency in Eqn. (2) still remains the same. Accordingly, the total efficiency in Eqn. (3) is modified into Eqn.(24)

$$\eta_{tot} = \eta_{core} \times \eta_{tr} \times \eta_{prop} \tag{24}$$

### 5.2.1 The effects of FPR and BPR

The first group to be evaluated is the FPR and BPR. The variations in the propulsive efficiency, the thermal efficiency, and the overall efficiency are studied and presented in Figure 5.2-Figure 5.4. The propulsive efficiency indicates how efficiently the available kinetic energy is converted into the thrust power. A higher propulsive efficiency implies lower residual kinetic energy in the jet wake. Therefore, it is a common practice to improve the propulsive efficiency by reducing the jet velocity. In a turbofan engine, the FPR and BPR have large effects on the jet velocity.

In Figure 5.2, the propulsive efficiency first increases as the FPR increase until it reaches the maximum. Then the propulsive efficiency starts reducing with the further increase in the FPR. Furthermore, this maximal value occurs at a lower FPR, when the BPR increases. The reasons are as below. The fan is driven by the LPT. Increasing the FPR requires more energy to be transferred from the core to the bypass stream; therefore, the core jet velocity reduces. Meanwhile, the jet velocity of the bypass increases. At the lower FPR, the average jet velocity reduces with the FPR increase; therefore, the propulsive efficiency is still improved. Until a certain value of the FPR is reached, beyond which the increase in the bypass jet velocity is dominant hence the averaged jet velocity increases again. The propulsive efficiency at this FPR is the maximum, and the corresponding FPR is the optimum FPR. Furthermore, the optimal FPR reduces as the BPR increases.

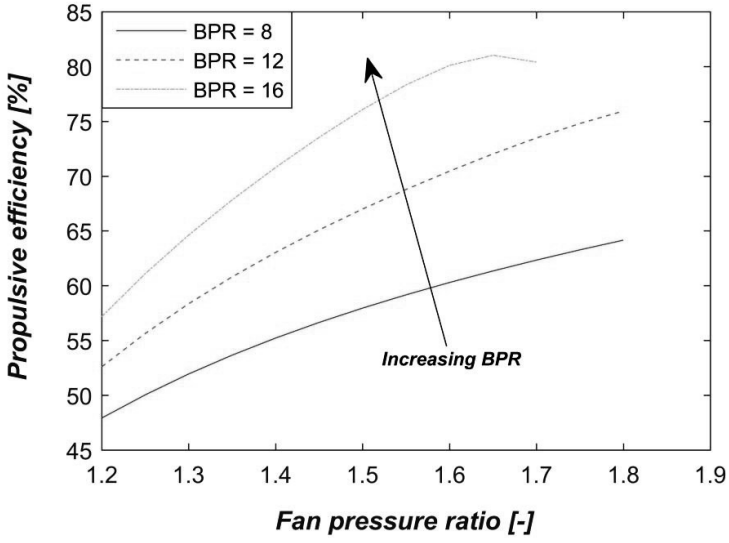


*Figure 5.2: Variation in propulsive efficiency versus FPR and BPR*

Figure 5.3 illustrates how the thermal efficiency varies with respect to the FPR and the BPR. Since in this study, the OPR and TIT remain unchanged, the core efficiency is therefore also constant. Accordingly, the variation in the thermal efficiency of the current study would be mainly due to the transfer efficiency. For a given BPR, the maximum transfer efficiency can be obtained at a particular FPR. Furthermore, the transfer efficiency decreases as the BPR increases.

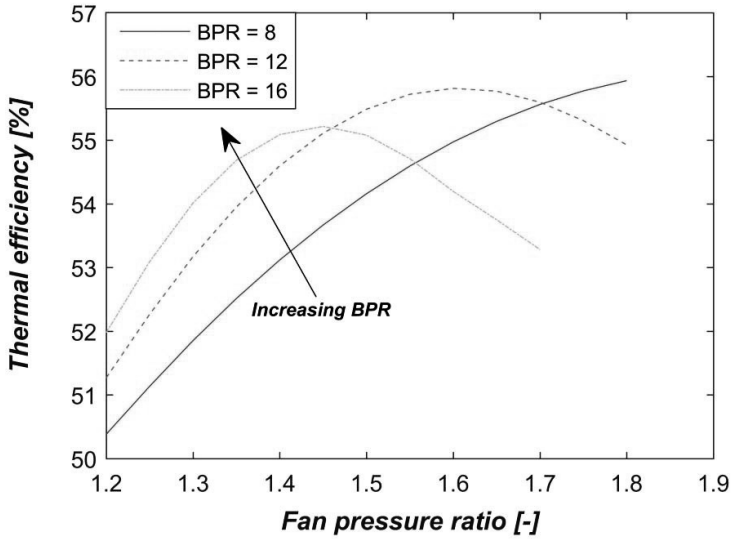


*Figure 5.3: Variation in thermal efficiency versus FPR and BPR*

As a product of the propulsive efficiency and the thermal efficiency, the overall efficiency in Figure 5.4 shows similarities as the propulsive efficiency. The higher BPR eventually helps to improve the overall efficiency of the engine cycle. Therefore, the general trend in the BPR development follows the continuous increment and this increment trend will very likely remain in future. The birth of the GTF engine has shown some evidence in this perspective.

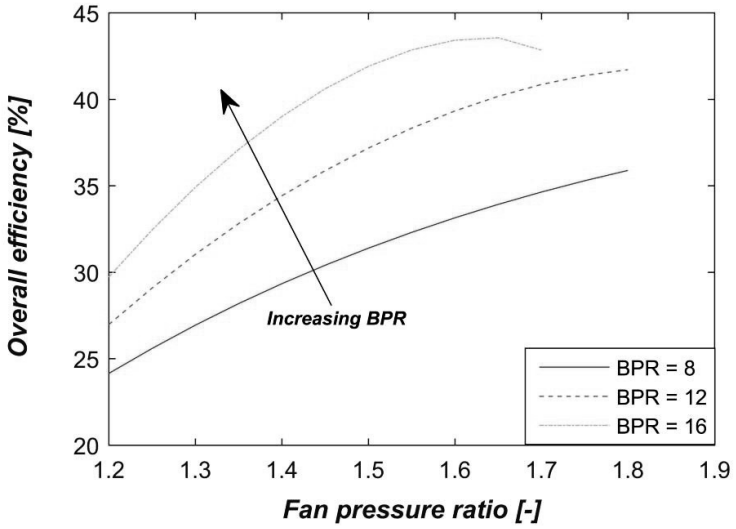


*Figure 5.4: Variation in overall efficiency versus FPR and BPR*

### 5.2.2 The effects of OPR and HPT inlet temperature

The OPR and HPT inlet temperature are dominant parameters on the gas generator performance. In this section, the analysis focuses on the effects of these two parameters. The comparison is made between the baseline engine (GTF) and the GITB (ITB energy fraction = 0.1). The variations of the thermal efficiency and the specific thrust are studied. In Figure 5.5, the cycle indicated by the solid line is the baseline engine cycle, whereas, the dashed line represents a classical turbofan cycle. The two cycles exhibit similar tendencies. For a given HPT inlet temperature, an optimal OPR corresponds to the maximal thermal efficiency can be observed. As the HPT inlet temperature increases, both thermal efficiency and the optimal OPR increase accordingly. Furthermore, the specific thrust of both engines always increases with increasing the HPT inlet temperature regardless to the OPR. Moreover, one can also observe that the cycle of the ITB engines overall exhibits the higher specific thrust but lower thermal efficiency. It proves that thermodynamically, an ITB engine is less efficient, but it enables a reduction in engine size smaller by improving the specific power.

Moreover, it should be noted that the current analysis has not taken into account the variations in the HPT efficiency due to the HPT cooling effect. As the ITB engine requires less turbine cooling air, which enables the HPT working more efficiently. Hence, the magnitude of the thermal efficiency increases would be even higher than the current value.

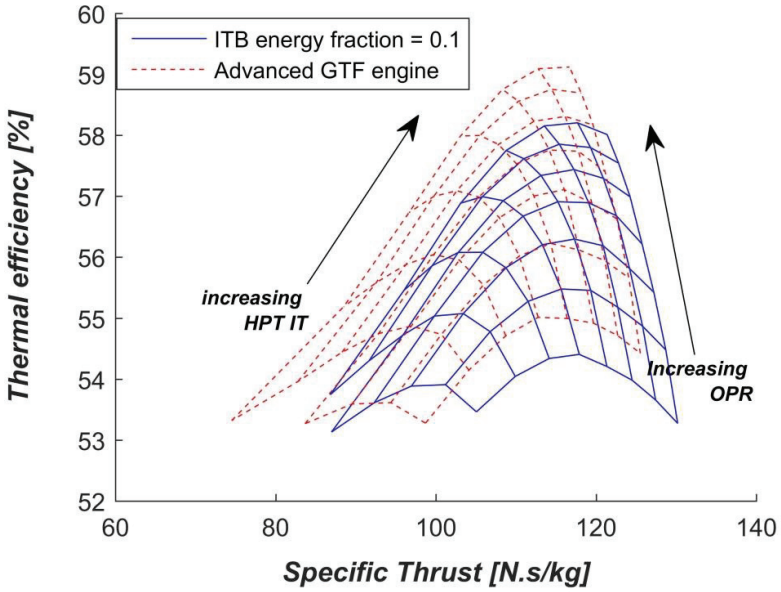


*Figure 5.5: Comparison of thermal efficiency and Specific thrust between two cycles*

### 5.2.3 The effects of the ITB energy fraction

The analysis above has been focused on the given ITB energy fraction of 0.1. In this section, the effects of the ITB on the engine performance will be studied.

In Figure 5.6, the variation of the thermal efficiency with respect to the FPR is illustrated again but versus different ITB energy fractions. Increasing the ITB energy fraction results in the higher temperature and velocity of the exhaust gas, implying the more exhaust heat loss and the residual kinetic energy. Therefore, the thermal efficiency reduces. Moreover, the optimal FPR increases with the ITB energy fraction increases. This is because the optimal FPR, in fact, corresponds to an optimal velocity ratio between the bypass jet and the core jet ($V_{j18}/V_{j8}$). At this optimal velocity ratio, the power transferred from the core to the bypass is maximal. Increasing the ITB energy fraction causes an increase in the core jet velocity. Therefore, the FPR has to increase such that the bypass jet velocity increases proportionally to maintain the optimal velocity ratio.

On the other hand, the propulsive efficiency reduces as the ITB energy fraction increases. This can be observed from Figure 5.7. The propulsive efficiency is inversely proportional to the average jet velocity, which increases as the ITB energy fraction increases. Therefore, at the higher ITB energy fraction, the propulsive efficiency is lower.

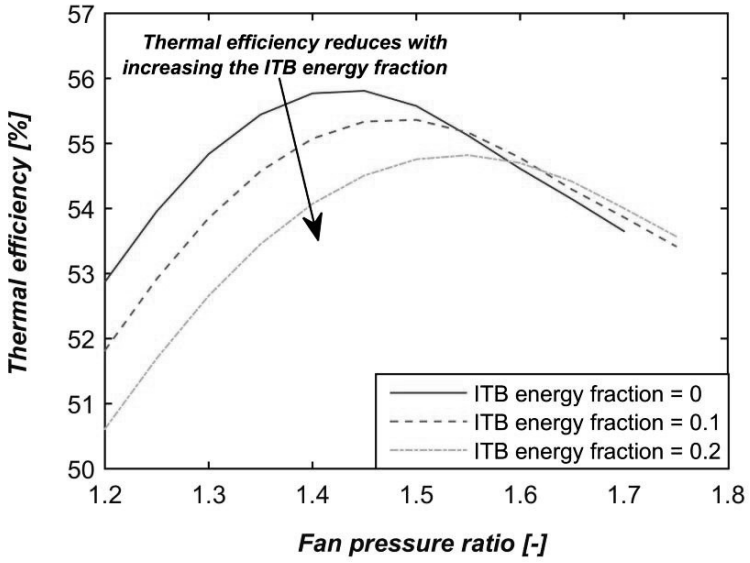


*Figure 5.6: Variation in thermal efficiency versus FPR at various ITB energy fractions.*

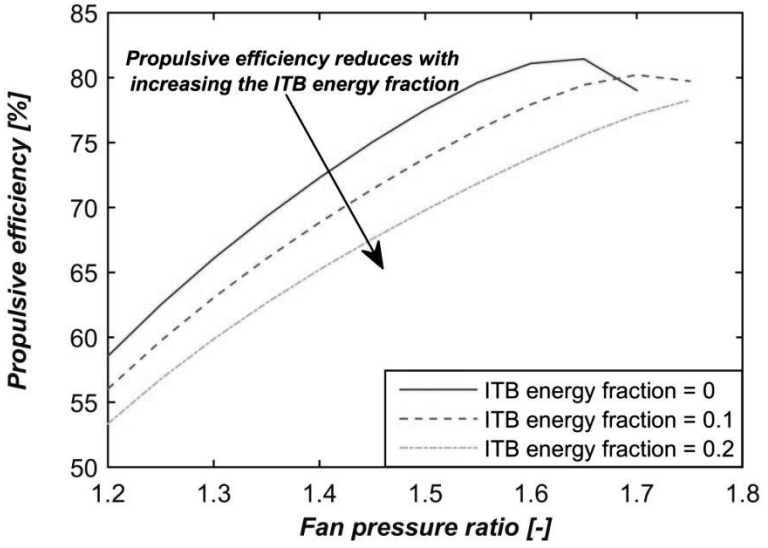


*Figure 5.7: Variation in propulsive efficiency versus FPR at various ITB energy fractions.*

The following study focuses on the variation in the engine performance with respect to the HPT inlet temperature ($T_{t4}$). Various ITB energy fractions are considered. The rest of the cycle parameters remain constant as in Table 5.2. In Figure 5.8, the variation of the TSFC with respect to the $T_{t4}$ is presented. One can see that there is a minimum TSFC at each ITB energy fraction and the minimum TSFC increases as the ITB energy fraction increases. Nevertheless the $T_{t4}$ value corresponding to the minimum TSFC reduces as the ITB energy fraction increases. This will be beneficial when the $T_{t4}$ increases significantly to realize the very high OPR cycle, which inevitably results in the increase in the NOx emissions. Under such circumstances, if one still attempts to maintain the very high OPR, using an ITB would be an option to prevent the NOx emissions from violating the limits.

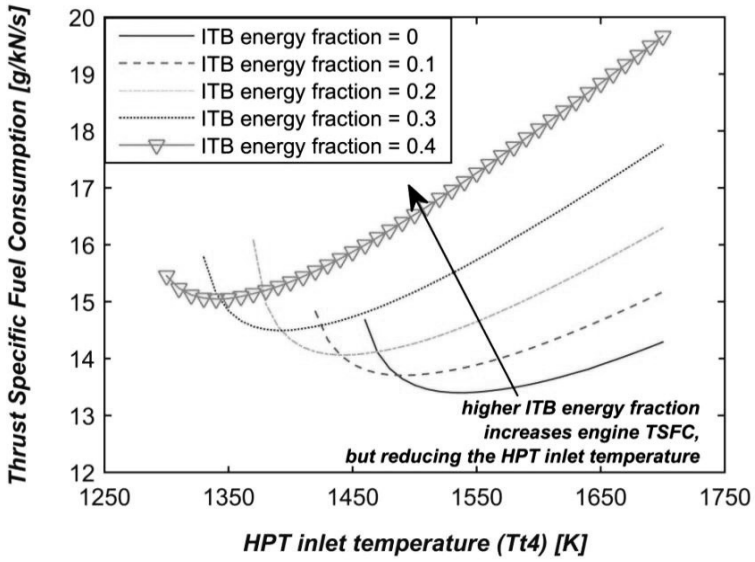


*Figure 5.8: Variation in Thrust Specific Fuel Consumption (TSFC) versus HPT inlet temperature at various ITB energy fractions.*

In Figure 5.9, the variation in the Specific Thrust (ST) with respect to the $T_{t4}$ at the various ITB energy fractions is displayed. First, the ST increases significantly as the ITB energy fraction increases at a given $T_{t4}$. This is also the reason why some researchers suggest the ITB engine as an alternative of a military engine, the design philosophy of which differs from a commercial aircraft engine. However, another tendency can be observed from Figure 5.9 is that if the ST is maintained unchanged, the $T_{t4}$ decreases progressively as the ITB energy fraction increases. This helps to reduce the turbine cooling air requirement.

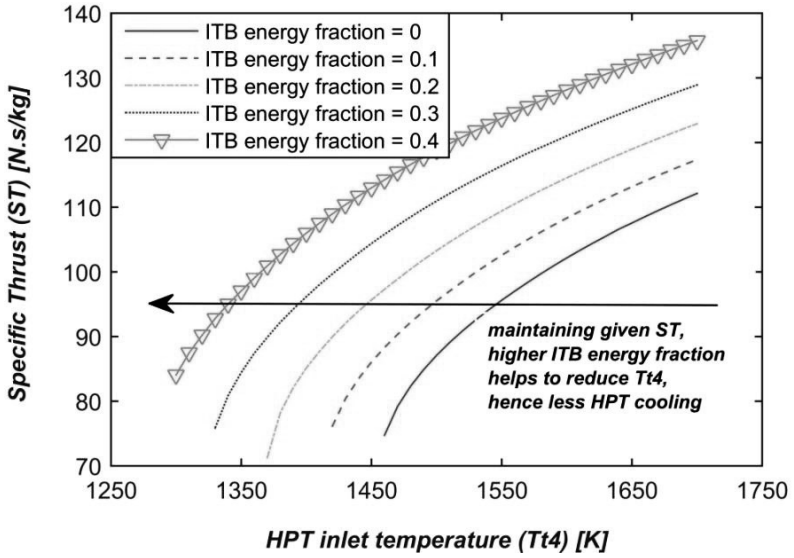


*Figure 5.9: Variation in Specific Thrust versus HPT inlet temperature at various ITB energy fractions.*

Both the Figure 5.8 and the Figure 5.9 tell that the HPT inlet temperature of an ITB engine can be much lower than that of a single combustor engine. This discovery is beneficial to reduce the turbine cooling air requirement and the NOx emissions. However, it is no way to avoid the penalty in the thermal efficiency. Nevertheless, it is possible to reduce the loss associated with the application of an ITB.

### 5.2.4 Sensitivity analysis of component efficiencies

In the previous analysis, the efficiencies of all components have been kept constant. In this section, a sensitivity analysis is performed to understand the effects of component efficiencies on a given engine cycle. All the design parameters in this analysis are constant as presented in Table 5.2. In this analysis, the component efficiency is increased by 1%, whereas, the pressure loss (indicated by $\Delta$PR) is decreased by 1%. Accordingly, the relative change in the specific fuel consumption and the specific thrust are shown in Figure 5.10.

The improvement in component efficiencies and the reduction in pressure losses are always helpful to improve the thermal efficiency, among which the most significant contribution is by reducing the pressure loss through the bypass duct followed by the improvement in the outer fan efficiency and the LPT efficiency. All these three terms are directly associated with the transfer efficiency. The improvement in any of these variables increases the transfer efficiency hence the

thermal efficiency of the cycle. Compared to the LP system, the components of the HP system mainly influence the core efficiency of a given cycle. Moreover, the improvement in the component efficiencies results in the reduction in propulsive efficiency mainly because the jet velocity increases. Since the increase in thermal efficiency is more substantial than the reduction in the propulsive efficiency, the overall efficiency increases eventually. Furthermore, the specific thrust increases for this given engine cycle.

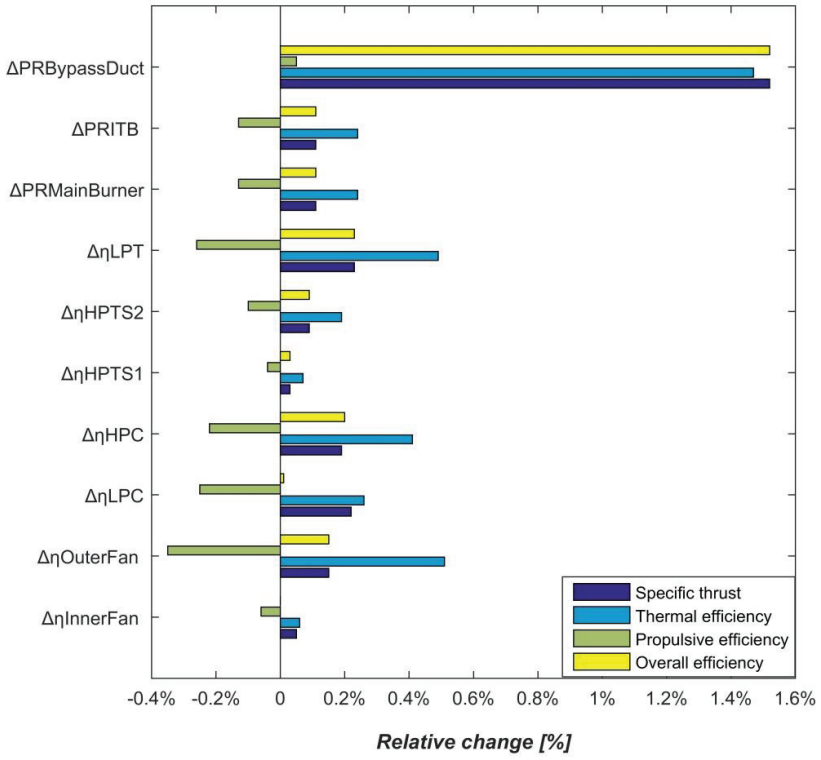


*Figure 5.10: The relative change in the cycle efficiency and the specific thrust resulted from 1% increase in component efficiency or 1% decrease in the pressure loss for a given GITB engine cycle.*

## 5.3 Cycle optimization

In this section, the cycle optimization is performed at the cruise condition. Considering a long haul aircraft, the fuel consumption at cruise contributes the most to the entire mission; therefore, the optimization is performed at cruise to minimize the cruise TSFC. The SLS hot-day condition is derived accordingly, where the effects of the ITB on the turbine cooling and the NOx emissions are evaluated. The

MATLAB fmincon optimizer [115] using Sequential Quadratic Programming (SQP) algorithm is implemented. Fundamentals of the SQP algorithm has been thoroughly discussed by Nocedal and Wright in [116].

### 5.3.1 Engine performance optimization

The thrust requirement at different operating conditions is provided in Table 5.3. The cruise condition is defined at the altitude of 11 km and the Mach number of 0.85. The maximum rated thrust of the engine is considered as the same with GEnx [1]. The baseline component efficiencies defined in Table 4.2 are applied. Depending on the turbine cooling air fraction, the cooled turbine efficiency is extrapolated from the curve represented by *thesis eff.* in Figure 4.11.

*Table 5.3: Engine performance requirement*

| | ***Altitude [km]*** | ***Mach number [-]*** | ***Ambient condition*** | ***Thrust [kN]*** |
|---|---|---|---|---|
| Cruise | 11 | 0.85 | ISA | 47 |
| SLS | 0 | 0 | ISA+15 K | 300 |
| TOC | 11 | 0.85 | ISA | 59 |

The same design space is defined for the advanced GTF engine and the advanced GITB engine, as given in Table 5.4. Optimization is executed with respect to ITB energy fraction (defined in Eqn. (21)) varying from 0 to 0.4. The inlet mass flow rate remains constant such that the engine size remains unchanged. This results in a constant specific thrust.

*Table 5.4: Bounds and constraints of design parameters.*

| ***Bounds of design parameters*** | | ***Constraints*** | |
|---|---|---|---|
| FPR | [1.2, 1.8] | OPR | <= 70 |
| LPC pressure ratio | [1.4, 5.0] | FN, [kN] | = 47 |
| HPC pressure ratio | [10, 20] | Inlet mass flow | Constant |
| Tt4, [K] | [1400, 1900] | | |
| BPR | [8, 15] | | |
| ITB energy fraction | [0, 0.4] | | |

The optimized engine cycles are presented in Table 5.5. The BPR of each engine reaches the upper limit to maximize the propulsive efficiency of the engine. Moreover, for constant OPR, the pressure ratio distribution between LPC, HPC is identical in all cases. The LPC pressure ratios of all engine cycles reach their maximum limit. This is explained from two aspects. At the lower ITB energy

1 http://www.geaviation.com/commercial/engines/genx/

fraction, the HPT inlet temperature is higher, which requires a large amount of HPT cooling. Considering the deterioration of turbine efficiency due to cooling, the HPT efficiency becomes much lower than that of the later stage LPT efficiency. Therefore, the optimizer tends to reduce the work output by the HPT such that the incurred loss can be minimized. This turbine work distribution is modified by increasing the LPC pressure ratio while reducing the HPC pressure ratio. Ultimately, the LPC pressure ratio reaches its upper limit. When the ITB energy fraction increases further, the optimizer tends to follow the path of increasing the ITB operating pressure by reducing the HPC pressure ratio. Lower HPC pressure ratio results in the reduction of HPT power output. This way the HPT exit or the ITB inlet pressure is higher. This is beneficial from the engine efficiency standpoint. Eventually, the LPC pressure ratio turns out always reach its upper limit.

*Table 5.5: Engine optimization results at cruise.*

| ***Design parameters*** | ***ITB energy fraction*** | | | |
|---|---|---|---|---|
| | 0 | 0.1 | 0.2 | 0.3 |
| BPR | 15 | 15 | 15 | 15 |
| FPR | 1.44 | 1.44 | 1.44 | 1.44 |
| LPCPR | 5 | 5 | 5 | 5 |
| HPCPR | 9.69 | 9.69 | 9.69 | 9.69 |
| HPT IT [K] | 1900 | 1689 | 1540 | 1431 |
| LPT IT [K] | 1177 | 1182 | 1190 | 1202 |

### 5.3.2 The effects of the ITB on turbine cooling

Figure 5.11 presents the variation in TSFC, HPT cooling fraction, and LPT cooling fraction for various ITB energy fractions. It shows that the HPT cooling fraction reduces substantially as the ITB energy fraction increases. This is due to the reduction in the HPT inlet temperature shown in Figure 5.12. The LPT inlet temperature increases slightly and has no cooling requirement. Furthermore, the higher HPT efficiency due to the lower HPT cooling requirement compensates the deterioration in the thermal efficiency by the ITB. It can be observed from Figure 5.11 that the increase in the cruise TSFC is less than 1% at the ITB energy fraction below 0.15. As the ITB energy fraction increases further, the negative effect of the ITB on the cycle thermal efficiency becomes increasingly dominant, thereby increasing the TSFC.

Figure 5.13 illustrates variations in the thermal efficiency and the propulsive efficiency versus the ITB energy fraction. Since the specific thrust remains unchanged, the propulsive efficiency also remains constant. However, due to the low operating pressure of the ITB, the engine thermodynamic efficiency deteriorates with increasing ITB energy fraction. Therefore, the overall efficiency reduces as the

ITB energy fraction increases. As discussed previously, this efficiency penalty is negligible at lower ITB energy fraction but becomes significant as the ITB energy increases.

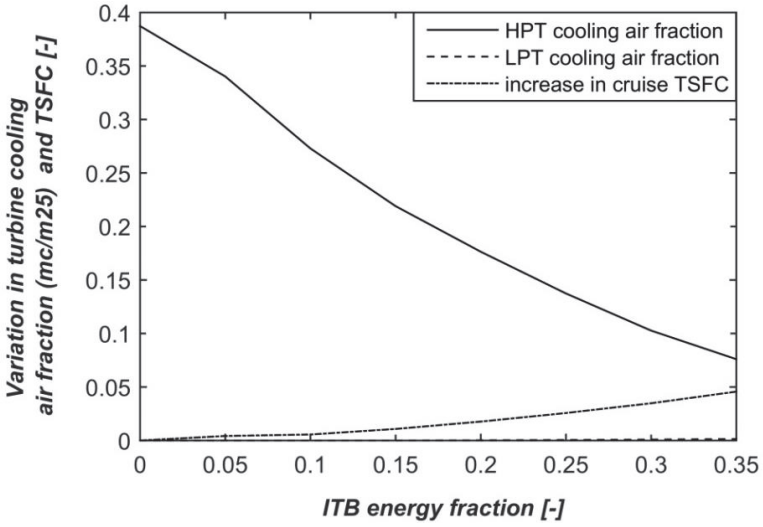


*Figure 5.11: Variation in turbine cooling air and TSFC versus the ITB energy fraction.*

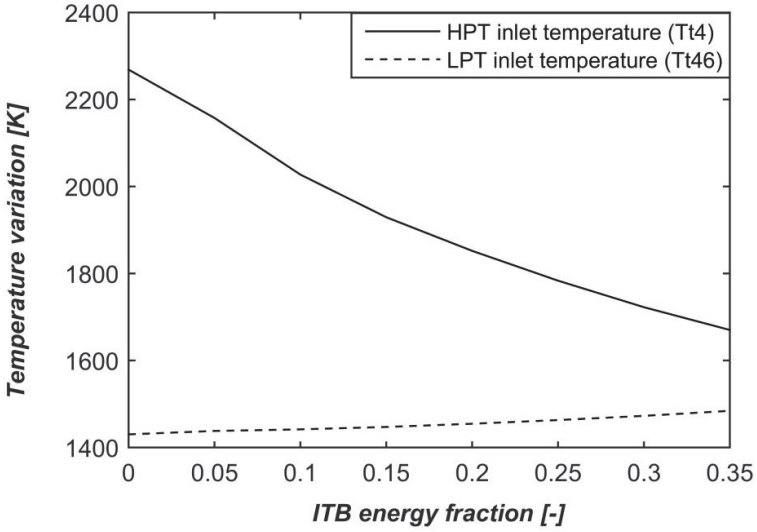


*Figure 5.12: Variation in TITs at SLS versus the ITB energy fraction.*

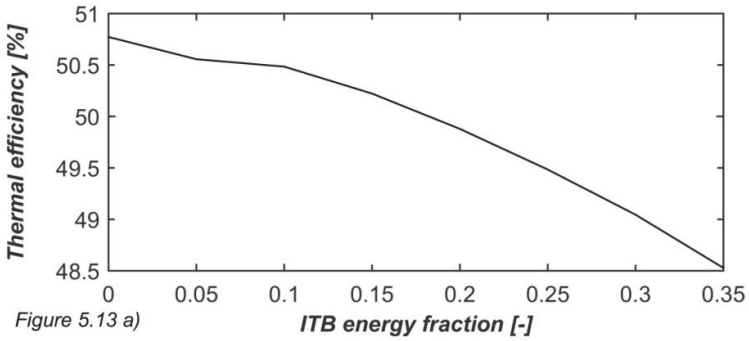


Figure 5.13 a)

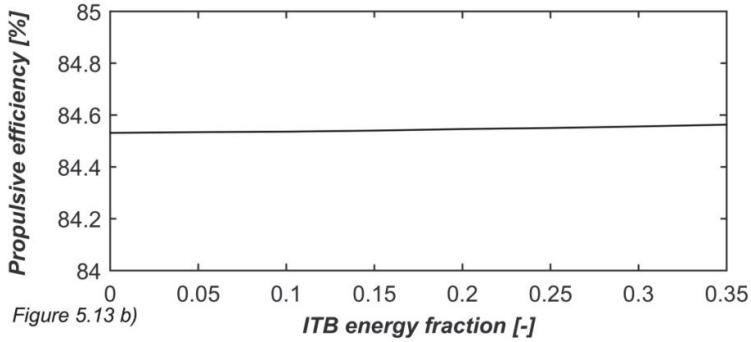


Figure 5.13 b)

*Figure 5.13: a) Variation in the thermal efficiency at cruise; b) Variation in the propulsive efficiency at cruise*

### 5.3.3 The effects of ITB on NOx emissions

The effects of the ITB on the NOx emissions are studied at the SLS hot day condition. The engine performance data is obtained from the previous section. The reactor setup presented in Figure 4.14 is applied. To calculate the NOx emissions, each combustor inlet conditions, including the pressure, temperature, and mass flow rate are required. The quantity of fuel burnt in each combustor is also an input parameter. Values of the corresponding parameters are given in Table 5.6.

*Table 5.6: Inputs for the NOx prediction*

| ***Input parameters*** | ***ITB energy fraction*** | | | |
|---|---|---|---|---|
| | 0 | 0.1 | 0.2 | 0.3 |
| $T_{t3}, K$ | 1049 | 1049 | 1049 | 1049 |
| $p_{t3}, Bar$ | 66.65 | 66.60 | 66.55 | 66.51 |
| $\dot{m}_3, kg/s$ | 46.83 | 55.58 | 62.93 | 68.49 |
| $\dot{m}_{f1}, kg/s$ | 1.98 | 1.8 | 1.62 | 1.45 |
| $T_{t45}, K$ | 1422 | 1353 | 1284 | 1214 |
| $p_{t45}, Bar$ | 16.14 | 15.76 | 15.22 | 14.52 |
| $\dot{m}_{45}, kg/s$ | 78.44 | 78.24 | 78.03 | 77.79 |
| $\dot{m}_{f2}, kg/s$ | 0 | 0.2 | 0.41 | 0.62 |

Figure 5.14 presents the variation in the NOx emissions against the ITB energy fraction. The baseline engine is the advanced GTF engine. It shows that the NOx emissions of the GITB engine are always lower. Depending on the ITB energy fractions, the reduction rate in the NOx emissions varies. The reduction in the NOx emissions is due to two reasons. On one hand, as the ITB energy fraction increases, the heat addition in the main combustor is less, which helps to reduce the NOx emissions. On the other hand, due to the re-burning process in the ITB, the NOx formed in the first combustor dissociates again in the ITB, hence reducing the total NOx emitted. Overall, the NOx emissions decrease as the ITB energy fraction increases. Constrained by the maximum ITB energy fraction of 0.4 defined beforehand, the reduction in the NOx emissions is about 30%.

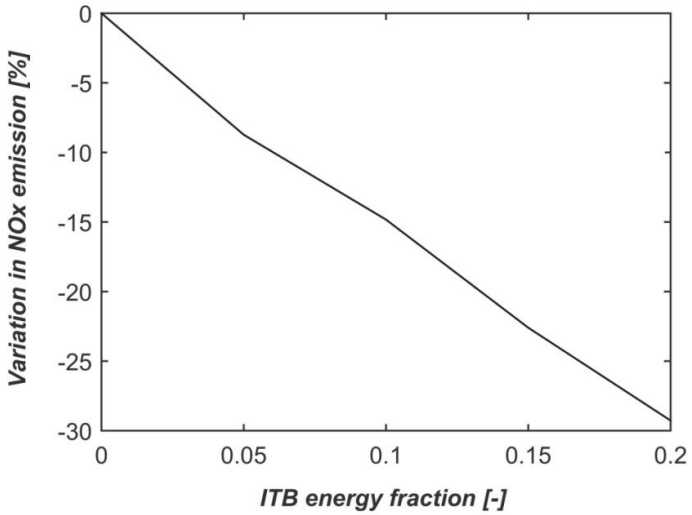


*Figure 5.14: Variation in the NOx emissions compared to the advanced GTF engine.*

## 5.4 Summary

This chapter investigates the characteristics of an Interstage Turbine Burner (ITB) engine. By defining the ITB energy fraction as the ratio of the additional heat of the ITB to the total thermal energy consumed, different engine cycles with or without an ITB can be realized. Overall, the thermal efficiency of ITB engine is worse than a normal turbofan engine. The parametric analysis shows that the optimal FPR of the ITB engine is higher than that of a classical engine. Moreover, the HPT inlet temperature reduces as the ITB energy fraction increases to maintain the identical specific thrust. This reduces the turbine cooling air by more than 50%. As a consequence, the penalty in the turbine efficiency reduces, which compensates the deterioration in the thermal efficiency by using an ITB. Furthermore, the reduction in the HPT inlet temperature helps to reduce the NOx emissions. The optimization performed in the later analysis of this chapter confirmed the benefits in this aspect. One can see that challenges and opportunities co-exist in ITB engines. If a proper configuration is selected, there is a large potential for using the ITB configuration to mitigate the environmental impact by the civil aviation. The AHEAD multi-fuel hybrid engine tends to follow this path. The further assessment of the multi-fuel hybrid engine is performed in the following chapters.

# Chapter 6 Characteristics of the multi-fuel hybrid engine

In chapter 3, the features of a novel multi-fuel hybrid engine concept have been elaborated. In this chapter, a thorough analysis is performed to investigate the characteristics of the multi-fuel hybrid engine. The analysis focuses on four aspects. Firstly, the parametric analysis is performed to study the effects of alternative fuels and the CBACS on the hybrid engine performance. The second part of this chapter is dedicated to optimizing the hybrid engine at cruise condition. The optimized engine performance is evaluated with respect to baseline engines. In the third part, the optimized engine is verified at the selected critical operating points. Finally, a mission analysis is performed based on a specific hybrid engine design. In the mission analysis, the performance of the MFBWB along with the hybrid engine is evaluated in terms of the energy consumption and emissions.

## 6.1 Characteristics of fuel sources

According to the predictions on the future aviation fuel sources in section 2.4.2, the fuel candidates can be classified into two categories. They are cryogenic fuels and liquid hydrocarbon fuels, among which the LNG, LH2, kerosene, and biofuels are considered in the hybrid engine. The arrangements of these fuels are illustrated in Figure 6.1. The cryogenic fuels are used in the first combustor, whilst, the normal liquid hydrocarbon fuels are used in the ITB. Since biofuels and kerosene share similar characteristics, kerosene can be substituted by biofuels without causing significant side effects on the engine performance. Hence, the analysis of the later contents mainly focuses on the fuel combinations of LH2-kerosene and LNG-kerosene.

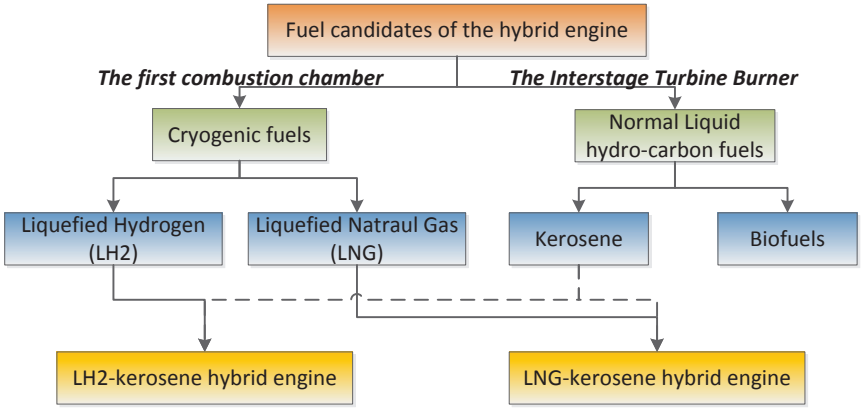


*Figure 6.1: Fuel combinations of the hybrid engine*

The relevant characteristics of kerosene, LNG, and LH2 are presented in Table 6.1. First of all, the chemical composition (C/H) differs significantly from each other, which directly affects the $CO_2$ emission. For instance, the C/H of LNG (0.25) is nearly half of that of kerosene (0.52), implying a 25% reduction in $CO_2$. Whilst, LH2 contains no carbon; therefore, the $CO_2$ can be eliminated by using hydrogen. Secondly, from the energy density point of view, the LHV of LNG is slightly higher than that of kerosene, whereas, the LHV of LH2 is more than doubled to kerosene and LNG. Therefore, to release the same amount heat, the mass flow of hydrogen would be the lowest, which helps to reduce the take-off weight of the aircraft. Nevertheless, the densities of both LNG and LH2 are lower, especially, the density of LH2 is merely 1/10 of kerosene. This extremely low density enlarges the fuel storage volume dramatically. On top of the larger volume requirement, the boiling temperatures of LNG and LH2 are substantially low. To prevent them from boiling off, an efficient insulation system would be appreciated. This insulation layer causes an extra increment in the storage volume, which aggravates the aerodynamic penalties. A preliminary analysis of the effects of LH2 on the volume and weight for a given mission is presented in Appendix A.

*Table 6.1: Fuel characteristics.*

| | ***Kerosene*** | ***LNG*** | ***LH2*** |
|---|---|---|---|
| Chemical formula | $C_{12}H_{23}$ | $CH_4$ | $H_2$ |
| Density $[kg/m^3]$ | 790-808 | 423 | 71 |
| C/H ratio | 0.52 | 0.25 | 0 |
| Lower Heating Value $[MJ/kg]$ | 42.8 | 50 | 120 |
| The Boling temperature at 1 $atm$ $[K]$ | 440 | 120 | 23 |

## 6.2 Parametric analysis

The design parameters of the hybrid engine are the FPR, BPR, OPR, the HPT inlet temperature, and the ITB energy fraction. The OPR is a product of the inner FPR, the LPC pressure ratio, and the HPC pressure ratio. The effects of the FPR, BPR, HPT inlet temperature, etc. have been studied in the previous chapter. The following study is mainly devoted to the hybrid engine performance with respect to the alternative fuels and the CBACS. The performance of the CBACS is represented by the effectiveness of the CHEX.

### 6.2.1 Effects of the alternative fuels

An optimized GITB engine using only kerosene at an ITB energy fraction of 0.1 is provided in Table 6.2 as the datum. The turbine cooling air is not considered in this analysis. Substituting kerosene in the first combustor of the GITB engine by LNG, an LNG-kerosene hybrid engine is formulated. The same fact is valid for the LH2-

kerosene hybrid engine. The cycles of these three engines are compared in Figure 6.2.

*Table 6.2: Design variables of the hybrid engine.*

| ***Variables*** | ***Notation*** | ***Datum value*** | ***Unit*** |
|---|---|---|---|
| Fan pressure ratio | FPR | 1.5 | [-] |
| Bypass ratio | BPR | 15 | [-] |
| LPC pressure ratio | LPCPR | 4 | [-] |
| HPC pressure ratio | HPCPR | 10.8 | [-] |
| Overall pressure ratio | OPR | 65 | [-] |
| HPT inlet temperature | Tt4 | 1689 | K |
| ITB energy fraction | ITB energy fraction | 0.1 | [-] |

Compared to the GITB kerosene engine, the thermal efficiency and specific thrust of the LNG-kerosene hybrid engine and the LH2-kerosene hybrid engine are improved. This behavior can be explained from the following perspectives: according to the analysis performed in [117], the isobaric heat capacity of the combustion products increases as the C/H reduces. This implies burning LNG or LH2 would yield the combustion products with the higher isobaric heat capacity. Therefore, to produce the required amount of the HPT power, the HPT expansion ration of the multi-fuel hybrid engine is less. This results in the higher ITB inlet temperature and pressure. Since the pressure at the ITB inlet is higher, the ITB combustion is more efficient. As a result, the deterioration in cycle thermal efficiency due to low combustion pressure of the ITB can be reduced slightly. Hence, it can be concluded that burning fuels with low C/H help to improve the thermal efficiency of the hybrid engine cycle. Moreover, the expansion ratio of LPT in the LH2-kerosene and the LNG-kerosene hybrid engine is also less. Therefore, the available kinetic energy increases to produce higher thrust.

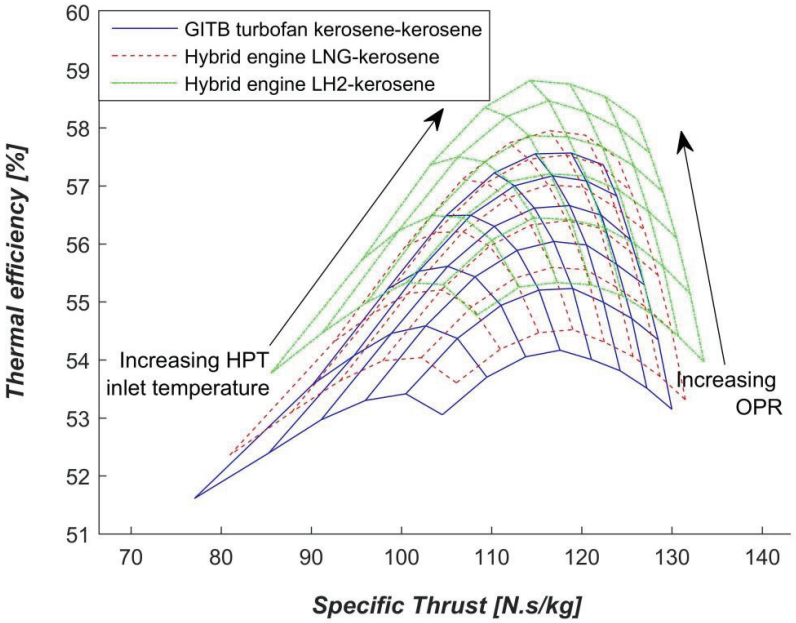


*Figure 6.2: Fuel effects on the engine cycle.*

### 6.2.2 Effect of Cryogenic Bleed Air Cooling System

The study in this section attempts to demonstrate the effects of the CBACS on the hybrid engine performance. The performance of the CBACS is represented by the effectiveness of the Cryogenic Heat Exchanger (CHEX) as defined in Chapter 4. The results of the LNG-kerosene and the LH2-kerosene hybrid engine are displayed independently.

#### 6.2.2.1 The LNG-kerosene hybrid engine

The analysis firstly identifies the effect of the CBACS on the turbine cooling quantity. This is performed at the SLS hot-day condition with respect to various ITB energy fractions at the given CHEX effectiveness. The baseline engine is an LNG-kerosene ITB engine without the CBACS. The discussions in Chapter 5 have illustrated that the reduction in the turbine cooling air can be facilitated by a reheat cycle under specific conditions (as described in Chapter 5). This feature is confirmed again by the solid curve of the baseline engine presented in Figure 6.3 b), where the turbine cooling air fraction ($\dot{m}_c/\dot{m}_{25}$) declines from 17% to about 5% as the ITB energy fraction varies from 0 to 0.3. When the CBACS is applied, the further reduction in turbine cooling air can be obtained at each given ITB energy fraction. The figure shows a 50% reduction in the turbine cooling air with the CHEX

effectiveness of 0.3. This is achieved mainly due to the reduction in the bleed air temperature, seen from Figure 6.3 a). The bleed air temperature reduces sharply along with the increase in the CHEX effectiveness. The reduction rate varies from 200 K at the effectiveness of 0.3 to about 600 K at the effectiveness of 0.7. Moreover, the Figure 6.3 b) shows that although a further reduction can be achieved by increasing the heat exchanger effectiveness to 0.5, the reduction rate is less substantial. In addition, one can see that curves in Figure 6.3 b) tend to converge with the increase in the ITB energy fraction. This gives an indication that the CBACS becomes less effective as the absolute turbine cooling air fraction decreases.

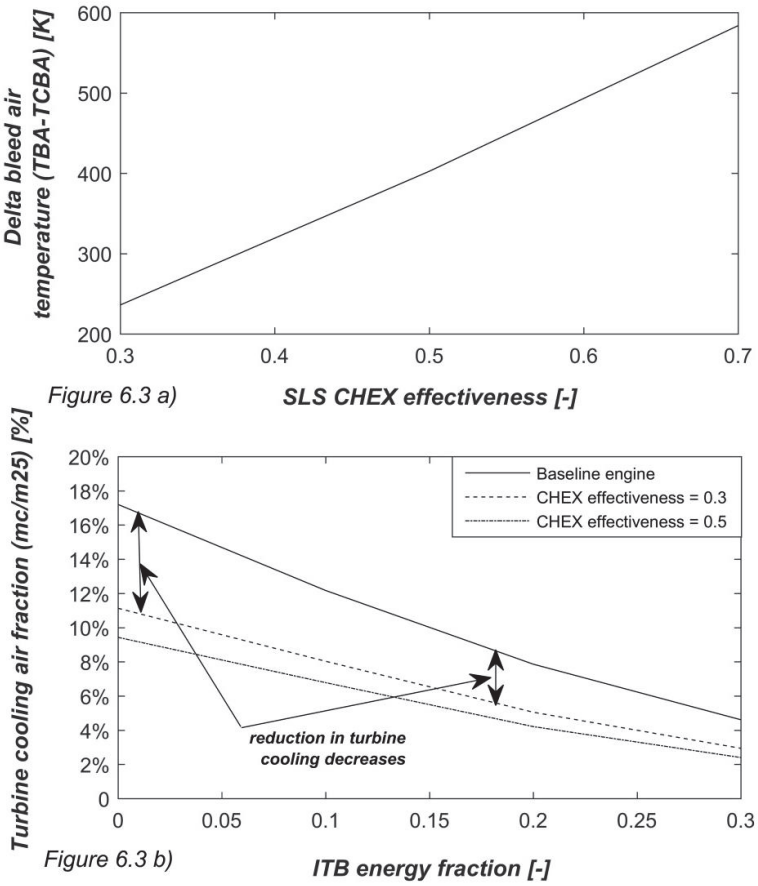


*Figure 6.3: a) Reduction of the bleed air temperature versus the heat exchanger effectiveness (TBA is the original Bleed Air temperature; TCBA is the Cooled Bleed Air temperature); b) Variation in turbine cooling air fraction.*

The effectiveness of CHEX at the SLS condition determines the turbine cooling air fraction, which is then applied to cruise condition. With the effectiveness of

CHEX at cruise known, the corresponding fuel temperature and the associated changes in the cycle performance are estimated. As one may have noticed, the role of the CHEX effectiveness varies at different operating conditions. Therefore, the design point of the CHEX has to be determined carefully such that the improvement in the cycle performance is maximized. Following this thought, a matrix consisting of the CHEX effectiveness at both cruise and SLS is composed. Correspondingly, a matrix containing the fuel temperature can be derived, with which the cycle performance at cruise is re-identified.

In Figure 6.4, the variation of the LNG temperature is presented in the coordinate of the SLS and cruise CHEX effectiveness varying from 0.3 to 0.7. The color bar represents the increment in the LNG temperature with the unit of Kelvin. The minimum temperature increment occurs at the right bottom corner of Figure 6.4, where the SLS CHEX effectiveness is maximal, and the cruise CHEX effectiveness is minimal. From Figure 6.3 a), it can be seen that the maximum SLS CHEX effectiveness allows the most reduction in the bleed air temperature; hence, the turbine cooling air under such circumstance is lowest. When this low turbine cooling air fraction is applied at cruise with lowest CHEX effectiveness assumed, the increment in fuel temperature becomes least. The maximum increase in the fuel temperature is at the maximum CHEX effectiveness.

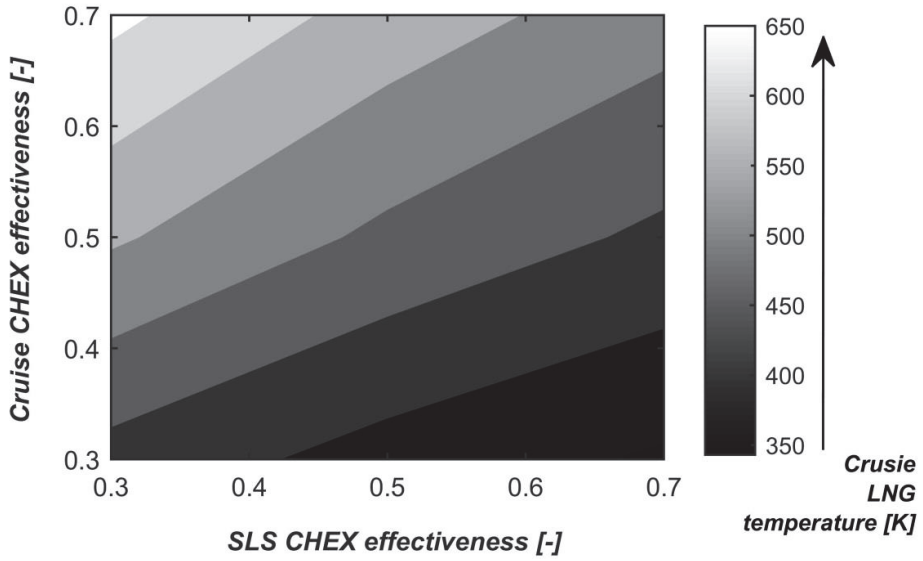


*Figure 6.4: Variation in cruise LNG temperature at ITB energy fraction of 0.1*

The corresponding thermal efficiency is presented in Figure 6.5. The variation is with respect to a baseline engine excluding the CBACS. The color bar indicates the variation margin. The minimum increase is about 1% in accordance with the lowest

fuel temperature increase. The most increase is more than 2% corresponds to the highest fuel temperature in Figure 6.4. This analysis also indicates that the maximum benefits in cycle efficiency are achieved when the optimum heat exchanger performance is at cruise condition.

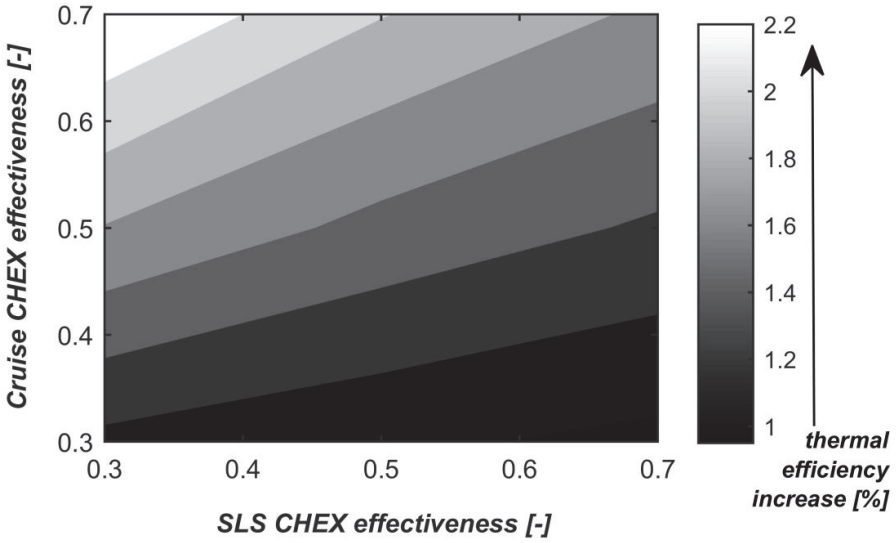


*Figure 6.5: Increase in cruise thermal efficiency at ITB energy fraction of 0.1.*

6.2.2.2 LH2-kerosene hybrid engine

The analysis in this section intends to identify the different features between the LNG-kerosene hybrid engine and the LH2-kerosene hybrid engine. The comparison is made from the following point of views: the bleed air temperature, the fuel temperature, and the turbine cooling air fraction. The ITB energy fraction of both engines is 0.1.

Figure 6.6 a) compares the increase in fuel temperature with respect to the CHEX effectiveness. The isobaric heat capacity of LH2 is larger than LNG, therefore, the temperature increase in LH2 at given CHEX effectiveness is less. The increment in the LNG temperature is ranging from 300 K to 400 K depending on the CHEX effectiveness. However, the LH2 temperature increases merely 150 K to 200 K. Moreover, since the initial temperature of LH2 is much lower than LNG, the temperature gradient between fuel and the bleed air is larger in the LH2-kerosene case. Therefore, the higher heat transfer rate would be expected in the LH2-kerosene engine. Hence, at a given effectiveness, the reduction in the bleed air temperature is more in the LH2-kerosene engine. This can be observed from Figure 6.6 b). Regarding the turbine cooling air fraction, the LH2-kerosene hybrid engine would

require less turbine cooling air compared to the LNG-kerosene engine as displayed in Figure 6.6 c).

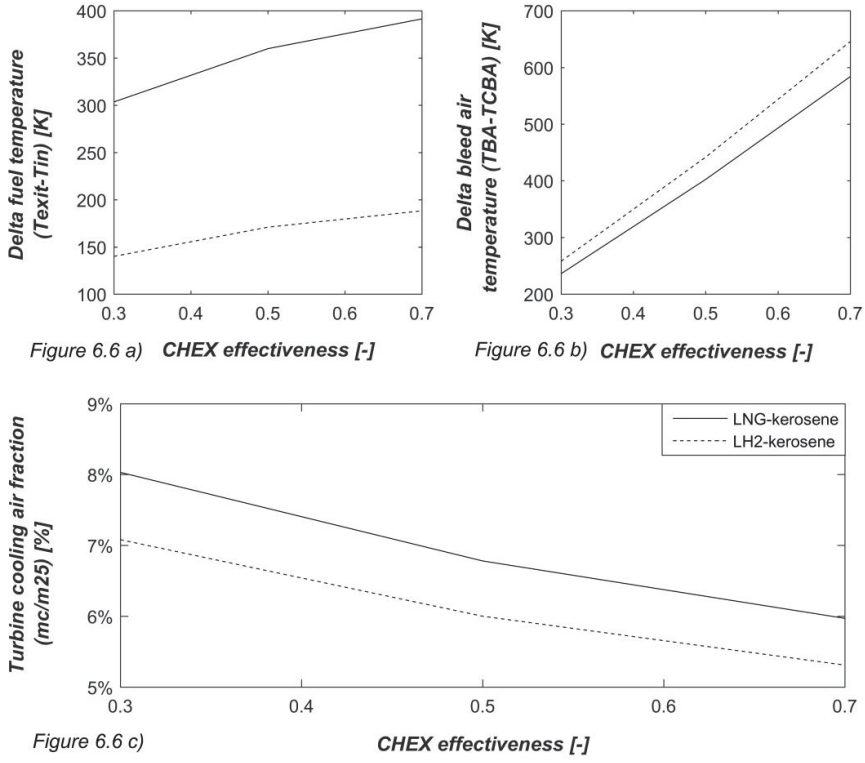


*Figure 6.6: a) Comparison of the fuel temperature between different fuel combinations; b) Comparison of the bleed air temperature between different fuel combinations; c) Variation in turbine cooling air fraction*

The parametric analysis in this section gives insights into the fundamental features of the multi-fuel hybrid engine. The messages delivered from the above analysis are summarized as following:

1) The analysis on the effects of the alternative fuels shows that using high H/C ratio fuels yields the combustion products with high isobaric heat capacity. This helps to improve the thermal efficiency of the engine cycle.
2) The application of the CBACS reduces the bleed air temperature significantly. Consequently, the turbine cooling air fraction decreases by more than 50%.

3) The analysis on the CBACS provides the evidence of selecting the design point of the CHEX. An essential aim of using the CHEX is to cool the bleed air such that the turbine cooling air reduces. From this perspective, it is reasonable to design the heat exchanger at the SLS condition. However, because the hybrid engine is proposed for a long-range commercial aircraft, to which an essential objective is to minimize the fuel consumption. According to Figure 6.5, the maximum thermal efficiency is achieved when the CHEX effectiveness at cruise is maximal. Therefore, the heat exchanger in this research is designed to cruise condition.

## 6.3 Cycle optimization of the hybrid engine

The cycle optimization of the hybrid engine is executed with respect to various ITB energy fractions (from 0 to 0.3), representing different quantities of the cryogenic fuel used. The same optimization program described in Chapter 5 is used. The component efficiencies are the same as presented in Table 4.2 except the turbine efficiency, where the effects of the turbine cooling are considered. The optimization is at cruise condition for the LH2-kerosene hybrid engine and the LNG-kerosene hybrid engine respectively. The turbine cooling air fraction is determined at the SLS ISA+25K condition and is applied to the cruise condition.

### 6.3.1 Specification of the design space

The design space of the hybrid engine is specified in Table 6.3. Compared to the design space defined for the GITB engine in the previous chapter, several differences can be observed. Since the fan of the hybrid engine needs to sustain more non-uniformity caused by ingesting the boundary layer flow, the FPR is confined to a maximum value of 1.5. Moreover, the thrust requirement of the hybrid engine is slightly higher. Additionally, the cruise altitude and flight Mach number also differ from that of the GITB engine. The effectiveness of the CHEX is extrapolated from the performance map presented in Chapter 4.

*Table 6.3: Bounds and constraints for optimization*

| ***Bounds of design parameters*** | | ***Constraints*** | |
|---|---|---|---|
| FPR | [1.2, 1.5] | OPR | <= 70 |
| LPC pressure ratio | [1.4, 5.0] | FN $[kN]$ | = 50 |
| HPC pressure ratio | [10, 20] | Inlet mass flow rate | constant |
| HPT inlet temperature $[K]$ | [1400, 1900] | | |
| BPR | [8, 15] | | |
| ITB energy fraction | [0,0.1,0.2,0.3] | | |

### 6.3.2 Optimization results

The optimization results of the multi-fuel hybrid engine are presented in this section. The ITB energy fraction varies from 0 to 0.3, which yields different engine cycles.

#### 6.3.2.1 Performance of the baseline engine

Three engine representatives are taken as the baseline.

1) An imaginary VHBPR turbofan engine burning kerosene, as presented in Chapter 5, but optimized at the same technology level with the hybrid engine, representing the year 2050 technology.
2) The second engine is the GEnx-1B64 model, the year 2014 technology.
3) The third engine is GE90-94B, the year 2000 technology.

The performance of these engines at cruise condition is displayed in Table 6.4. The $CO_2$ and $H_2O$ emission are determined based on the complete combustion process.

*Table 6.4: The baseline engine performance at cruise condition*

| | ***Advanced turbofan*** | ***GEnx-1B64*** | ***GE90-94B*** |
|---|---|---|---|
| ***Design Parameters*** | | | |
| BPR | 15 | 9.1 | 8.6 |
| FPR | 1.44 | 1.65 | 1.62 |
| OPR | 70 | 41 | 39 |
| Tt4 [K] | 1900 | 1438 | 1447 |
| ***Engine Performance*** | | | |
| Thermal efficiency [%] | 50.2 | 46.7 | 45 |
| Propulsive efficiency [%] | 83.0 | 82.6 | 81.2 |
| TSFC $[g/kN/s]$ | 13.2 | 14.1 | 14.7 |
| Kerosene $[kg/s]$ | 0.66 | 0.76 | 1.14 |
| $CO_2$ emission $[kg/s]$ | 2.09 | 2.40 | 3.6 |
| $H_2O$ emission $[kg/s]$ | 0.82 | 0.94 | 1.41 |

6.3.2.2 Performance of the LNG-kerosene hybrid engine

The performance of the LNG-kerosene hybrid engine is presented in Table 6.5. The cooled bleed air temperature is 600 K, and the LNG temperature varies with the ITB energy fraction. As the ITB energy fraction increases, the HPT inlet temperature reduces from 1593 K to 1387 K. The LPT inlet temperature of each engine remains nearly constant at around 1200 K. The thermal efficiency reduces as the ITB energy fraction increases, whereas, the propulsive efficiency remains constant. The mass flow rate of LNG reduces as the ITB energy fraction increases, whilst, the mass flow rate of kerosene increases. With an assumption of complete combustion taking place, the mass flow rates of $CO_2$ and $H_2O$ are derived.

*Table 6.5: The optimized LNG-kerosene hybrid engine*

| ***LNG & Kerosene*** | ***ITB energy fraction*** | | | |
|---|---|---|---|---|
| | ***0*** | ***0.1*** | ***0.2*** | ***0.3*** |
| ***Design Parameters*** | | | | |
| BPR | 15 | 15 | 15 | 15 |
| FPR | 1.48 | 1.48 | 1.48 | 1.48 |
| LPC pressure ratio | 5 | 5 | 5 | 5 |
| HPC pressure ratio | 9.48 | 9.48 | 9.48 | 9.48 |
| HPT inlet temperature $[K]$ | 1593 | 1521 | 1451 | 1387 |
| LPT inlet temperature $[K]$ | 1177 | 1187 | 1200 | 1215 |
| ***Engine Performance*** | | | | |
| Thermal efficiency [%] | 52.5 | 51.7 | 50.7 | 49.7 |
| Propulsive efficiency [%] | 82.6 | 82.6 | 82.6 | 82.6 |
| LNG $[kg/s]$ | 0.5436 | 0.4968 | 0.4494 | 0.4018 |
| Kerosene $[kg/s]$ | 0 | 0.0645 | 0.1312 | 0.2011 |
| Bleed air temperature $[K]$ | 602 | 603 | 604 | 604 |
| LNG temperature $[K]$ | 528 | 478 | 424 | 366 |
| $CO_2$ emission $[kg/s]$ | 1.49 | 1.57 | 1.65 | 1.74 |
| $H_2O$ emission $[kg/s]$ | 1.22 | 1.2 | 1.17 | 1.15 |

6.3.2.3 Performance of the LH2-kerosene hybrid engine

The optimization results of the LH2-kerosene hybrid engine are presented in Table 6.6. The bleed air at the exit of the CHEX is about 560 K, which is slightly lower as compared to the LNG-kerosene case. The LH2 temperature is also significantly lower than that of LNG. The $CO_2$ and $H_2O$ are calculated based on the complete combustion.

*Table 6.6: The optimized LH2-kersoene hybrid engine*

| ***LH2 & Kerosene*** | ***ITB energy fraction*** | | | |
|---|---|---|---|---|
| | ***0*** | ***0.1*** | ***0.2*** | ***0.3*** |
| ***Design Parameters*** | | | | |
| BPR | 15 | 15 | 15 | 15 |
| FPR | 1.48 | 1.48 | 1.48 | 1.48 |
| LPC pressure ratio | 5 | 5 | 5 | 5 |
| HPC pressure ratio | 9.48 | 9.47 | 9.47 | 9.469 |
| HPT inlet temperature $[K]$ | 1555 | 1496 | 1430 | 1368 |
| LPT inlet temperature $[K]$ | 1157 | 1171 | 1184 | 1200 |
| ***Engine Performance*** | | | | |
| Thermal efficiency [%] | 53 | 52 | 51.1 | 50 |
| Propulsive efficiency [%] | 82.5 | 82.5 | 82.6 | 82.6 |
| LNG $[kg/s]$ | 0.2245 | 0.2057 | 0.1861 | 0.1663 |
| Kerosene $[kg/s]$ | 0 | 0.0641 | 0.1304 | 0.1998 |
| Bleed air temperature $[K]$ | 562 | 565 | 564 | 564 |
| LNG temperature $[K]$ | 219 | 194 | 161 | 123 |
| $CO_2$ emission $[kg/s]$ | 0 | 0.2 | 0.41 | 0.63 |
| $H_2O$ emission $[kg/s]$ | 2.02 | 1.93 | 1.84 | 1.74 |

## 6.4 Hybrid engine performance evaluation

The performance of the hybrid engine is assessed with respect to the baseline engines. Attentions are paid to the cycle thermal efficiency, $CO_2$ emission, and $H_2O$ emission with respect to the ITB energy fraction from 0 to 0.3.

The comparison between the LNG-kerosene hybrid engine and the baseline engines is presented in Figure 6.7. The maximum increment of the thermal efficiency is achieved at the ITB energy fraction of 0. Compared to the advanced GTF engine, the thermal efficiency improves by approximately 5% mainly due to the utilization of LNG. Compared to GEnx and GE90, the improvement is even larger by 12% and 17% approximately. As the ITB energy fraction increases, benefit in thermal efficiency reduces progressively. When the ITB energy fraction reaches 0.3, the thermal efficiency of the hybrid engine becomes lower than that of the advanced GTF. The propulsive efficiency of the hybrid engine has no significant change compared to the all the baseline engines. The $CO_2$ emission of the hybrid engine is much lower about 20% less than the most advanced baseline engine, 30% less than GEnx, and more than 50% less than GE90. However, using LNG emits more water vapor than burning kerosene.

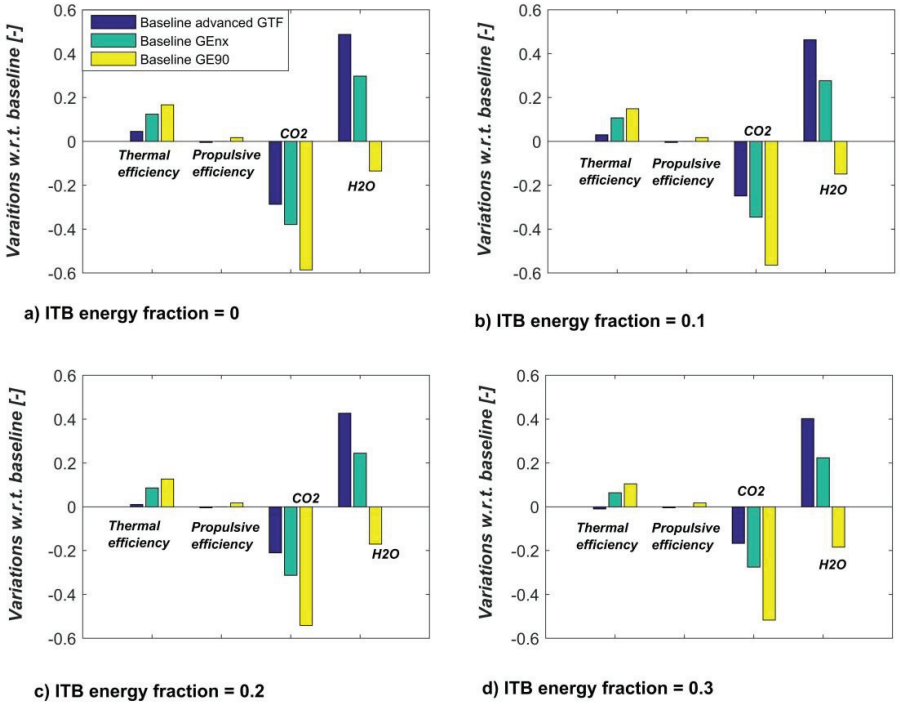


*Figure 6.7: Comparison of the LNG-kerosene hybrid engine to baselines*

Figure 6.8 compares the LH2-kerosene hybrid engine to the baseline engines. A similar trend to Figure 6.7 is observed but with different magnitudes. The increment in the thermal efficiency using LH2 is slightly more than using LNG. The main difference is exhibited in the variations of $CO_2$ and $H_2O$ emissions. When only LH2 is in use (ITB energy fraction is equal to 0), $CO_2$ can be eliminated. As the ITB

energy fraction increases, the mass flow rate of kerosene increases, therefore, more $CO_2$ is produced. The reduction in $CO_2$ is overall significant by using LH2. Even at the ITB energy fraction of 0.3 in the study case, the $CO_2$ emission decreases by more than 70% compared to all the baseline engines. Moreover, burning LH2 has a lot stronger negative effects on the water vapor emission.

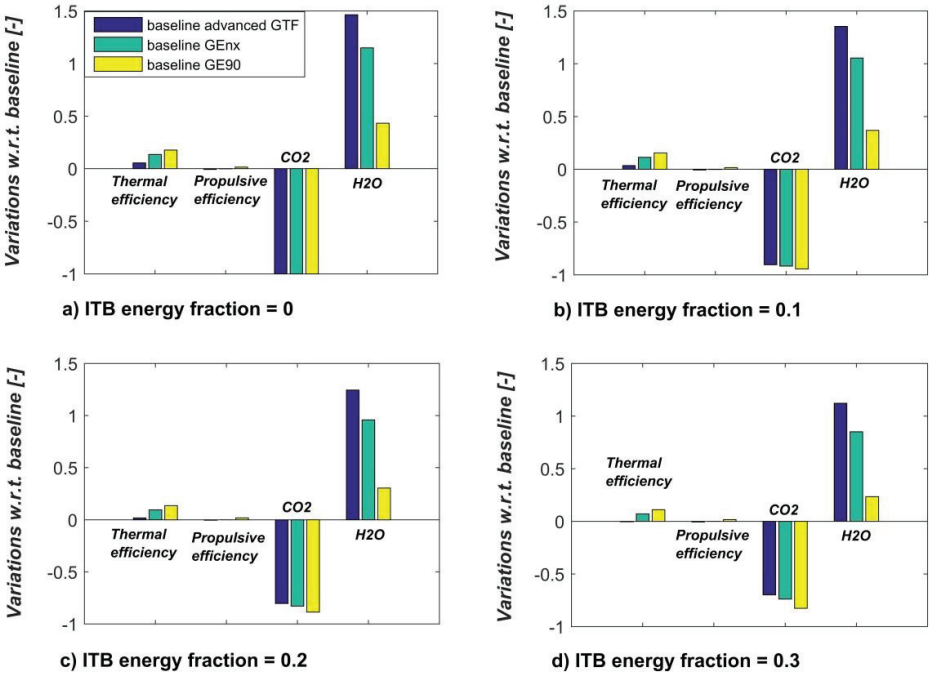


*Figure 6.8: Comparison of the LH2-kerosene hybrid engine to baselines*

The water vapor at high altitude and certain atmospheric condition condenses into droplets to form contrails, which have an important impact on the global warming. Especially in the middle and upper troposphere, water vapor is considered as one of the dominant greenhouse gasses [118]. Therefore, it is essential to evaluate the global warming effect of the hybrid engine from this perspective such that the hybrid engine design considers this impact.

## 6.5 Verification of the hybrid engine design

The engine has to perform under various conditions. If the engine cannot meet the performance requirement, the engine design has to be modified. In this section, the characteristics of the hybrid engine at several typical off design conditions are verified. The performance requirements are presented in Table 6.7.

*Table 6.7: Performance requirement of the hybrid engine*

| Operating points | Ambient condition | Mach number | Thrust [kN] |
|---|---|---|---|
| Max static | SLS ISA | 0 | 280 |
| Takeoff | SLS ISA | 0.2 | 250 |
| TOC | 12 km, ISA | 0.8 | 56 |
| Ground idle | SLS ISA | 0 | N2 55% |

The optimized hybrid engine cycles in the previous section have been taken as the design conditions. Accordingly, the steady-state performance at the operating points selected in Table 6.7 is derived. The results of the spool speed and the compressor surge margin are illustrated in Figure 6.9. It has been observed that increasing the ITB energy fraction results in a reduction in the LPC surge margin, especially at the low thrust. Therefore, a variable bleed valve has been applied to bleed off the air from the end of LPC in case the LPC surge margin violates its limit. Overall, when the hybrid engine operates at the selected points, the operating limits are satisfied. The same procedure has also been implemented to verify the LH2-kerosene hybrid engine. In the next section, one of the optimized hybrid engines is used to analysis the mission performance of the MFBWB together with the hybrid engine.

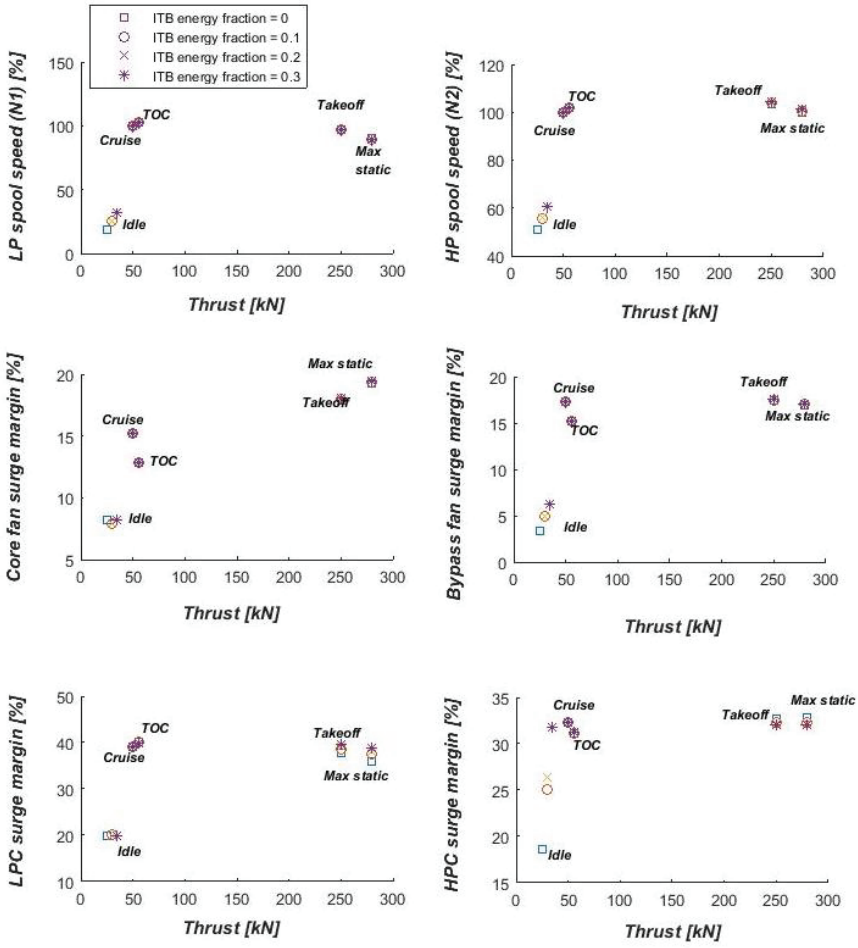


*Figure 6.9: Verification of the LNG-kerosene hybrid engine design.*

## 6.6 Flight mission analysis

The mission analysis is performed to evaluate the energy consumption and emissions of the MFBWB aircraft along with the hybrid engine. The comparison is made between the LH2-kerosene BWB, the LNG-kerosene BWB, the baseline Boeing777-200ER, and the Boeing 787-8. A typical flight mission profile as presented in Chapter 4 is used. The data obtained in the following contents have been based on the hybrid engine performance at the ITB energy fraction of 0.3 during the entire flight mission.

### 6.6.1 City pairs selection

The analysis in this section is a preparation for the final assessment of the climate impact of the MFBWB, which has been performed by the research group of the AHEAD project. The aim is to evaluate the mean climate impact in terms of the changes in the near-surface temperature over 100 years after the fleet of the aircraft entry into service. Depending on the flight latitude, longitude, and altitude, the long-term effects of emissions on the global climate can be predicted. The comparison has been made between the LNG-kerosene BWB, LH2-kerosene BWB, and the baseline aircraft. The final results can be found in [119].

To support the full assessment, ten city pairs in Table 6.8 have been selected following certain criterions, for instance, long-range, covering the globe widely, etc. The corresponding flight routes are given in Figure 6.10. The energy consumption and emissions for the given flight mission between all city pairs are calculated and provided as inputs for the climate assessment.

*Table 6.8: Selected city pairs.*

| ***Airport A*** | ***Airport B*** | ***Flight range (nm)*** |
|---|---|---|
| ATL(Atlanta) | NRT (Tokyo) | 5953 |
| MAD (Madrid) | PVG (Shanghai) | 5556 |
| DXB (Dubai) | SYD (Sydney) | 6500 |
| AMS(Amsterdam) | EZE(Buenos Aires) | 6176 |
| JFK (New York) | JNB (Johannesburg) | 6925 |
| SYD (Sydney) | JNB (Johannesburg) | 5963 |
| JFK (New York) | HKG (Hong Kong) | 7014 |
| BOM (Bombay) | EWR (New Jersey) | 6784 |
| DXB (Dubai) | GRU (Sao Paulo) | 6597 |
| DOH(Doha) | IAH(Houston) | 6994 |


*Figure 6.10: City pairs selected.*

### 6.6.2 Mission analysis

This section focuses on the mission energy consumption and emissions of the MFBWB along with the hybrid engine. Among those city pairs in Table 6.8, three are selected as examples representing different flight ranges. For the purpose of comparison, long range Boeing 787-8 and Boeing 777-200ER are selected as a baseline aircraft. The engines of both aircraft are GEnx and GE90 respectively. Piano X [120] is used to generate mission profiles for B787 and B777. With this calculation tool, emissions of an existing aircraft for a given flight mission can be predicted. The NOx emissions of the hybrid engine are calculated using the emission prediction tool for the hybrid combustion system described in section 4.4.3. The $CO_2$ emission and $H_2O$ emission are derived based on the complete combustion process.

The design of the MFBWB has been mainly focused on the LNG-kerosene versions. The installation effect of the LH2-kerosene hybrid engine is stronger on the aerodynamic performance of the aircraft. According to the analysis performed in [121], over a long range mission flight using LH2 increases the block energy consumption by about 10% if considering the variations in aircraft size and weight. Although the multi-fuel configuration is expected to improve this situation, the analysis on the LH2-kerosene BWB is based on the most pessimistic scenario. Therefore, it is assumed that the LH2-kerosene BWB would consume 10% extra energy. Accordingly, the energy consumption and emissions of the LH2-kerosene BWB are estimated. The results for various aircraft models are presented in Table 6.9 - Table 6.11. The comparison is made in Figure 6.11 - Figure 6.14.

*Table 6.9: Emissions and energy consumption per payload per unit distance (SYD-DXB 12000km).*

| | ***B777-200ER*** | ***B787-8*** | ***LNG-kerosene BWB*** | ***LH2-kerosene BWB*** |
|---|---|---|---|---|
| Energy consumption, kJ/payload/km | 8.3 | 7.1 | 4.95 | 5.4 |
| NOx emission, mg/payload/km | 3.12 | 1.93 | 0.4 | 0.62 |
| $CO_2$ emission, mg/payload/km | 610.65 | 522.78 | 297.45 | 120.68 |
| $H_2O$ emission, mg/payload/km | 242.32 | 207.45 | 201.58 | 333.39 |

*Table 6.10: Emissions and energy consumption per payload per unit distance (AMS-EZE 11000km)*

| | ***B777-200ER*** | ***B787-8*** | ***LNG-kerosene BWB*** | ***LH2-kerosene BWB*** |
|---|---|---|---|---|
| Energy consumption, kJ/payload/km | 7.63 | 6.54 | 4.77 | 5.25 |
| NOx emission, mg/payload/km | 2.89 | 1.81 | 0.38 | 0.6 |
| $CO_2$ emission, mg/payload/km | 561.5 | 481.4 | 286.7 | 116.3 |
| $H_2O$ emission, mg/payload/km | 222.8 | 191 | 194.3 | 321.3 |

*Table 6.11: Emissions and energy consumption per payload per unit distance (MAD-PVG 10000km)*

| | ***B777-200ER*** | ***B787-8*** | ***LNG-kerosene BWB*** | ***LH2-kerosene BWB*** |
|---|---|---|---|---|
| Energy consumption, kJ/payload/km | 6.62 | 5.78 | 4.67 | 5.14 |
| NOx emission, mg/payload/km | 2.56 | 1.6 | 0.36 | 0.58 |
| $CO_2$ emission, mg/payload/km | 487.5 | 425.2 | 280.7 | 113.9 |
| $H_2O$ emission, mg/payload/km | 193.4 | 168.7 | 190.2 | 314.6 |

In Figure 6.11, compared to B777, the LNG-kerosene BWB can reduce the NOx emissions by more than 80%. The maximum reduction in $CO_2$ is 50%, in $H_2O$ is about 20%, and in the energy consumption is 40% at the longest flight distance. Since the B787 is more efficiency than B777, the LNG-kerosene BWB is also less advantageous than B787, which can be observed from Figure 6.12. A similar trend as Figure 6.11 is exhibited with an exception for the $H_2O$. At the shorter distance (11000 km and 10000 km in the current study), the water vapor emitted by the LNG-kerosene BWB is more than B787. As explained in the earlier contents, more water vapor at high altitude tends to aggravate the global warming effect.

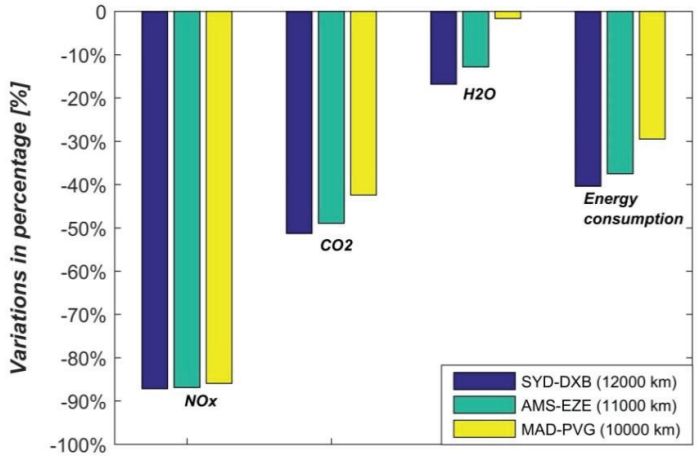


*Figure 6.11: Comparison of the LNG-kerosene BWB to B777.*

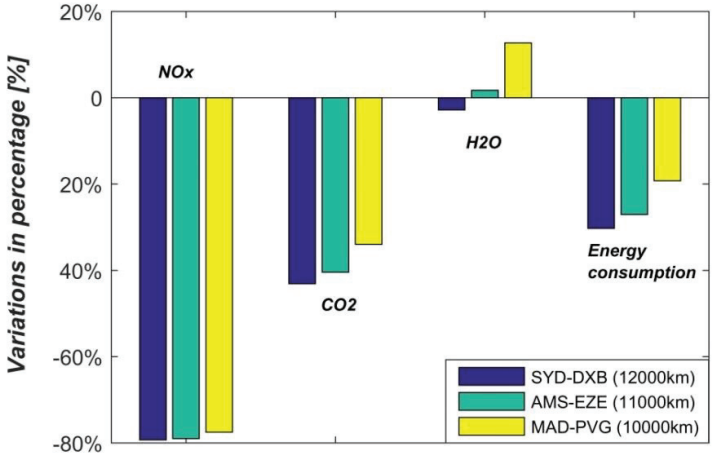


*Figure 6.12: Comparison of the LNG-kerosene BWB to B787.*

The LH2-kerosene BWB is compared to the B777 and B787 in Figure 6.13 and Figure 6.14. Although the optimization results in the earlier analysis exhibit the performance of the LH2-kerosene hybrid engine being superior to the LNG-kerosene hybrid, the installation effect of the LH2-kerosene engine is also stronger. Therefore, the mission analysis shows that the advantages of the LH2-kerosene BWB are less. Compared to the B777, the energy consumption of the LH2-kerosenen BWB is 35% lower (40% in the LNG-kerosene case). The reduction in the NOx emissions is less than 80%. The $CO_2$ emission decreases more substantial

owing to the utilization of LH2. However, the unfavorable increase in the water vapor is also observed.

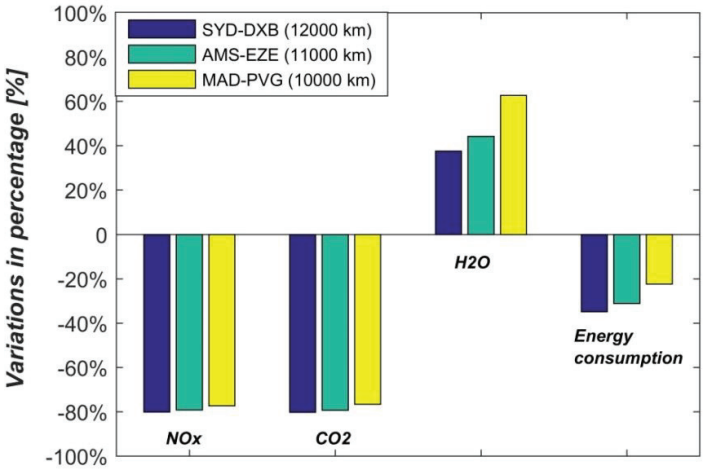


*Figure 6.13: Comparison of the LH2-kerosene BWB to B777.*

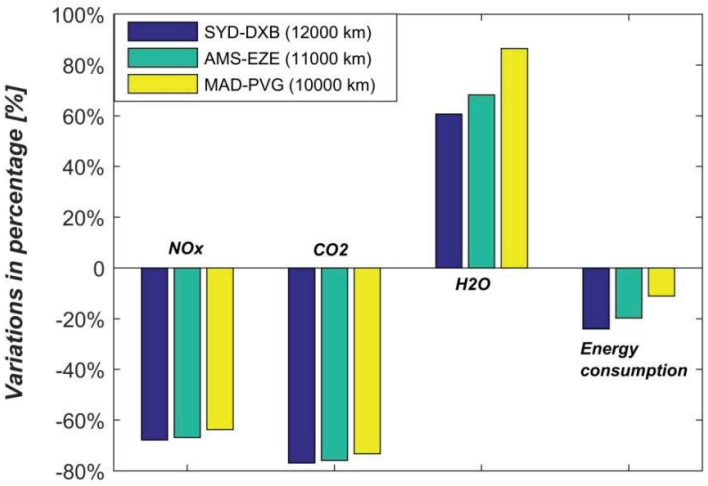


*Figure 6.14: Comparison of the LH2-kerosene BWB to B787.*

## 6.7 Summary

In this chapter, the characteristics of the hybrid engine have been studied. Both the LNG-kerosene and the LH2-kerosene versions are analyzed. Based on the results, the following aspects are highlighted:

- The isobaric heat capacity of the combustion products from the high H/C ratio fuels, like LNG or LH2, is higher, which is beneficial to improve the thermal efficiency of the engine cycle. However, using the high H/C ratio fuels yields the significant increase in water vapor, especially as LH2 is concerned. The final evaluation of the hybrid engine on global warming effect should consider this effect.
- Using LH2 or LNG as a coolant, the bleed air temperature reduces significantly, enabling more than 50% reduction in the turbine cooling air mass flow rate. Moreover, the increment in fuel temperature is also substantial, which is beneficial in the cycle efficiency.
- The benefits in the reduction of the turbine cooling are more substantial in a normal single combustor turbofan engine than in an ITB engine.
- The parametric analysis suggests that the heat exchanger should be designed to cruise to enable the maximum effectiveness at cruise. This ensures the maximum increment in the thermal efficiency.
- The hybrid engine is optimized at cruise with respect to different ITB energy fraction from 0 to 0.3. The standalone LH2-kerosene hybrid engine exhibits superior performance to the LNG-kerosene hybrid engine in terms of the improvement in the thermal efficiency and the reduction of $CO_2$.
- In the mission analysis, the LNG-kerosene BWB shows the highest superiority in terms of energy consumption and low emissions. Although the standalone LH2-kerosene hybrid engine is more efficient, the installation effect of the LH2-kerosene is also stronger. The LH2-kerosene BWB exhibits fewer advantages.

# Chapter 7 Operating strategy for the hybrid engine

The hybrid engine differs from conventional turbofan architecture in several aspects; the most critical one from an engine control point of view is the hybrid sequential combustion system. The motivation of this chapter is to develop a control strategy for the hybrid engine taking into account the additional degree of freedom provided by the hybrid sequential combustor. The hybrid engine has been optimized with respect to various ITB energy fractions in the previous chapter. For a given hybrid engine design, how is the dual combustor system operated at various off-design conditions? Would the operating strategy remain identical as for the design condition? If not, what could be changed in order to improve the control strategy?

## 7.1 Operating limiters

Throughout the off-design performance analysis, limits are set for several essential parameters in Table 7.1. The speeds of the high pressure spool and the low pressure spool are constrained by the upper limits. At hot day, the compressor exit temperature might surpass the maximum allowable material temperature. Therefore, the upper limit has been set as 1000 K. Since the NOx emissions increase exponentially when the temperature exceeds 1800 K; the HPT inlet temperature is confined to 1800 K. Moreover, the LPT inlet temperature is limited by 1500 K to minimize the LPT cooling requirement and the associated unfavorable effects. The ITB energy fraction is restricted to the maximum value of 0.3 such that the negative effects of having an ITB on the cycle efficiency can be reduced.

Moreover, surge margin is another key parameter to identify compressor surge. The surge margin on a compressor map can be defined by the distance of the operating point to the surge line at a constant speed or constant mass flow rate. In GSP, the latter one is applied as presented in Eqn. (25) [122],

$$SM = \frac{PR_{SL} - PR_{OL}}{PR_{SL}} \times 100 \tag{25}$$

where $PR_{SL}$ and $PR_{OL}$ represent the pressure ratio on the surge line and the operating line.

The determination of minimum required surge margin depends on various issues, for instance, the deteriorations of the component working line and surge line, the transient allowance, the inlet distortion, etc. In Table 7.1, typical surge margin requirements corresponding to the ISA SLS maximum rating condition are presented [79] and will be applied in the analysis in this chapter.

*Table 7.1: Operating limits*

| *Variables* | *Notation* | *Value* | *Description* |
|---|---|---|---|
| High pressure spool speed [%] | N2 | 100 | Max |
| Low pressure spool speed [%] | N1 | 100 | Max |
| Fan surge margin [%] | SM_fan | 10 | Min |
| LPC surge margin [%] | SM_LPC | 20 | Min |
| HPC surge margin [%] | SM_HPC | 25 | Min |
| HPC exit temperature [K] | $T_{t3}$ | 1000 | Max |
| HPT inlet temperature [K] | $T_{t4}$ | 1800 | Max |
| LPT inlet temperature [K] | $T_{t46}$ | 1500 | Max |
| ITB energy fraction | [-] | 0.3 | Max |

## 7.2 Various thrust at SLS ISA condition

The analysis in this section is performed at SLS ISA condition to simulate the hybrid engine undergoing a procedure from the ground idle until the maximum static power to take off. The thrust schedule is given as an input. Attentions are paid to those critical parameters defined in Table 7.1

### 7.2.1 Component characteristics

In Figure 7.1, the variations in the low pressure spool speed (N1) and the high pressure spool speed (N2) with respect to various thrust are displayed. The ITB energy fraction exhibits no essential effects on N1. The N1 only varies with the changes in thrust. This is because, in a very high BPR turbofan like the hybrid engine, more than 80% of thrust is produced by the bypass stream. Therefore, the variation in thrust is mainly subjected to the fan speed which is subjected to the low pressure shaft speed. No matter how the ITB energy fraction varies, the low pressure shaft speed remains nearly unchanged to produce the required thrust. If the thrust requirement changes, the N1 varies correspondingly.

However, the N2 is dependent on both thrust and the ITB energy fraction. It is illustrated in Figure 7.1 that N2 increases with thrust. For the reason that the N1 has to increase to produce more thrust, hence, more fuel is injected. With the ITB energy fraction remains unchanged, the fuels added into two combustors shall increase simultaneously. As a result, the N2 increases with the increase in thrust. Nevertheless, N2 reduces as the ITB energy fraction increase. This is beneficial at the higher thrust where the high pressure spool can likely exceed its maximum speed as indicated by the dashed line in Figure 7.1. At an ITB energy fraction of 0, the N2 surpasses its threshold when the thrust is beyond 55% of the maximum. As the ITB energy fraction increases, the less fuel is injected into the main combustor, which helps to prevent the N2 from over speeding.

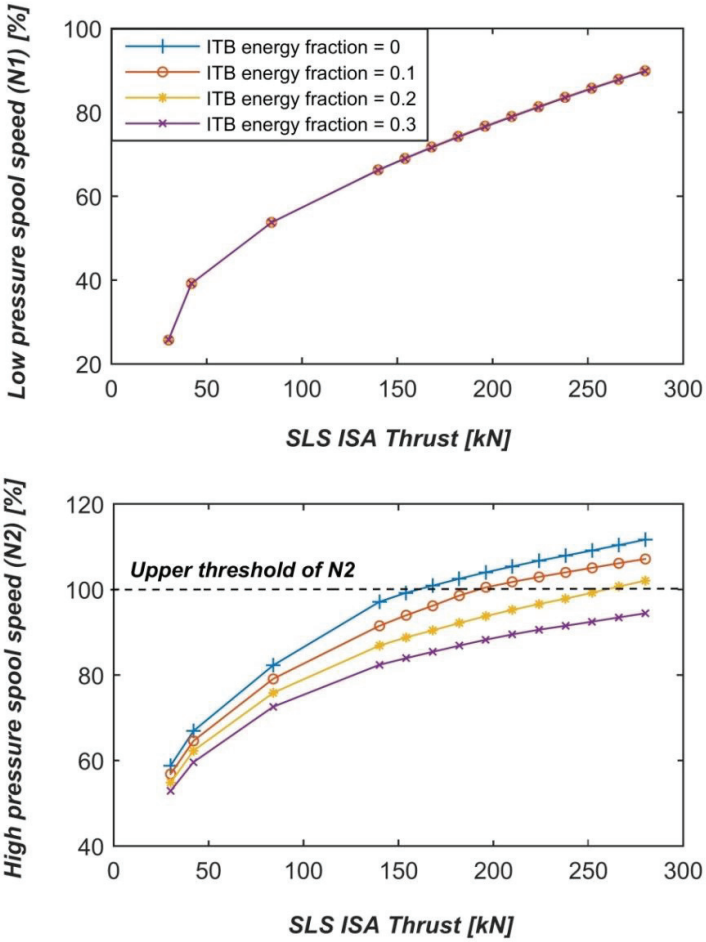


*Figure 7.1: Variation in shaft speed versus SLS ISA thrust.*

The surge margins of the fan and compressors have also been studied and illustrated in Figure 7.2. The ITB energy fraction has no significant effect on the surge margin of the fan, but the thrust does. This is because the inlet condition of the fan is determined by the ambient condition. Since the N1 is nearly unchanged as the ITB energy fraction varies, the corrected speed and the corrected mass flow rate (defined in Chapter 4) of the fan are, therefore, nearly constant. According to the modeling principle at off-design conditions described in Chapter 4, knowing the corrected speed and the corrected mass flow rate, the FPR is also determined. In the current analysis, it varies very slightly at the given thrust. Therefore, the fan surge margin is not sensitive to the ITB energy fraction.

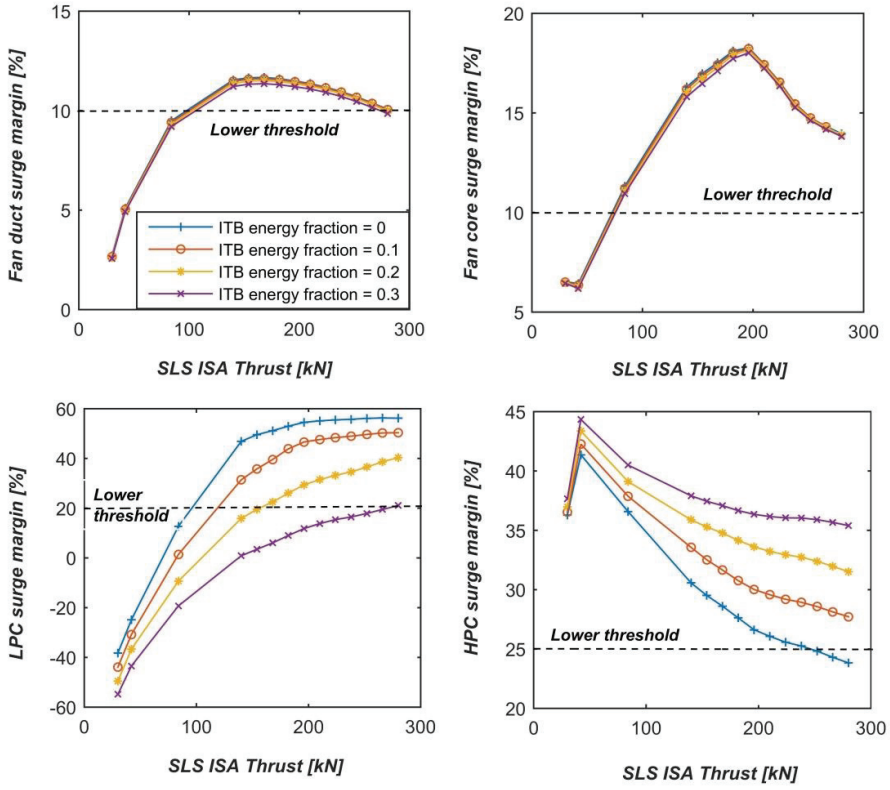


*Figure 7.2: Variation in surge margin with SLS ISA thrust.*

However, the LPC surge margin undergoes large variations with the ITB energy fraction and thrust. As the ITB energy fraction increases, more fuel is injected into the ITB, leading to an increase in the LPT inlet temperature. Consequently, the core mass flow rate reduces. The characteristics of fan are nearly independent of the ITB energy fraction as discussed above. Therefore, the inlet pressure and temperature of the LPC do not vary with the ITB energy fraction either. However, the core mass flow rate reduces. As a result, the corrected mass flow rate through the LPC decreases, whereas, the corrected rotational speed remains unchanged. Thereby, the operating points shift towards to the surge line in LPC map. After a certain point, the LPC encounters surge as displayed in Figure 7.2. On the other hand, fuel flow rate of the main combustor decreases as the ITB energy fraction increases, leading to a decrease in the HPT inlet temperature, thereby, reducing the HPT power output. Accordingly, the HPC pressure ratio reduces. The consequence is to drive the operating line of the HPC moving away from the surge line.

Variations in HPC exit temperature, HPT inlet temperature, and LPT inlet temperature are presented in Figure 7.3. From the curves in this figure, it can be seen that the temperature limits defined in Table 7.1 are all satisfied. Furthermore, increase in the fuel flow rate of ITB results in a significant reduction in temperatures at the HPT inlet and the HPC exit. This is beneficial not only from the material point of view but also from the NOx emissions point of view.

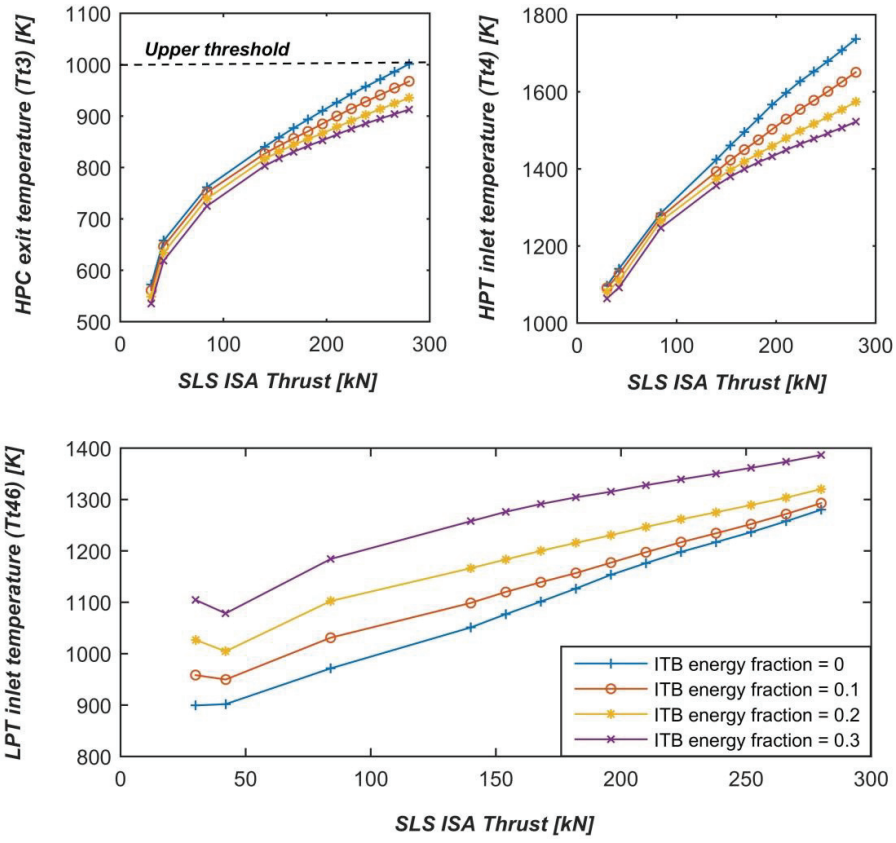


*Figure 7.3: Temperature with the SLS ISA Thrust*

To summarize, operating the two combustors simultaneously is beneficial in the following aspects: 1) It is helpful to protect the N2 from exceeding its limit; 2) The HPC exit temperature and HPT inlet temperature are reduced without conflicting the LPT inlet temperature limit. The disadvantage is the LPC surge margin decreases significantly, which creates a high risk of the LPC encountering surge. In the next section, the analysis is performed mainly in this regard to improve the performance of components.

### 7.2.2 The fuel control schedule for various thrust

According to the analysis performed above, the N2 speed and the LPC surge margin are the most stringent parameters. Making use of the operational flexibility provided by this unique combustor system, a control strategy of the fuel flow is proposed. Depending on the thrust variation, the fuel flow rates to the two combustors vary such that both the N2 and the LPC surge margin are in their safe region. After comparing the curves representing the N2 speed and the LPC surge margin, a control schedule for fuel flow rates is derived as can be seen in Figure 7.4. At the lower thrust, the ITB is switched off such that the N2 is below 100 until thrust reaches 55% of the maximum. Beyond this percentage, the fuel flow rate of the ITB increases progressively until the ITB energy fraction is 0.1. When the thrust increases further until the 90%, the fuel flow rate of the ITB continuously increases until the ITB energy fraction is 0.2. If the thrust is higher than 90% of the maximum, the ITB energy fraction of 0.3 will have to be maintained.

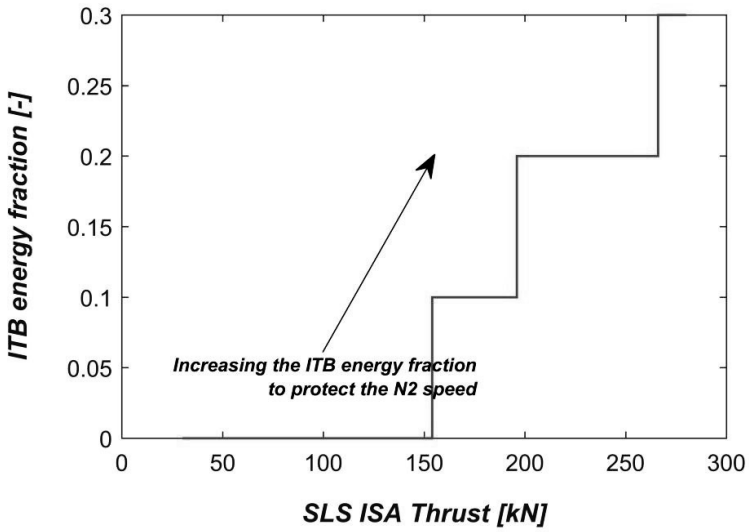


*Figure 7.4: Fuel control schedule proposed for various thrust at SLS ISA.*

The same control schedule is valid to mitigate the LPC surge margin problem. However, as can be seen in Figure 7.2, even with the ITB switched off, the surge margin of the LPC is still not satisfied. To overcome this, the current technology is to use variable geometries, for example, 1) Variable Bleed Valve (VBV) which is applied to bleed air directly from a compressor. This solution is convenient to apply and has an immediate effect on the compressor surge, yet it deteriorates the engine performance. 2) Variable Stator Vanes (VSVs) which are employed to vary the flow angel incoming to the turbine blade, hence modifying the surge line position. Compared to the VBV, the VSVs are more sophisticated, but it creates extra

complexity. In this study, the VBV is used, the schedule of which is suggested as in Figure 7.5. These two schedules will be applied together in the next section study.

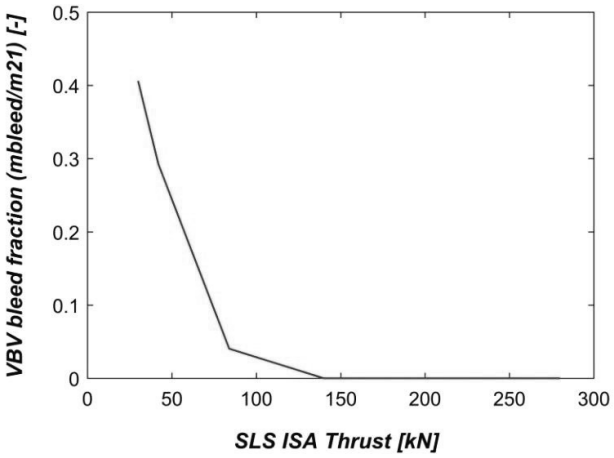


*Figure 7.5: The VBV control schedule for various thrust at SLS ISA*

### 7.2.3 Verification of the control strategy for various thrust

Following the control strategy suggested above, the problem of over speeding encountered by the N2 speed can be eliminated, which can be observed in Figure 7.6. It can be seen that following the combined fuel control schedule the high-pressure spool speed remains below its maximum.

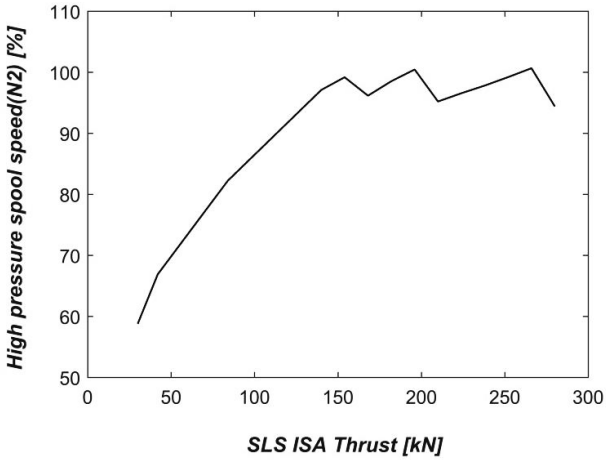


*Figure 7.6: Improved high pressure spool speed with the fuel control schedule*

The LPC surge margin resulted from this control schedule is displayed in Figure 7.7. The solid line represents the variation resulted from purely using the fuel control schedule, whilst, the dashed line shows the improvement due to the VBV applied. When thrust is below 40%, the ITB is switched off while the VBV is left open to bleed off air. As the thrust increases, the VBV starts closing progressively until the thrust reaches 40%. By doing so, the downstream air mass flow rate reduces. A drop in delivery pressure accompanies the reduction in the mass flow rate. As a result, the LPC pressure ratio drops and the operating line moves away from the surge line. When the thrust is beyond 40%, the single fuel control schedule is enough to satisfy both the N2 and LPC surge margin requirements. Of course, the other parameters would still be operating within their limits.

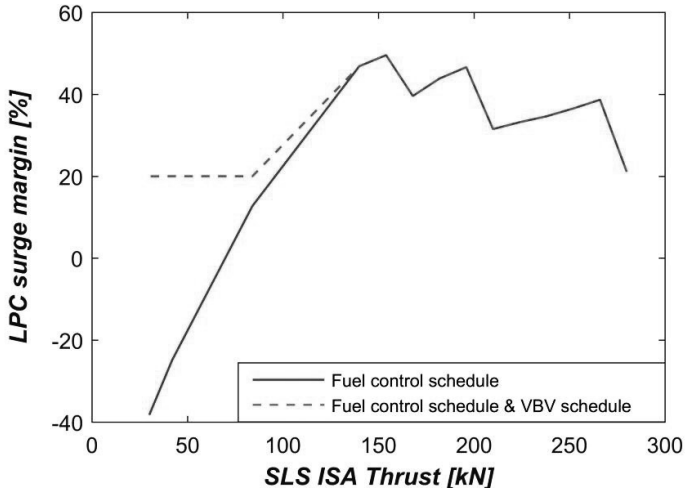


*Figure 7.7: Improved LPC surge margin with the fuel control schedule*

## 7.3 Flat rating at SLS

Flat rating is to offer constant allowable power or thrust level over a range of ambient temperature. Rating levels are designed to ensure satisfactory engine life while achieving the power or thrust required by an aircraft at key operating conditions [79], for example, take-off, climb, cruise, flight idle and ground idle. A generic example of maximum thrust rating at SLS is depicted in Figure 7.8. The maximum thrust is only achievable below the flat rating temperature. Above this temperature, the thrust decreases with increase in temperature. Depending on the engine design, the flat rating temperature can vary. The maximum thrust level corresponds to the maximum allowable value of several limiting parameters for engine integrity. In general, temperatures or mechanical speeds are the limitations on hot take-off, while the pressure level limits operations on cold days.

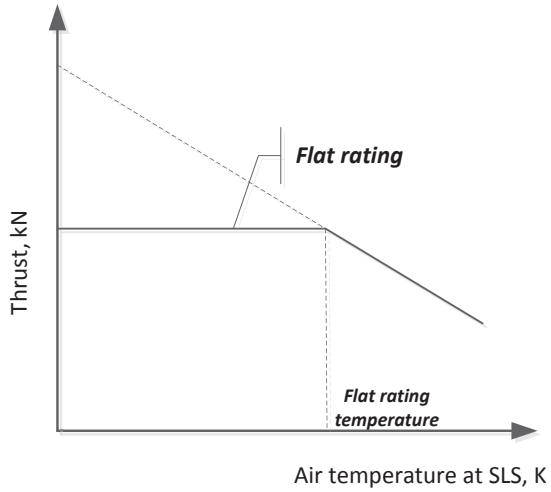


*Figure 7.8: Typical flat rating*

The analysis in this section is carried out to determine the flat rating temperature of the hybrid engine at SLS condition. Maximum thrust requirement for the hybrid engine is 280 kN at the SLS ISA condition. This thrust is maintained at other nonstandard atmosphere conditions. The operating limits defined in Table 7.1 still remain valid. At the first step, component characteristics with respect to ambient temperatures at different ITB energy fractions are studied to identify the stringent parameters. The next step is to develop a control strategy such that challenges can be overcome. Finally, the control schedule is verified.

### 7.3.1 Component characteristics

In Figure 7.9, variations in N1 and N2 with respect to different ambient temperatures are presented. The maximum thrust is maintained at each point. The fuel flow rates into two combustors are controlled to ensure that the ITB energy fraction varying from 0 to 0.3. The N1 doesn't change with respect to the ITB energy fraction, whilst, the N2 increases with the increase in the ITB energy fraction. Both N1 and N2 show linear growth with the increase in ambient temperature. Moreover, the N2 tends to violate its upper threshold at the lower ITB energy fraction. In particular, at the ITB energy fraction of 0, the N2 surpasses its limit over the entire temperature range, implying that the engine operating with only a single combustor is not feasible to meet the required thrust. Therefore, the dual combustors have to be always operated simultaneously to produce the maximum static thrust. Otherwise, the engine would have to oversized to satisfy the requirement.

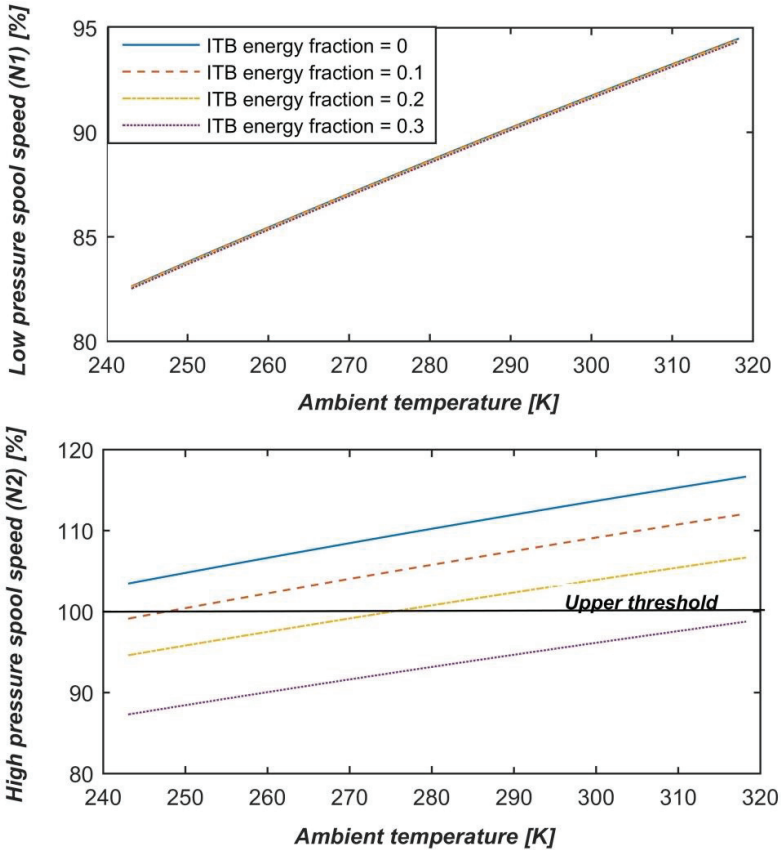


*Figure 7.9: Variation in spool speeds with ambient temperature.*

The surge margins of the fan, LPC and HPC are examined as presented in Figure 7.10. The surge margin of each component has been within the limit regardless the ITB energy fraction and the ambient temperature.

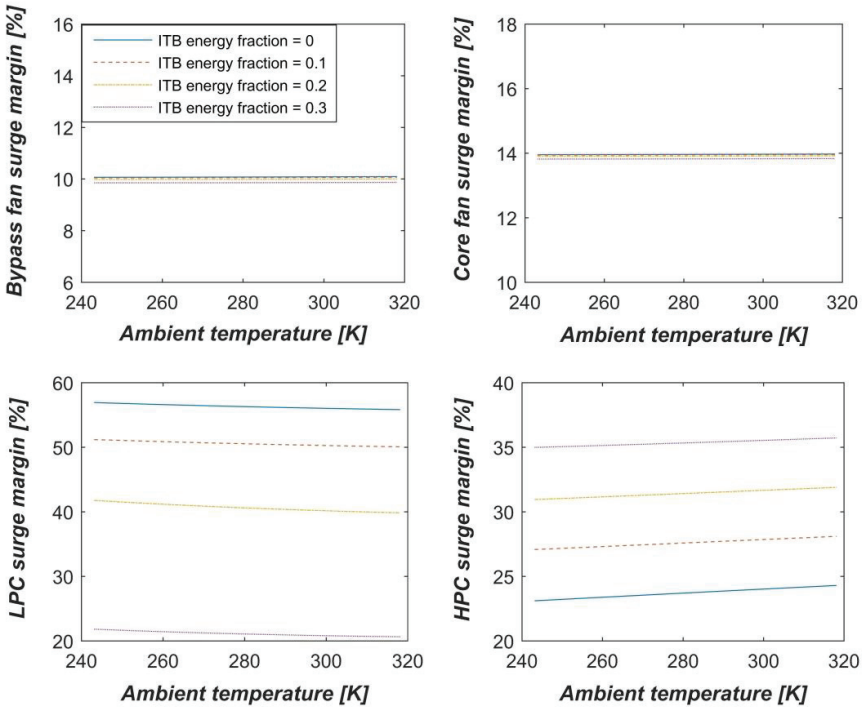


*Figure 7.10: Variation in surge margins with ambient temperature.*

Furthermore, the temperature limits have been reviewed under all circumstances, as displayed in Figure 7.11. All the station temperatures increase linearly with the increase in the ambient temperature. When increasing the ITB energy fraction, the LPT inlet temperature shows opposite variation tendency as the HPC exit temperature and the HPT inlet temperature. At the lower ITB energy fraction, the HPC exit temperature and the HPT inlet temperature have risks to exceed their limits when the ambient temperature becomes hotter. Overall, the flat rating temperature increases with the increment in the ITB energy fraction.

From the analysis above, it can be observed that the ITB has beneficial effects on:

- HPC exit temperature
- HPT inlet temperature
- HPC surge margin
- High pressure spool speed

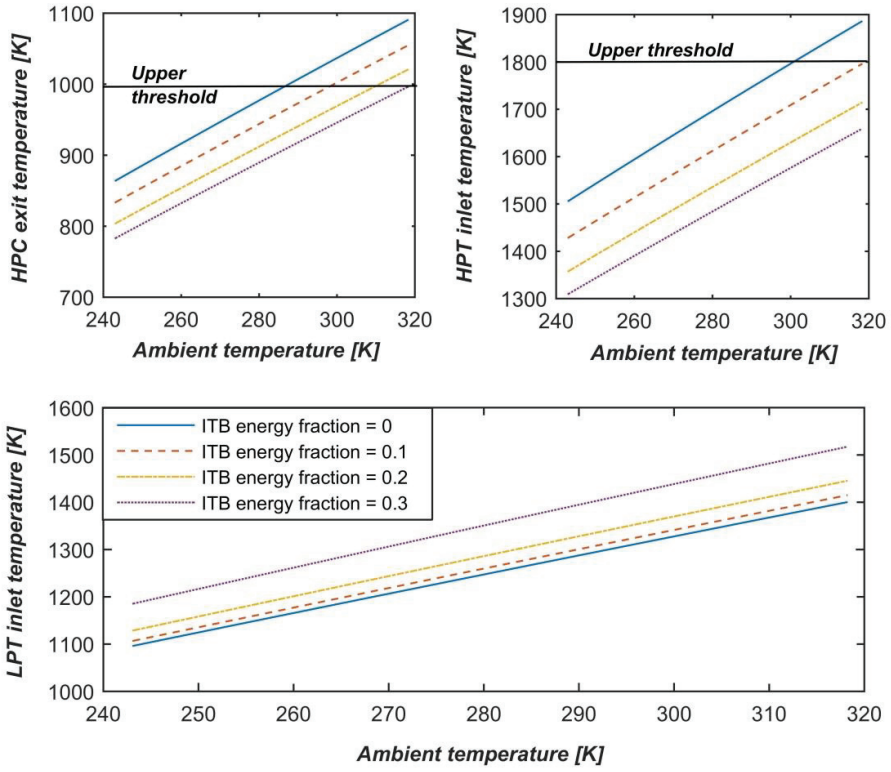


*Figure 7.11: Variation in station temperatures with ambient temperature*

### 7.3.2 The fuel control schedule for flat rating

According to the analysis in the previous section, it can be concluded that for the maximum thrust at SLS, the N2 speed, the HPC exit temperature ($T_{t3}$), and the HPT inlet temperature ($T_{t4}$) are the main parameters, which might violate their limits. To satisfy the operating limits presented in Table 7.1, a regulation strategy for fuel flow rate have been developed and illustrated in Figure 7.12. The $T_{t4}$ exceeds its limit only at the hotter ambient temperature when the ITB is not in use. However, the analysis in Figure 7.9 suggests that the single combustor operating strategy should be discarded to ensure the N2 from surpassing its limit. As a consequence, the risk of $T_{t4}$ exceeding its limit is avoided. Ultimately the control strategy mainly focuses on how to ensure the $T_{t3}$ and N2 within their allowable operating ranges.

There are multiple options for the $T_{t3}$ protection as been presented by the solid and dashed line in Figure 7.12. However, the solution to overcome the N2 from over speeding is unique. Eventually, the solid line is selected. The regulation procedure is described in Table 7.2. When the ambient temperature is below 248.15 K (-25°C),

the fuel flow rate of both combustors is regulated to maintain the ITB energy fraction equal to 0.1. Between 248.15 K and 276.15 K (-25°C to 3°C), the fuel flow rate of the ITB increases such that the ITB energy fraction is 0.2. When the ambient temperature increases further, the ITB energy fraction continues increasing to ensure each component operates under its own favourable condition. This control strategy is then verified at the SLS maximum thrust condition.

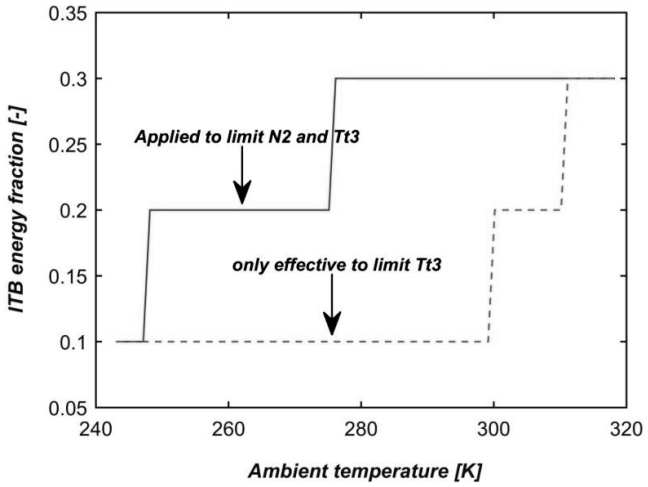


*Figure 7.12: Fuel control strategy for flat rating*

*Table 7.2: Control schedule for flat rating.*

| *Temperature range [K]* | *ITB energy fraction [-]* |
|---|---|
| Ta<248.15 | 0.1 |
| 248.15≤Ta<276.15 | 0.2 |
| 276.15≤Ta≤315.15 | 0.3 |

### 7.3.3 Verification of the control strategy for flat rating

By applying the control schedule in Table 7.2, the component characteristics discussed in section 7.3.1 are expected to be altered. In Figure 7.13, the N1 and N2 corresponding to the control schedule is presented. Over the entire operating range, the N2 speed represented by the dashed line remains safely under its upper limit. The kink in this curve has been due to the switch between different ITB energy fractions. The N1 increases with the increment of the ambient temperature, yet it never exceeds the maximum.

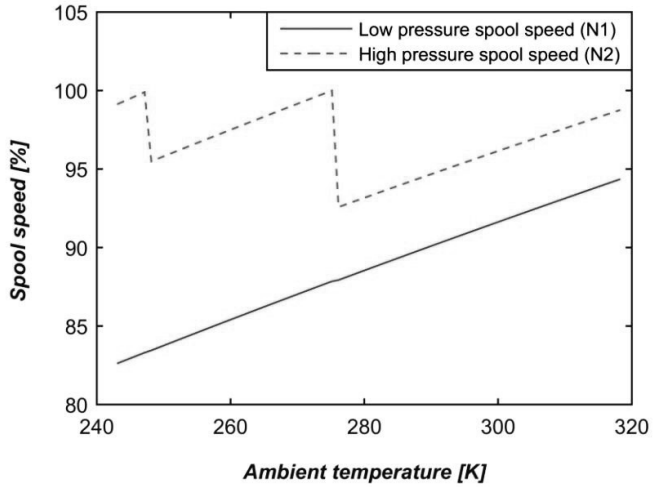


*Figure 7.13: Variation in shaft speeds for the flat rated thrust.*

Apart from the spool speeds, the variations in surge margins of the associated components are presented in Figure 7.14. The core and bypass fan surge margin exhibits nearly no relevance to the ambient temperature since the thrust setting in all cases is identical. This constant thrust results in also constant fan corrected speed, hence constant FPR. The surge margins of LPC and HPC show a contrary tendency. As the fuel flow rate of the ITB increases, the pressure ratio of LPC becomes higher causing a reduction in its surge margin. On the other hand, this is beneficial to enhance the HPC surge margin.

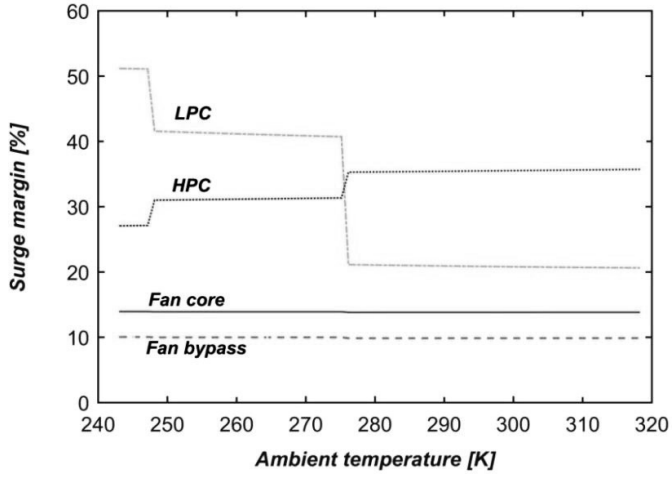


*Figure 7.14: Variation in surge margins for the flat rated thrust*

In Figure 7.15, the variations in engine station temperatures are shown with respect to various ambient temperatures. The $T_{t3}$ and $T_{t4}$ increase with the ambient temperature becomes hotter. Following the fuel flow regulation strategy, the fuel added in the main combustor decreases gradually. The $T_{t4}$ and N2 decreases correspondingly; hence, the HPT power output reduces. As a result, the HPC pressure ratio becomes small (hence lower HPC exit temperature). However, the $T_{t46}$ increases monotonically with an increase in the ambient temperature. Yet it is still under the limit.

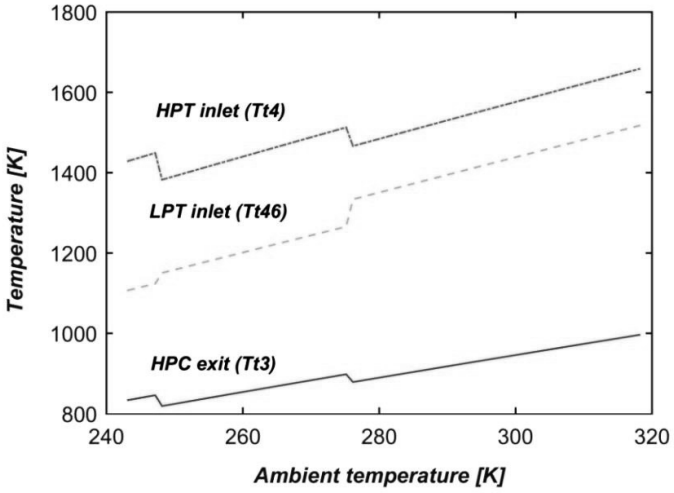


*Figure 7.15: Variation in station temperatures for the flat rated thrust*

Figure 7.16 shows the variation of the thermal efficiency when the regulation strategy of Figure 7.12 is applied. As the ITB energy fraction increases to ensure the engine design variables do not violate their limits, the thermal efficiency decreases progressively, which can result in higher energy consumption during take-off phase. However, the take-off process lasts only for a short time compared to the overall mission; the mechanical and thermal loading at this operating point would play roles that are more important.

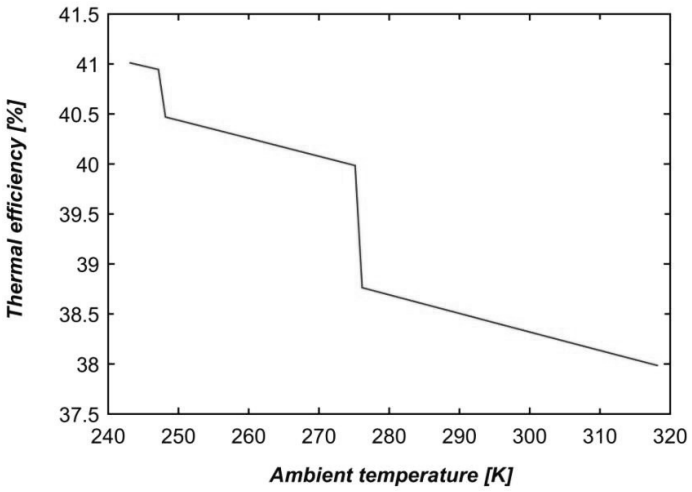


*Figure 7.16: Thermal efficiency for the flat rated thrust*

In this section, a fuel control law has been developed for the flat rating at SLS condition. After performing the verification, it can be concluded that the following this control schedule, the flat rating temperature of the hybrid engine would reach 40°C (ISA+25 K), which is much higher than the current engine flat rating temperature (ISA+15 K). This is realized at the expenses of the fuel consumption during take-off.

## 7.4 Summary

In this chapter, the control strategy for the hybrid engine has been developed and verified to fulfill various requirements at two operating conditions. Overall, using ITB is beneficial for the high pressure spool speed, the HPC exit temperature, and the HPT inlet temperature. However, the limit of the LPC surge margin is violated as increasing the ITB energy fraction. In the first part, the analysis is performed at the SLS ISA condition with respect to various thrust requirements. By following the suggested fuel control schedule with the assist of the VBV schedule, the engine performance at various thrust levels is guaranteed. The second part has been focused on the flat rating for the hybrid engine at SLS condition. Operating the dual combustion chambers simultaneously following the developed control law, the flat rating temperature can reach 40°C (ISA+25 K), which is 10°C higher than the current value.

# Chapter 8 Conclusions and recommendations

The research conducted in this thesis focuses on optimizing the architecture and performance of a multi-fuel hybrid engine concept. The main pillars of this thesis are as follows:

1. Development of a model framework consisting of an engine performance module, a cryogenic heat exchanger module, and an emission prediction module
2. A fundamental study and analysis of turbofan engine with ITB
3. Characterization and optimization of the proposed hybrid engine architecture
4. Development of a control strategy for the proposed hybrid engine

Accordingly, conclusions are drawn and presented in this chapter, followed by recommendations for future work.

## 8.1 The standalone ITB turbofan burning pure kerosene

The basis of the hybrid engine originates from an ITB turbofan engine configuration. Due to its higher specific thrust and SFC, the ITB engine architecture was only considered for military applications. However, the analysis performed in this research is the first to prove the applicability of such an engine configuration to future civil aircraft. The research on an advanced ITB turbofan engine burning pure kerosene has shown the following

- Using an ITB reduces the maximum temperature of the cycle (Tt4) substantially. The analysis showed that the Tt4 reduces from 2300 K to about 1700 K when the ITB energy fraction is increased from 0 to 0.3.
- The reduction in Tt4 reduces the cooling air requirement up to 70% when compared to a contemporary normal turbofan engine with the Tt4 of 2300 K.
- The reduction in the NOx emission for an ITB engine is around 30% due to the low Tt4 and the partial disassociation of NOx formed in the first combustion chamber in the ITB.
- The specific thrust of an ITB turbofan engine is higher than a conventional turbofan engine, implying that the size of the ITB engine would be smaller at the same power output level.
- The increase in SFC due to ITB is negligible up to ITB energy fraction of 0.2.

## 8.2 The characteristics of the multi-fuel hybrid engine

The characteristics of the standalone hybrid engine are assessed with respect to three baseline engines, including an advanced turbofan engine (an imaginary single combustor turbofan engine at the same technology level with the hybrid engine), GEnx, and GE90. The main discoveries are highlighted from the following aspects:

- The isobaric heat capacity of the combustion products from LNG / LH2 is higher, which is beneficial to improve the thermal efficiency of the hybrid engine cycle.
- Using cryogenic fuel as a coolant, the turbine cooling air temperature reduces significantly by about 500K, thereby, the turbine cooling air mass flow rate reduces by 50% compared to a contemporary engine with the uncooled turbine cooling air.
- The benefit of using cooled turbine cooling in a classical turbofan engine is more substantial than in an engine with an Interstage Turbine Burner.
- Compared to the advanced turbofan engine, the thermal efficiency of the LH2-kerosene hybrid engine is about 5% higher. When compared to GEnx and GE90, the improvement is up to 13% and 18% respectively. Moreover, the reduction in $CO_2$ varies from 70% to 100% depending on the fraction of LH2 used.
- The improvement of the thermal efficiency in the LNG-kerosene hybrid engine is slightly less, about 4% higher than the advanced turbofan, 12% higher than GEnx, and 16% higher than GE90. The reduction in $CO_2$ emission by the LNG-kerosene hybrid engine varies from 20% to 50% depending on the LNG fraction.
- The $H_2O$ emission by both hybrid engines increases, which should be considered to evaluate the climate impact.

Furthermore, the mission analysis has been performed to evaluate the characteristics of the MFBWB with the hybrid engine installed. The baseline aircraft are the Boeing 787-8 and the Boeing 777-200ER. The following conclusion is derived:

- Compared to the B777-200ER and B787-8, the LH2-kerosene BWB is able to reduce $CO_2$ emission up to 80%; meanwhile, reduce the NOx emissions by 70% to 80%. Furthermore, the LNG-kerosene BWB reduces $CO_2$ emission by 40% to 50%, and the NOx emissions by more than 80%. The energy consumption by MFBWB is also reduced significantly for the assessed mission. Last but not least, the advantages of the MFBWB are more explicit when the flying distance is longer.

## 8.3 Operating strategy of the hybrid engine

The operating strategy of the hybrid engine is developed making use of the extra degree of freedom provided by the sequential combustion system.

- A fuel control schedule with the assist of a VBV schedule has been proposed for various thrust at SLS ISA condition. Below 55% of the maximum thrust, there is no need to operate the ITB. The VBV is left open during the start-up to prevent the LPC from the surge. As the thrust increases, the VBV commence opening progressively to bleed off the air from the end of the LPC until the thrust reaches 40% of the maximum. As the thrust increases to 55%, the ITB starts to operate until the ITB energy fraction of 0.3 is encountered.
- For the flat rating at SLS, a different operating strategy has been suggested, which ensures the flat rating temperature of the hybrid engine to be at 40°C, about 10°C higher than the current standard.

## 8.4 Recommendations

These are few recommendations suggested for the continuation of further research on the multi-fuel hybrid engine concept.

- To assess the effect of a contra-rotating fan, more sophisticated fan map is required.
- The Interstage Turbine Burner increases the exhaust temperature and thus results in higher exhaust heat losses. Therefore, the ITB engine configuration is slightly less efficient than a conventional turbofan engine for the same component technology level. As an alternative, the exhaust heat can be recovered by using a recuperator or a suitable bottoming cycle like Supercritical $CO_2$ or Organic Rankine Cycle.
- Currently, it is considered that the cryogenic fuel is used to cool the bleed air such that the amount of the turbine cooling air can be reduced, hence improving the engine performance. However, the analysis has shown that the benefits in turbine cooling reduction due to lower bleed air temperature decrease when turbine cooling becomes less. Therefore, instead of cooling the bleed air the cryogenic fuel can be used for intercooling or other systems where the heat sink is required.
- A highly integrated multi-disciplinary framework tool is necessary to support a fully automatic engine design process taking into account various disciplines, for example, thermodynamic, engine structure, engine weight, combustion emissions, etc.

- The performance analysis in this thesis neglects the engine installation effect, like boundary layer ingestion and some of the other interference caused due to the engine. It is recommended to consider the aircraft–engine integration aspects in the future.

# Appendix A Preliminary analysis on cryogenic fuel tanks

The boiling temperature of LNG and LH2 are 112 K and 23 K respectively. To maintain the LNG and LH2 as a liquid phase, an efficient insulation layer is necessary. Moreover, as the fuel gets boil off, the internal the tank pressure increases progressively. This is challenging for the tank material. In this appendix, sensitivity analysis is performed how the fuel tank and insulation layer influence the volume and weight of entire fuel storage system.

The analysis is conducted in the following procedure: firstly, a baseline aircraft Boeing 787-8 is flown over a given long range mission. The energy consumption by B787 during this flight is calculated by a professional aircraft performance analysis tool [120]. Afterward, this mission energy consumption is maintained for the LH2-kerosene fuel combinations with the energy fraction between the LH2 and kerosene varying. As the energy contribution of the LH2 increases the LH2 mass increases accordingly, hence the tank and insulation weight and dimension are calculated.
The LH2 tank considerations

The design choice of LH2 fuel tank is given in Table A.1. A cylindrical tank with hemispherical end caps shape is selected. The fuel tank volume is confined to its maximum of the minimum boundary. As long as the fuel volume is beyond the maximum tank volume, another fuel tank would be added. The minimum volume if specified since the smaller tank volume to area ratio penalizes the aerodynamic performance of aircraft seriously[40]. The diameter of each fuel tank is restricted as 1 meter. Although the fuel tank is well insulated, fuel boil off cannot be eliminated. This boiling off fuel increases the storage pressure inside the fuel tank. A cryogenic fuel tank design has to take this into consideration. In this analysis, a safety factor of 5 is considered. The internal operating pressure of the fuel tank is 1.5 Bar.

*Table A.1: Tank design choice.*

| ***Elements*** | ***Specification*** |
|---|---|
| Shape | Cylindrical tank with hemispherical end caps |
| Maximum tank volume, $m^3$ | 30 |
| Minimum tank volume, $m^3$ | 10 |
| Diameter, $m$ | 1 |
| Boil off rate | 5% volume |
| Inside operating pressure, $Bar$ | 1.5 |
| Safety Factor | 5 |

Different materials, which might be suitable for the LH2 tank, are presented in Table A.2. They are typically considered for the cryogenic fuel tank application. It

can be seen that the carbon composite has the smallest density but highest strength, which is an ideal candidate. The thickness of the tank is a function of material stress, internal operating pressure, and the diameter of the tank. The analysis in the later paragraph is based on these four tank materials.

*Table A.2: Material properties of pressure tank [123].*

| ***Material*** | ***Density*** $kg/m^3$ | ***Yield Strength*** $Mpa$ |
|---|---|---|
| Steel (quenched and tempered alloy ASTM-A514) | 7860 | 690 |
| Aluminum (4.4% Cu 2014-T6) | 2800 | 410 |
| Titanium Alloy (6% AL, 4% V) | 4460 | 825 |
| Carbon Composite | 1530 | 1900 |

## A.1 Insulation considerations

The material of the insulation layer is chosen as *Rigid closed cell polymethacrylimide*. Density of this material is 35.3 $kg/m^3$ . The thermal conductivity of this material is 0.0096$\frac{W}{m \cdot K}$. The thickness of insulation layer is determined by boil off rate and heat transfer rate.

## A.2 Heat transfer mechanism

In this section, detailed heat transfer analysis is performed to determine the insulation layer for given design considerations. The cross section of an insulated fuel tank is depicted in Figure A.1. It is divided into three sections. The inner section is the LH2 storage compartment. Radius of this section is defined as $r_1$. The surrounding of fuel is the tank wall. The tank wall thickness is calculated by Eqn. (26). The most external layer is the insulation layer. The insulation thickness is given by Eqn. (27). The maximum radius including tank and insulation thickness ($r_3$) is confined to 0.5 meter.

$$t_{tank} = r_2 - r_1 \tag{26}$$

$$t_{insulation} = r_3 - r_2 \tag{27}$$

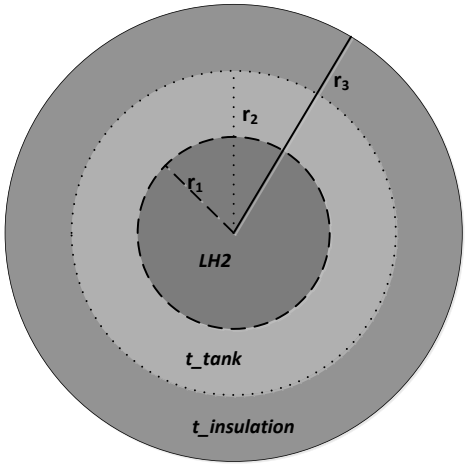


*Figure A.1: Cross section of the LH2 fuel tank.*

Before the analysis is performed, temperatures on each interface are symbolized in Table A.3. Starting from the external environmental, the heat transfer mechanisms involved in this system are heat convention from external environment to the insulation outer surface, heat conduction from the insulation outer surface to its inner surface, heat conduction from the inner surface of the insulation layer to the inner surface of the tank, heat conduction from the inner surface of the tank to the LH2 itself, and finally heat conventional between LH2 and the tank inner wall. Heat radiation is neglected throughout the entire process. Basic heat transfer calculation tool described in [124] is applied.

*Table A.3: Notation of temperatures.*

| ***Notation*** | ***Descriptions*** |
|---|---|
| $T_{\infty}$ | External environment temperature |
| $T_{s\_insulation}$ | Temperature at external surface of insulation layer |
| $T_{s\_tank}$ | Temperature at external surface of the tank |
| $T_{s\_LH2}$ | Temperature at the inner tank surface attaching to the LH2 |
| $T_{LH2}$ | The stored LH2 temperature |

## A.3 Results

The analysis is performed in three aspects: 1) tank and insulation weight fraction with respect to the LH2 energy fraction; 2) system weight variation with respect to the LH2 energy fraction; 3) system volume variation with respect to the LH2 energy fraction. The baseline is single kerosene providing identical mission energy.

One can see from Figure A.2 that the tank and insulation weight with respect to the total fuel total decreases as the LH2 energy fraction increases. When the LH2 fraction is beyond 0.4, the tank and insulation layer weight is only 14% of the total weight and tends to stabilize.

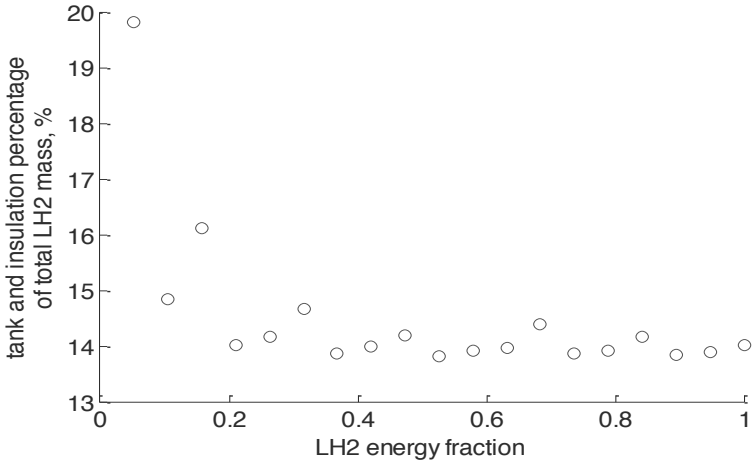


*Figure A.2: The fuel tank and insulation to the total LH2 fraction.*

In Figure A.3, the variation of overall mass with respect to the baseline is presented. Various tank materials are compared. The baseline case excludes the tank and insulation. It can be observed that if including the tank and insulation weight, the weight reduction changes from maximum 65% to 50% depending on the tank material. Therefore, the weight reduction by LH2 is still substantial compared to the kerosene aircraft system.

In Figure A.4, variation in volume with respect to the increase of the LH2 is illustrated. The volume requirement of the entire system increases as the LH2 energy fraction. If excluding the fuel tank and insulation, the volume increase by only LH2 is maximal 4 times of the kerosene aircraft. On top of the fuel volume increases, extra volume is required by insulation. The tank material has no essential effect on the volume increase. Since the heat transfer rate and boil off rate are constant, the insulation thickness also remains identical. The maximum increase would be 4.5 times of the volume occupied by the pure kerosene system. However, how much this volume increase penalizes the over aircraft size is not studied in this analysis.

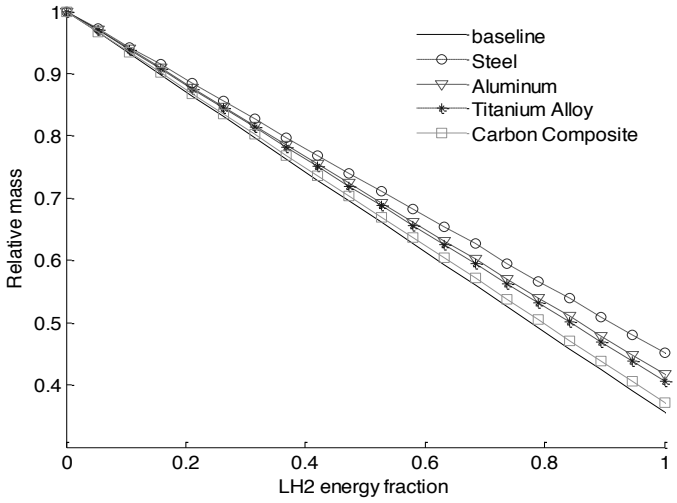


*Figure A.3: The system mass variation w.r.t. the baseline.*

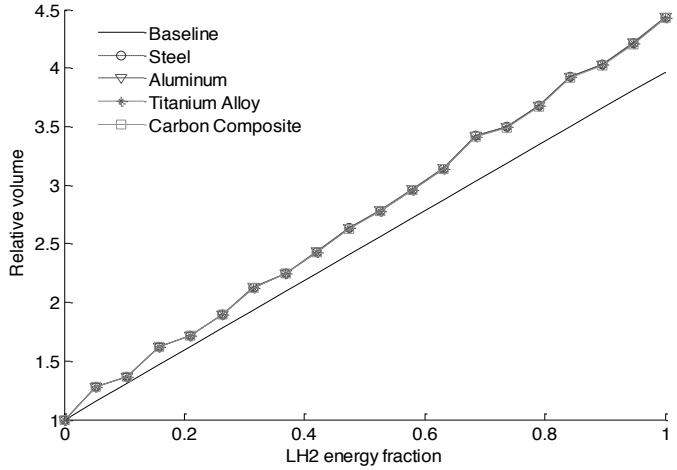


*Figure A.4: Variation of the volume w.r.t. the baseline.*

## A.4 Discussions

According to the analysis performed in this section, it can be seen that the overall benefits of the weight reduction due to LH2 are still substantial even taking into account the fuel tank and insulation weight. On the other hand, the volume required due to low fuel density is large. The tank and insulation add maximum half point

volume on top of the fuel volume itself, which is a relatively small portion. The overall volume increase might enlarge the fuselage of the aircraft hence more wet area and higher aerodynamic drag, which was not studied in this section.

# Bibliography


1. ATAG, *The economic & social benefits of air transport*, 2005.

2. Airbus, *Nevigating the future*, 2012.

3. IPCC, *Aviation and the global atmosphere*, 1999.

4. Lee, D. S., Fahey, D. W., Forster, P. M., Newton, P. J., Wit, R. C. N., Lim, L. L., Owen, B., and Sausen, R., *Aviation and global climate change in the 21st century,* Atmospheric Environment, 2009. 43.

5. Lee, D. S., Pitari, G., Grewe, V., Gierens, K., Penner, J. E., Petzold, A., Prather, M. J., Schumann, U., Bais, A., Berntsen, T., Iachetti, D., Lim, L. L., and Sausen, R., *Transport impacts on atmosphere and climate: Aviation,* Atmospheric Environment, 2010. 44(37): p. 4678-4734 DOI: http://dx.doi.org/10.1016/j.atmosenv.2009.06.005.

6. ACARE, *Flightpath 2050 Europe's vision for aviation*, 2011.

7. ATAG, *The economic and social benefits of air transport 2008*, 2008.

8. Epstein, A. H., *Aeropropulsion for Commercial Aviation in the Twenty-First Century and Research Directions Needed,* AIAA Journal, 2014. 52(5): p. 901-911 DOI: 10.2514/1.J052713.

9. *http://www.ahead-euproject.eu/*, [cited 2015 3rd August].

10. Tang, K., *Next Generation Aircraft Propulsion: Concept Study of a Hybrid Turbofan Engine*. 2010. Delft University of Technology.

11. IATA, *The IATA technology roadmap report*, 2009.

12. Saravanamuttoo, H. I. H., Rogers, G. F. C., and Cohen, H., *Gas turbine theory*. 6th ed. 2008: Longman imprint.

13. Roth, B. A., *The role of thermodynamic work potential in aerospace vehicle design*. in *ISABE conference*. 2003.

14. Grönstedt, T., Irannezhad, M., Lei, X., Thulin, O., and Lundbladh, A., *First and Second Law Analysis of Future Aircraft Engines,* Journal of Engineering for Gas Turbines and Power, 2013. 136(3): p. 031202-031202 DOI: 10.1115/1.4025727.

15. *http://www.pw.utc.com/PurePowerPW1000G_Engine*, 2015.

16. Tsague, L., Tsogo, J., and Tatietse, T. T., *Prediction of the production of nitrogen oxide in turbojet engines,* Atmospheric Environment, 2006. 40(29): p. 5727-5733 DOI: http://dx.doi.org/10.1016/j.atmosenv.2006.05.055.

17. Tsague, L., Tatietse, T. T., Ngundam, J., and Tsogo, J., *Prediction of emissions in turbojet engines exhausts: relationship between nitrogen oxides emission index (EINOx) and the operational parameters,* Aerospace Science and Technology, 2007. 11(6): p. 459-463 DOI: http://dx.doi.org/10.1016/j.ast.2007.04.005.

18. Kurzke, J., *Aeroengine design: from state of the art of turbofans towards innovative architectures.*, in *von Karman Institute for FLuid Dynamics Lecture Series 2013-2014*. 2013.

19. Riegler, C. and Bichlmaier, C., *The Geared Turbofan Technology– Opportunities, Challenges and Readiness Status*. in *Proceedings of the 1st CEAS European Air and Space Conference, Berlin, Germany*. 2007.

20. *http://www.purepowerengine.com/*, 2015 [cited 2015 1st August].

21. Blythe, A. and Smith, P., *Prospects and problems of advanced open rotors for commercial aircraft,* 1985. DOI: 10.2514/6.1985-1191.

22. *http://www.cleansky.eu/content/page/sage-sustainable-and-green-engines*, 2015 [cited 2015 1st August].

23. Guynn, M. D., Berton, J. J., Haller, W. J., Hendricks, E. S., and Tong, M. T., *Performance and environmental assessment of an advanced aircraft with open rotor propulsion*, 2012.

24. Czech, M. J. and Thomas, R. H., *Open Rotor Aeroacoustic Installation Effects for Conventional and Unconventional Airframes*. 2013.

25. Boggia, S., *Intercooled recuperated gas turbine engine concept,* 2005.

26. *http://www.newac.eu/86.0.html*, 2015 [cited 2015 3rd August].

27. Wilfert, G., Sieber, J., Rolt, A., Baker, N., Touyeras, A., and Colantuoni, S., *New environmental friendly aero engine core concepts*, in *18th ISABE conference*. 2007: Beijing, China.

28. Roth, B. A. and Mavris, D. N., *A work availability perspective of turbofan engine performance*. 2001.

29. Kyprianidis, K. G., Grönstedt, T., Ogaji, S. O. T., Pilidis, P., and Singh, R., *Assessment of Future Aero-engine Designs With Intercooled and Intercooled*

*Recuperated Cores,* Journal of Engineering for Gas Turbines and Power, 2011. 133(1): p. 011701 DOI: 10.1115/1.4001982.

30. Sirignano, W. and Liu, F., *Performance increases for gas-turbine engines through combustion inside the turbine,* Journal of Propulsion and Power, 1999. 15(1): p. 111-118.

31. Liu, F. and Sirignano, W. A., *Turbojet and turbofan engine performance increases through turbine burners,* Journal of Propulsion and Power, 2001. 17(3): p. 695-705.

32. Liew, K., Urip, E., and Yang, S., *Parametric cycle analysis of a turbofan engine with an interstage turbine burner,* Journal of propulsion and power, 2005. 21(3): p. 546-551.

33. Güthe, F., Hellat, J., and Flohr, P., *The reheat concept: the proven pathway to ultralow emissions and high efficiency and flexibility,* Journal of Engineering for Gas Turbines and Power, 2009. 131(2): p. 021503.

34. Deffeyes, K. S., *Hubbert's peak: the impending world oil shortage*. 2001: Princeton University Press.

35. Hubbert, M. K., *Nuclear energy and the fossil fuels*. Vol. 95. 1956: Shell Development Company, Exploration and Production Research Division Houston, TX.

36. Hirsch, R. L., Bezdek, R., and Wendling, R., *Peaking of world oil production: Impacts, mitigation, & risk management*, 2005.

37. Brand, J., Sampath, S., Shum, F., Bayt, R. L., and Cohen, J., *Potential use of hydrogen in air propulsion*. in *AIAA/ICAS International Air and Space Symposium and Exposition: The Next 100 Y*. 2003. Dayton, Ohio.

38. Pohl, H. W. and Malychev, V. V., *Hydrogen in future civil aviation,* International Journal of Hydrogen Energy, 1997. 22(10-11): p. 1061-1069 DOI: http://dx.doi.org/10.1016/S0360-3199(95)00140-9.

39. Janic, M., *Is liquid hydrogen a solution for mitigating air pollution by airports?,* International Journal of Hydrogen Energy, 2010. 35(5): p. 2190-2202 DOI: http://dx.doi.org/10.1016/j.ijhydene.2009.12.022.

40. Ponater, M., Pechtl, S., Sausen, R., Schumann, U., and Hüttig, G., *Potential of the cryoplane technology to reduce aircraft climate impact: A state-of-the-art assessment,* Atmospheric Environment, 2006. 40(36): p. 6928-6944 DOI: http://dx.doi.org/10.1016/j.atmosenv.2006.06.036.

41. Klug, H. G. and Faass, R., *CRYOPLANE: hydrogen fuelled aircraft—status and challenges,* Air & Space Europe, 2001. 3(3): p. 252-254.

42. Ponater, M., Marquart, S., Strom, L., Gierens, K., Sausen, R., and Huttig, G., *On the potential of the CRYOPLANE technology to reduce aircraft climate impact*, in *AAC conference*. 2003: Friedrichshafen, Germany.

43. Airbus-Deutschland-GmbH, *Liquid hydrogen fuelled aircraft-system analysis fianl technical report*, 2003.

44. Liebeck, R. H., *Design of the blended wing body subsonic transport,* Journal of aircraft, 2004. 41(1): p. 10-25.

45. Qin, N., Vavalle, A., Le Moigne, A., Laban, M., Hackett, K., and Weinerfelt, P., *Aerodynamic considerations of blended wing body aircraft,* Progress in Aerospace Sciences, 2004. 40(6): p. 321-343.

46. Hileman, J., Spakovszky, Z., Drela, M., and Sargeant, M., *Airframe design for 'silent aircraft',* AIAA paper, 2007. 453: p. 2007.

47. Li, P., Zhang, B., Chen, Y., Yuan, C., and Lin, Y., *Aerodynamic Design Methodology for Blended Wing Body Transport,* Chinese Journal of Aeronautics, 2012. 25(4): p. 508-516 DOI: http://dx.doi.org/10.1016/S1000-9361(11)60414-7.

48. Rao, A. G., Yin, F., and Buijtenen, J. P. v., *A hybrid engine concept for multi-fuel blended wing body,* Aircraft Engineering and Aerospace Technology, 2014. 86(6): p. 483-493 DOI: doi:10.1108/AEAT-04-2014-0054.

49. Plas, A., Sargeant, M., Madani, V., Crichton, D., Greitzer, E., Hynes, T., and Hall, C., *Performance of a boundary layer ingesting (BLI) propulsion system*, in *45th AIAA Aerospace Sciences Meeting and Exhibit*. 2007: Reno, Nevada.

50. Hardin, L., Tillman, T., Sharma, O. P., Berton, J., and Arend, D. J., *Aircraft System Study of Boundary Layer Ingesting Propulsion,* 2012.

51. Hanlon, C. J., *Engine design implications for a blended wing-body aircraft with boundary later ingestion*. 2003. Massachusetts Institute of Technology.

52. Liu, F. and Sirignano, W. A., *Turbojet and turbofan engine performance increase through turbine burners*, in *38th AIAA Aerospace Sciences Meeting and Exhibit*. 2000: Reno, Nevada.

53. Sirignano, W. A. and Liu, F., *Performance increase for gas turbine engines through combustion inside the turbine,* Journal of Propulsion and Power, 1999. 15(1).

54. Wünning, J. and Wünning, J., *Flameless oxidation to reduce thermal NO-formation,* Progress in energy and combustion science, 1997. 23(1): p. 81-94.

55. Wünning, J., *Flameless combustion and its applications,* Natural Gas Technologies. Orlando (USA), 2006. 30.

56. Levy, Y., Sherbaum, V., and Arfi, P., *Basic thermodynamics of FLOXCOM, the low-NOx gas turbines adiabatic combustor,* Applied Thermal Engineering, 2004. 24(11–12): p. 1593-1605 DOI: http://dx.doi.org/10.1016/j.applthermaleng.2003.11.022.

57. Rao, G. and Levy, Y., *A new combustion methodology for low emission gas turbine engines*. in *8th HiTACG conference, Poznan*. 2010.

58. Brewer, G. D., *Hydrogen aircraft technology*. 1991: CRC Press.

59. Rao, A. G., Yin, F., and van Buijtenen, J. P., *A novel engine concept for aircraft propulsion*, in *20th International Symposium Air Breathing Engines*. 2011: Gothenburg, Sweden.

60. Reichel, T. G., Terhaar, S., and Paschereit, O., *Increasing Flashback Resistance in Lean Premixed Swirl-Stabilized Hydrogen Combustion by Axial Air Injection,* Journal of Engineering for Gas Turbines and Power, 2015. 137(7): p. 071503.

61. van Dijk, I. P., Rao, A. G., and van Buijtenen, J. P., *Stator cooling & hydrogen based cycle improvements*. in *ISABE 2009*. 2009. Montreal.

62. Polacsek, C. and Barrier, R., *Numerical simulation of counter-rotating fan aeroacoustics,* 2007.

63. Jérôme Talbotec, M. V., *Snecma counter rotating fan aerodynamic design logic & tests results*, in *27th International Congress of Aeronautical Sciences*. 2010.

64. Lengyel, T., Voß, C., Schmidt, T., and Nicke, E., *Design of a counter rotating fan. an aircraft engine technology to reduce noise and CO2–emissions*. in *ISABE Conference on Air Breathing Engines, Montreal, Canada, ISABE Paper No. 2009-1267*. 2009.

65. Lengyel-Kampmann, T., Bischoff, A., Meyer, R., and Nicke, E., *Design of an Economical Counter Rotating Fan: Comparison of the Calculated and Measured Steady and Unsteady Results*. in *ASME Turbo Expo 2012: Turbine Technical Conference and Exposition*. 2012. American Society of Mechanical Engineers.

66. Sanghi, V., *Technical notes: Sensitivity of design point choice on engine cycle selection,* Journal of Propulsion and Power, 1999. 15(5).

67. Kurzke, J., *http://www.gasturb.de/*, 2015.

68. *http://www.wolverine-ventures.com/index.php?option=com_content&view=article&id=2&Itemid=2*, [cited 2015 30 April].

69. Claus, R. W., Evans, A. L., Lylte, J. K., and Nichols, L. D., *Numerical Propulsion System Simulation,* Computing Systems in Engineering, 1991. 2(4): p. 357-364 DOI: http://dx.doi.org/10.1016/0956-0521(91)90003-N.

70. Lytle, J. K., *The numerical propulsion system simulation: an overview,* 2000.

71. *http://www.ecosimpro.com/description_proosis.php*, [cited 2015 29th April].

72. Ruimtevaartlaboratorium, N. L.-e., *http://www.gspteam.com/*, 2015.

73. Visser, W. P. J. and Broomhead, M. J., *GSP A generic object-oriented gas turbine simulation environment*, 2000.

74. W.P.J. Visser, H. P., M. Oostveen, E. van Dorp, *Experience with GSP as a Gas Path Analysis Tool*. in *ASME Turbo Expo 2006*. 2006. Barcelona, Spain.

75. GSP-Development-Team, *Gsp 11 user manual - version 11.1.0*. 2010: National Aerospace Laboratory NLR.

76. Farokhi, S., *Aircraft Propulsion*. 2014: Wiley.

77. Visser, W., *Generic Analysis Methods for Gas Turbine Engine Performance: The development of the gas turbine simulation program GSP*. 2015. TU Delft, Delft University of Technology.

78. Kurzke, J., *How to get component maps for aircraft gas turbine performance calculations*. in *ASME 1996 International Gas Turbine and Aeroengine Congress and Exhibition*. 1996. American Society of Mechanical Engineers.

79. Walsh, P. P. and Flectcher, P., *Gas Turbine Performance*. 2nd ed. 2004: Blackwell Science Ltd.

80. Tiemstra, F., *Design of a Semi-Empirical Tool for the Evaluation of Turbine Cooling Requirements in a Preliminary Design Stage*. 2014. Delft University of Technology.

81. Han, J.-C., Dutta, S., and Ekkad, S., *Gas turbine heat transfer and cooling technology*. 2012: CRC Press.

82. Florschuetz, L., Truman, C., and Metzger, D., *Streamwise flow and heat transfer distributions for jet array impingement with crossflow,* Journal of Heat transfer, 1981. 103(2): p. 337-342.

83. Levy, Y., Rao, A. G., Erenburg, V., Sherbaum, V., Gaissinski, I., and Krapp, V., *Pressure losses for jet array impingement with crossflow*. in *ASME Turbo Expo 2012: Turbine Technical Conference and Exposition*. 2012. American Society of Mechanical Engineers.

84. Metzger, D., Shepard, W., and Haley, S., *Row resolved heat transfer variations in pin-fin arrays including effects of non-uniform arrays and flow convergence*. in *31st international gas turbine conference and exhibit*. 1986.

85. Metzger, D., Fan, Z., and Shepard, W., *Pressure loss and heat transfer through multiple rows of short pin fins*. in *Heat Transfer 1982, Volume 3*. 1982.

86. Baldauf, S., Scheurlen, M., Schulz, A., and Wittig, S., *Correlation of Film-Cooling Effectiveness From Thermographic Measurements at Enginelike Conditions,* Journal of Turbomachinery, 2002. 124(4): p. 686-698.

87. Stearns, E. M., *Energy efficient engine core design and performance report,* 1982.

88. Halila, E., Lenahan, D., and Thomas, T., *Energy efficient engine high pressure turbine test hardware detailed design report,* 1982.

89. Horlock, J., *The basic thermodynamics of turbine cooling,* Journal of turbomachinery, 2001. 123(3): p. 583-592.

90. Horlock, J., Watson, D., and Jones, T., *Limitations on gas turbine performance imposed by large turbine cooling flows,* Journal of engineering for gas turbines and power, 2001. 123(3): p. 487-494.

91. Wilcock, R., Young, J., and Horlock, J., *The effect of turbine blade cooling on the cycle efficiency of gas turbine power cycles,* Journal of Engineering for Gas Turbines and Power, 2005. 127(1): p. 109-120.

92. Young, J. and Wilcock, R., *Modeling the Air-Cooled Gas Turbine: Part 1—General Thermodynamics,* Journal of Turbomachinery, 2002. 124(2): p. 207-213.

93. Hartsel, J., *Prediction of effects of mass-transfer cooling on the blade-row efficiency of turbine airfoils*, in *AIAA paper 7211*. 1972.

94. Kurzke, J., *Performance modeling methodology: efficiency definitions for cooled single and multistage turbines*. in *ASME Turbo Expo 2002: Power for Land, Sea, and Air*. 2002. American Society of Mechanical Engineers.

95. Young, J. and Horlock, J., *Defining the efficiency of a cooled turbine,* Journal of turbomachinery, 2006. 128(4): p. 658-667.

96. Horlock, J. and Torbidoni, L., *Calculations of cooled turbine efficiency,* Journal of Engineering for Gas Turbines and Power, 2008. 130(1): p. 011703.

97. Łapkaa, P., Seredyńskia, M., Ćwikb, A., and Domańskia, R., *Preliminary study on supercritical hydrogen and bleed air heat exchanger for aircraft application*, in *22nd ISABE conference* 2015: Phoenix AZ USA.

98. Fohmann, K. G., *Design of a cooling system for the hybrid engine*
*Design of a heat exchanger for cooling bleed air with liquefied natrual gas*. 2015. Delft University of technology.

99. Shah, R. K. and Sekulic, D. P., *Fundamentals of Heat Exchanger Design*. 2003: Wiley.

100. Lefebvre, A. H., *Fuel effects on gas turbine combustion-liner temperature, pattern factor, and pollutant emissions,* Journal of Aircraft, 1984. 21(11): p. 887-898.

101. Rizk, N. K. and Mongia, H. C., *Emissions predictions of different gas turbine combustors*, in *32nd AIAA Aerospace Sciences Meeting & Exhibit*. 1994.

102. Lefebvre, A. H. and Ballal, D. R., *Gas Turbine Combustion: Alternative Fuels and Emissions, Third Edition*. 2010: CRC Press.

103. Rizk, N. K. and Mongia, H., *Semianalytical correlations for NOx, CO, and UHC emissions,* Journal of Engineering for Gas Turbines and Power, 1993. 115(3): p. 612-619.

104. Shakariyants, S. A., *Generic methods for aero-engine exhaust emission prediction*. 2008: TU Delft, Delft University of Technology.

105. http://www.cantera.org/docs/sphinx/html/reactors.html, [cited 2015 August].

106. Dagaut, P., *On the kinetics of hydrocarbons oxidation from natural gas to kerosene and diesel fuel,* Physical Chemistry Chemical Physics, 2002. 4(11): p. 2079-2094 DOI: 10.1039/B110787A.

107. Honnet, S., Seshadri, K., Niemann, U., and Peters, N., *A surrogate fuel for kerosene,* Proceedings of the Combustion Institute, 2009. 32(1): p. 485-492 DOI: http://dx.doi.org/10.1016/j.proci.2008.06.218.

108. Rao, A. G. and Bhat, A., *Hybrid Combustion System for Future Aero Engines*. in *Proceedings of the 2nd National Propulsion Conference*. 2015. IIT Bombay, Powai, Mumbai.

109. *http://nl.mathworks.com/discovery/genetic-algorithm.html*.

110. Konak, A., Coit, D. W., and Smith, A. E., *Multi-objective optimization using genetic algorithms: A tutorial,* Reliability Engineering & System Safety, 2006. 91(9): p. 992-1007 DOI: http://dx.doi.org/10.1016/j.ress.2005.11.018.

111. Rao, S. S., *Engineering optimization: theory and practice*. 4th ed. 2009: John Wiley & Sons.

112. Lakshminarayana, B., *Methods of predicting the tip clearance effects in axial flow turbomachinery,* Journal of Fluids Engineering, 1970. 92(3): p. 467-480.

113. Kyprianidis, K. G. and Rolt, A. M., *On the Optimization of a Geared Fan Intercooled Core Engine Design,* Journal of Engineering for Gas Turbines and Power, 2015. 137(4): p. 041201.

114. Drawin, S., Heilmaier, M., Jéhanno, P., Wu, X., Belaygue, P., Tsakiropoulos, P., Vilasi, M., Guédou, J., Novak, P., and Delabrouille, F., *THE EU-FUNDED "ULTMAT" PROJECT: ULTRA HIGH TEMPERATURE MATERIALS FOR TURBINES*. in *25th International Congress of the Aeronautical Sciences*. 2006.

115. *http://nl.mathworks.com/help/optim/ug/fmincon.html*, [cited 2015 August].

116. Nocedal, J. and Wright, S., *Numerical optimization*. 2nd ed. 2006: Springer Science & Business Media.

117. Kyprianidis, K. G., Sethi, V., Ogaji, S. O., Pilidis, P., Singh, R., and Kalfas, A. I., *Thermo-Fluid Modelling for Gas Turbines—Part I: Theoretical Foundation and Uncertainty Analysis*. in *ASME Turbo Expo 2009: Power for Land, Sea, and Air*. 2009. American Society of Mechanical Engineers.

118. Held, I. M. and Soden, B. J., *Water vapor feedback and global warming 1,* Annual review of energy and the environment, 2000. 25(1): p. 441-475.

119. GREWE, V., BOCK, L., BURKHARDT, U., DAHLMANN, K., GIERENS, K., HÜTTENHOFER, L., UNTERSTRASSER, S., RAO, A. G., BHAT, A., YIN, F., REICHEL, T. G., PASCHEREIT, O., and LEVY, Y., *Assessing the climate impact of the AHEAD multi-fuel blended wing body,* 2015. DOI: 10.1127/metz/2014/0123.

120. *http://www.lissys.demon.co.uk/PianoX.html*, 2015 [cited 2015 4th August].

121. CRYOPLANE-Group, *Liquid Hydrogen Fuelled Aircraft-System Analysis*, 2003.

122. *http://www.gspteam.com/GSPsupport/OnlineHelp/index.html?surge_margin.htm*, [cited 2015 11th August].

123. Colozza, A. J., *Hydrogen storage for aircraft applications overview*. 2002.

124. Bergman, T. L., Incropera, F. P., and Lavine, A. S., *Fundamentals of Heat and Mass Transfer*. 2011: Wiley.

# Acknowledgement

The research presented in this thesis was under the project AHEAD founded by the European Union Commission. I would like to thank all the partners of this project for their support. Moreover, I was financially supported by the China Scholarship Council (CSC). Without this scholarship, I would not be able to complete my PhD research. Therefore, I would like to express my appreciations to CSC.

Exploring unknown world is never an easy task. During my six years research period, many people have come into my life with their knowledge, friendliness, and love. If there were no them, I would not be enjoying the work and life as much as what I am now. I am so grateful and I would like particularly to thank some of them here.

I would like to thank my promoter prof. Jos van Buijtenen. Jos, I understand it is not a short distance for you to visit TUDelft, I really appreciate every discussion between us. I still remember our meetings at the very beginning when I just arrived. Those discussions had deep influences on my research approaches later on. Without your feedbacks, the quality of my thesis wouldn't have been as good as what it is now.

My thanks are expressed further to my co-promoter Dr. Arvind G. Rao. Arvind, as my daily supervisor, you are the one who I talked to the most in the past years. You're busy with all kinds of things, however, you've been always available for shearing knowledge whenever you could. I just wonder how many wonderful ideas are hidden in your mind. Your insights into aviation inspire me a lot on my research. Moreover, I've learnt a lot from you the way to communicate with people, which is as valuable as the knowledge itself.

I would like also to thank prof. Piero Colonna and prof. Leo Veldhuis to host me in the group. Moreover, thank you, Wilfried and Oscar for your unconditional support for GSP that I have been using during my entire PhD research period. Thank you, Maurice and Tomas, to help me translating my thesis summary. Mo Li, thank you so much for helping me with my thesis cover design. Also, my thanks go further to Nana and Bettie for all your help.

In the past years, acquaintances left and strangers came, having become friends again. Thanks to all these alterations, my life has become as colorful as how it is now. My sincerely appreciations are expressed to all those interesting conversations with them. Hereby I would like to first thank Abhishek, my former officemate. Every lunch discussion with you was so interesting. I'm very much impressed by your knowledge in such broad area, especially your deep interests into history, which has also become my interest later on. Moreover, I would like to thank my other officemates either former or current ones: Ali (until now you are still the most

efficient one among people I've ever met to finish their PhDs), Wim (with whom I had a long competition to collect labels from various apple brands), Dipanjay, Haiqiang, Andre, Peijian, Imco, Lucia, Sebastian, Antonio, Adam, Salvatore. My thanks are also expressed to Reinier, Jan, Xiaojia, and Fred. I missed all those moments of hanging out with you guys. I must say standing on a square in Den Haag at 01:00 am with a strange gesture is probably the most silly thing that I have ever done… but it was so much fun. I really missed it.

No surprisingly, there is a big Chinese community around, which makes me feel at home. It wouldn't be realistic to name all, still I would like to thank some of them here. Hui Yu, Huajie, Fengnian, Peijun, Zaoxu, Yannian, Qingxi, Chang Wang, Liu Liu, Xiaoyu. Thanks to you, my trip is full of warmness and happiness.

I would like to thank my parents and my brother. 8000 km is not short at all as I imagined. When I made the decision to leave home, I had never been aware that it would be for such a long period. Persistence is the only thing that I can do. Thanks for your understanding and love. If there were not your unconditional support, I would not be able to complete this journey.

Finally yet importantly, I would like to thank my beloved husband, Xiaodong. Meeting you has been the most beautiful part of my journey. The list of things I would like to thank you is too long, which I will be telling you in the rest of my life.

# About the author

Feijia Yin was born on 20th April 1986, in Liquan, Shaanxi Province, China. In 2004, she entered Northwestern Polytechnical University (NPU) in Xi'an, China as a bachelor student. She received her BSc. Degree in Automation, 2008. After two years, she received her MSc. Degree in Control Theory and Engineering from the faculty of Power and Energy in NPU.

Since October 2010, she started her Ph.D. research in the group of Flight Performance and Propulsion (FPP), Faculty of Aerospace engineering, Delft university of Technology. The research topic is modeling and characteristics of a novel multi-fuel hybrid engine for future aircraft. Starting from June 2016, Feijia has been employed by the group of Aircraft Noise and Climate Effects (ANCE) in the same faculty as a postdoc researcher. The research topic is flight trajectory optimization to reduce the climate impact.